Journal of Computational Physics 348 (2017) 298–342

Contents lists available at ScienceDirect

Journal of Computational Physics

www.elsevier.com/locate/jcp

High order ADER schemes for a unified first order hyperbolic formulation of Newtonian continuum mechanics coupled with electro-dynamics

Michael Dumbser [a,*], Ilya Peshkov [b,c], Evgeniy Romenski [c,d], Olindo Zanotti [a]

[a] Department of Civil, Environmental and Mechanical Engineering, University of Trento, Via Mesiano 77, 38123 Trento, Italy
[b] Institut de Mathématiques de Toulouse, Université Toulouse III, F-31062 Toulouse, France
[c] Sobolev Institute of Mathematics, 4 Acad. Koptyug Avenue, 630090 Novosibirsk, Russia
[d] Novosibirsk State University, 2 Pirogova Str., 630090 Novosibirsk, Russia

ARTICLE INFO

Article history:
Received 6 December 2016
Received in revised form 9 June 2017
Accepted 10 July 2017
Available online 17 July 2017

Keywords:
Symmetric hyperbolic thermodynamically compatible systems (SHTC)
Unified first order hyperbolic model of continuum physics (fluid mechanics, solid mechanics, electro-dynamics)
Finite signal speeds of all physical processes
Arbitrary high-order ADER Discontinuous Galerkin schemes
Path-conservative methods and stiff source terms
Nonlinear hyperelasticity

ABSTRACT

In this paper, we propose a new unified *first order hyperbolic* model of Newtonian continuum mechanics coupled with electro-dynamics. The model is able to describe the behavior of moving elasto-plastic dielectric solids as well as viscous and inviscid fluids in the presence of electro-magnetic fields. It is actually a very peculiar feature of the proposed PDE system that viscous fluids are treated just as a special case of elasto-plastic solids. This is achieved by introducing a *strain relaxation* mechanism in the evolution equations of the distortion matrix $\boldsymbol{A}$, which in the case of purely elastic solids maps the current configuration to the reference configuration. The model also contains a hyperbolic formulation of heat conduction as well as a dissipative source term in the evolution equations for the electric field given by Ohm's law. Via formal asymptotic analysis we show that in the stiff limit, the governing first order hyperbolic PDE system with relaxation source terms tends *asymptotically* to the well-known viscous and resistive magnetohydrodynamics (MHD) equations. Furthermore, a rigorous derivation of the model from variational principles is presented, together with the transformation of the Euler–Lagrange differential equations associated with the underlying variational problem from Lagrangian coordinates to Eulerian coordinates in a fixed laboratory frame. The present paper hence extends the unified first order hyperbolic model of Newtonian continuum mechanics recently proposed in [110,42] to the more general case where the continuum is coupled with electro-magnetic fields. The governing PDE system is *symmetric hyperbolic* and satisfies the first and second principle of thermodynamics, hence it belongs to the so-called class of symmetric hyperbolic thermodynamically compatible systems (SHTC), which have been studied for the first time by Godunov in 1961 [61] and later in a series of papers by Godunov and Romenski [67,69,119]. An important feature of the proposed model is that the propagation speeds of all physical processes, including dissipative processes, are *finite*. The model is discretized using high order accurate ADER discontinuous Galerkin (DG) finite element schemes with *a posteriori* subcell finite volume limiter and using high order ADER-WENO finite volume schemes. We show numerical test problems that explore

* Corresponding author.
E-mail addresses: michael.dumbser@unitn.it (M. Dumbser), peshkov@math.nsc.ru (I. Peshkov), evrom@math.nsc.ru (E. Romenski), olindo.zanotti@unitn.it (O. Zanotti).

http://dx.doi.org/10.1016/j.jcp.2017.07.020

a rather large parameter space of the model ranging from ideal MHD, viscous and resistive MHD over pure electro-dynamics to moving dielectric elastic solids in a magnetic field.

1. Introduction

1.1. Electrodynamics of moving media

In this paper, we propose a new unified *first order hyperbolic* model of Newtonian continuum mechanics coupled with electro-dynamics. The model is the extension of our previous results [42], hereafter Paper I, on a unified formulation of continuum mechanics towards the coupling of the time evolution equations for the matter with the electric and magnetic fields. The problem of determining the force acting on a medium in an electromagnetic field, as well as the related problem of determining the energy-momentum tensor of an electromagnetic field in a medium, has been discussed in the literature over the years since the work by Minkowski [93] and Abraham [2]. However, to the best of our knowledge, a universally accepted solution to this problem has been absent to date [83,88,60,51,34].

In this respect, our work can be broadly considered as a contribution to the modeling of electrodynamics of moving continuous media. We do not claim to give an ultimate solution to the problem, but rather to show that, within our formalism, all the equations can be obtained in a consistent way with rather good mathematical properties (symmetric hyperbolicity, first order PDEs, well posedness of the initial value problem, finite speeds of perturbation propagation even for dissipative processes in the diffusive regime) and that the corresponding physical effects are correctly described. By an extensive comparison with the numerical and analytical solutions to the well established models as the Maxwell equations, ideal MHD equations and viscous resistive MHD (VRMHD) equations, we demonstrate that the proposed nonlinear hyperbolic dissipative model is able to describe dielectrics ($\eta \to \infty$), ideal conductors ($\eta \to 0$), and resistive conductors ($0 < \eta < \infty$) as particular cases, where η is the resistivity. Thus, the applicability range of the proposed model is larger than those for ideal and resistive MHD models, because the electric and magnetic fields are genuinely independent and are governed by their own time evolution equations as in the Maxwell equations.

In Paper I and [110], we provided a unified first-order hyperbolic formulation of the equations of continuum mechanics, showing for the first time that the dynamics of fluids and solids can be cast in a *single mathematical framework*. This becomes possible due to the use of a characteristic strain dissipation time τ, which is the characteristic time for continuum particle *rearrangements*. By its definition, the characteristic time τ, as opposed to the viscosity coefficient, is applicable to the dynamics of both fluids and solids (see the discussions in [110] and Paper I) and is a continuum interpretation of the seminal idea of the so-called *particle settled life time* (PSI) of Frenkel [54], who applied it to describe the fluidity of liquids, see also [18,16,17] and references therein. In addition, the definition of τ assumes the continuum particles to have a *finite scale* and thus to be deformable as opposed to the *scaleless mathematical points* in classical continuum mechanics. We note that the model studied in [110] and Paper I was used by several authors, e.g. [118,91,114,57,10,66,53,115,9,99,109,139] to cite just a few, in the solid dynamics context since its original invention in 1970th by Godunov and Romenski [68,64] but the recognition that the same model is also applicable to the dynamics of viscous fluids and its extensive validation in the fluid dynamics context was made only recently in [110] and Paper I.

1.2. Symmetric hyperbolic equations, well-posedness, causality

When one deals with nonlinear dynamical phenomena, and thus with **nonlinear** time-dependent partial differential equations (PDEs), perhaps, the first examination a new model has to pass is to verify if the initial value problem (IVP) is well-posed, at least locally, i.e. whether the solution to the system of PDEs with given initial data exists, is unique and stable (depends continuously on the initial data). We emphasize that the well-posedness of the IVP should not be considered as a purely mathematical requirement but as a fundamental physical observation about the time evolution of physical systems, i.e. exactly as we consider causality, conservation and thermodynamic principles, Galilean or Lorentz invariance to be essential features of macroscopic time evolution. In other words, a model describing the time evolution of a physical system and having an ill-posed IVP should be regarded as wrong. Moreover, the well-posedness of the IVP is a fundamental property of time-dependent PDEs in order to be numerically solvable.

From the mathematical viewpoint, the well-posedness of the IVP cannot be guaranteed for a general nonlinear system of PDEs. This even cannot be guaranteed for a first order quasi-linear system [12,49,96], or for models which were consistently derived from microscopic theories as, for example, the Burnett equations derived from the gas kinetic theory [14,128,138]. However, there is a class of nonlinear PDEs for which the IVP is locally well-posed in time, which is the class of hyperbolic PDEs. Unfortunately, it is hardly possible to prove that a given non-linear first order system is globally (not in time but in the space of physically relevant state parameters) hyperbolic because this would require to prove the global existence of the full basis of eigenvectors for a matrix whose entries can be highly nonlinear. For example, the model considered in this paper has nonlinear terms up to power 4 and to find analytical expressions for the eigenvalues and eigenvectors, and thus

to prove hyperbolicity in this way, seems impossible. So how can we be sure that the IVP for the proposed nonlinear model is well-posed, i.e. that the model is hyperbolic?

The model proposed in this paper was developed within a very important *subclass* of first order nonlinear hyperbolic systems whose non-dissipative part can be written in the following quasi-linear form

$$\mathcal{M}(\mathbf{p})\frac{\partial \mathbf{p}}{\partial t}+\mathcal{H}_k(\mathbf{p})\frac{\partial \mathbf{p}}{\partial x_k}=0, \tag{1}$$

$\mathcal{M}^{\mathrm{T}}=\mathcal{M}>0$ and $\mathcal{H}_k^{\mathrm{T}}=\mathcal{H}_k$, for which (local) well-posedness is known to hold true [80,12,96,121]. This subclass is called *symmetric hyperbolic systems of PDEs* and it is a generalization of Friedrichs-symmetrizable linear systems [55]. One may naturally question how restrictive it is for a model to be symmetric hyperbolic? As it was shown by Godunov [61–63] and later by others [56,15,122] there is an intimate connection between the symmetric hyperbolicity and thermodynamics, i.e. a first order system of PDEs is symmetric hyperbolic if it admits an extra conservation law for a *convex potential* which plays the role of the total energy for the system. Therefore, such a subclass of hyperbolic PDEs can be associated with the thermodynamically compatible systems of first order time-dependent PDEs.

The considered nonlinear system for electrodynamics of moving media has been developed within such a class of symmetric hyperbolic systems with convex energy. Therefore, one can be certain that, *despite the highly nonlinear terms*, the proposed model is globally hyperbolic and the IVP for it is well-posed, and hence the model can be solved numerically.

What concerns a mathematical guide to derive symmetric hyperbolic time evolution equations, as in [110] and Paper I, we follow the so-called formalism of ***S**ymmetric **H**yperbolic **T**hermodynamically **C**ompatible systems of conservation laws*, or simply SHTC formalism here. This formalism is described in Section 2.

Eventually, we recall that apart of the well-posedness of the IVP the *hyperbolicity* also naturally accounts for another fundamental observation about time evolution of physical systems, namely the finite velocity for any perturbation propagation, i.e. *causality*.

1.3. Hyperbolic PDEs with stiff relaxation source terms

By passing from the non-dissipative dynamics described by symmetric hyperbolic PDEs of type (1) to dissipative dynamics (viscous momentum, heat and charge transfer), we do not want to destroy the fundamental physical properties discussed above, i.e. the well-posedness and causality. Thus, we believe that the only compromise is to model dissipative processes by adding *algebraic source terms* of relaxation type to the right hand side of (1). Thus, we shall consider the following generalization of (1)

$$\mathcal{M}(\mathbf{p})\frac{\partial \mathbf{p}}{\partial t}+\mathcal{H}_k(\mathbf{p})\frac{\partial \mathbf{p}}{\partial x_k}=-\frac{1}{\tau}\mathbf{S}(\mathbf{p}), \tag{2}$$

where τ is a dissipation time scale[1] that can be a function of the state parameters $\mathbf{p}$ as well. This option preserves both features (well-posedness and causality) because the hyperbolic character of the PDEs is defined by the leading terms only, i.e. by the symmetric matrices $\mathcal{M}$ and $\mathcal{H}_k$. As shown in Paper I, the relaxation source terms can be successfully used to describe viscous momentum and heat transfer which, for many years, in classical continuum mechanics was believed to be possible only in the framework of second order parabolic PDEs.

An *attractive* feature of using algebraic relaxation source terms is the possibility of a straightforward generalization to a nonlinear transport theory via $\tau=\tau(\mathbf{p})$ (e.g. non-Newtonian fluids, elasto-plastic solids, non-Fourier heat conduction) without any increase in the complexity of the mathematical formulation, because no new analytical and numerical techniques are required to treat the model with $\tau(\mathbf{p})$. For example, the same family of ADER finite volume and discontinuous Galerkin methods that was used in paper I for the simulation of Newtonian flows with $\tau=const$ was also applied to the modeling of nonlinear elasto-plastic deformation in solids in [139] where the dissipation time was not constant but varies over ~ 15 orders of magnitude.

At this point, we stress that the SHTC formalism is *radically different* from the well-known Maxwell–Cattaneo approach to construct hyperbolic relaxation models [25] typically used in extended irreversible thermodynamics (EIT) [79]. The noticeable difference between the Maxwell–Cattaneo and the SHTC approach is that the relaxation affects the differential terms in the Maxwell–Cattaneo approach while it is introduced in a *purely algebraic manner* in the SHTC formalism. In Maxwell–Cattaneo-type models the flux Jacobian as well as the corresponding sound speeds depend on a relaxation parameter ϵ as ϵ^{-1} [142]. In particular, in order to approach Newtonian flows with a Maxwell–Cattaneo-type model, the shear sound speed has to go to infinity[2] which of course violates the causality principle. In the SHTC formalism, as demonstrated in paper I via the dispersion analysis, the sound speeds are always finite, also in the limit $\tau\to 0$. Another apparent consequence

[1] There may be, of course, multiple dissipation time scales τ_1, τ_2, …, etc. corresponding to different physical processes (viscous dissipation, dissipation due to heat transfer, chemical reactions, etc.). In equation (2), we write a single time τ just for simplicity of notation and only to emphasize the main character of the source terms used in this paper.

[2] This defect, however, was removed in the version of EIT by Müller and Ruggeri [96] due to a more elaborate structure of the equations, in which the relaxation is introduced in a purely algebraic manner and does not affect the differential terms, as in our formalism.

of the structure of the relaxation terms of the Maxwell–Cattaneo-type models is that the generalization to a more realistic case with $\epsilon = \epsilon(\mathbf{p})$ inevitably affects the hyperbolicity of a model [49] because the matrices of the quasi-linear form now depend on $\epsilon(\mathbf{p})$. In addition, the differences between the approaches become also apparent if one takes a look at the physical meaning of the state variables used in both approaches. We recall that in the EIT the *fluxes* are typically used as the extra state variables (in addition to the conventional ones like mass, momentum and energy), which usually leads to the situation that the PDEs have no apparent structure (new *differential* terms may appear or disappear depending on the choice of the closure for the system). In the SHTC formalism, only density fields may serve as state variables which, in fact, due to the fundamental *conservation principle* allows to obtain equations in a rather complete form with an elegant structure, see Section 2. Last but not least, it is well known that for Maxwell–Cattaneo-type models the choice of an objective time derivative (objective frame rate) for the fluxes can not be addressed in a unique manner since an infinite number of objective time derivatives is possible [142,49]. This is not the case for the SHTC formalism because it is frame invariant by construction [65].

1.4. Numerical solution of hyperbolic PDEs with stiff relaxation

Although the SHTC formalism provides a consistent framework for the modeling of time-dependent nonlinear dissipative phenomena the use of hyperbolic relaxation models (2), as it is well known, imposes certain difficulties for the numerical solution in the case when the dissipation time scale defined by the relaxation time $\tau \ll T$ is much smaller than the macroscopic time scale $T \sim 1/c_{\max}$ defined by the maximum characteristic speed $c_{\max}$ of the non-dissipative part of the model (i.e. by the left hand side of (2)). In such a case, the source term in (2) is called a *stiff* source term. The presence of a stiff source term may let the original system tend towards an asymptotically reduced system (see [26,124]) that may even have a different structure than the original one, see e.g. [42].

For nondissipative hyperbolic PDEs (1), only a numerical flux must be chosen, or an appropriate fluctuation for non-conservative products [24,104]. In this case, the classical properties required are consistency, stability and accuracy. For dissipative hyperbolic PDEs (2) with relaxation source terms also an appropriate numerical source term must be chosen. Here, not only the three classical properties are required, but some additional properties are needed for the global numerical scheme: It should be *well-balanced*, i.e. able to preserve certain relevant steady state solutions also numerically. It should be robust also on coarse grids if the source term is stiff. A coarse grid is a grid whose size does not take into account the source term, i.e. the characteristic space and time steps are based on the associated homogeneous system (1) only. Finally, the scheme should be *asymptotically consistent* or in other words asymptotic preserving (AP) if the source term is stiff. This means that the scheme should give the correct asymptotic behavior even if the source term is *under resolved*.

In this paper, we do not aim to provide new developments concerning the numerical treatment of hyperbolic systems with stiff relaxation. The reader is referred to the extensive literature on the subject, see e.g. the following non-exhaustive list of references [85,107,108,78,21,124,19,22,105,98,87,92,40,75,20] and references therein. Our numerical results fully rely on the unified family of ADER finite volume (FV) and ADER discontinuous Galerkin (DG) methods developed previously in [40,36,41,46,75] and successfully applied to the modeling of viscous Newtonian flows (i.e. in the stiff relaxation limit) in Paper I within the SHTC framework, see [42]. The ADER finite volume methods are based on a three stage procedure. First, a high-order non-oscillatory WENO reconstruction procedure is applied to the cell averages at the current time level. Second, the temporal evolution of the reconstruction polynomials is computed locally inside each cell using the governing equations. In the original ENO scheme of Harten et al. [74] and in the ADER schemes of Toro and Titarev [130,137,131,132], this time evolution is achieved via a Taylor series expansion where the time derivatives are computed by repeated differentiation of the governing PDEs with respect to space and time, i.e. by applying the so-called Cauchy–Kowalevski procedure. However, this approach is not able to handle stiff source terms, unless an *implicit* Cauchy–Kowalevski method is used, see recent developments documented in [136]. Therefore, a new strategy was proposed in [40], which only replaces the Cauchy–Kowalevski procedure compared to the previously mentioned schemes. For the time-evolution part of the algorithm, a *local* space–time discontinuous Galerkin (DG) finite element scheme was introduced, which is able to handle also stiff source terms. This step is the only part of the algorithm which is *locally implicit*, and thus allows the use of a time step for the final numerical scheme that has to obey only a classical CFL-type stability condition based on the maximum wave speed $c_{\max}$ of the advective processes and not based on the relaxation time τ. The third and last step of the fully-discrete ADER family of schemes consists of a fairly standard *explicit* integration over each space–time control volume, using the local space–time DG solutions at the Gaussian integration points for the intercell fluxes and for the space–time integral over the source term. Compared to ADER-FV schemes, in the case of ADER-DG methods there is no need for the high order WENO reconstruction operator, since the discrete solution is directly evolved in the space of higher order piecewise polynomials. However, these schemes require proper limiting at shock waves, see e.g. [48,145,144] for recent developments.

The ADER-FV and ADER-DG framework is now well established and has already been applied to many different systems of PDEs [36,39,41,35,46,48,145,144,42], including hyperbolic systems with stiff relaxation.

1.5. Computational advantages of using hyperbolic dissipative models

From the computational performance viewpoint, a clear difference between classical parabolic theories such as the Navier–Stokes–Fourier (NSF) equations or the viscous and resistive magnetohydrodynamics (VRMHD) equations and our

hyperbolic approach is that the latter uses a much larger set of state variables (2 scalar fields, namely the mass density and the total energy density, + 3 components of the momentum density + 9 components of the non-symmetric distortion tensor + 3 components of the thermal impulse vector + 6 components of the electro-magnetic fields), that is a total number of 23 evolution equations. This obviously requires more memory and computational effort if compared with only 5 equations for the NSF equations or 8 equations for VRMHD. However, we can also list some benefits in utilizing first order hyperbolic models. As discussed in [42,89,90], one may point out the following computational advantages when using hyperbolic models over conventional parabolic models

- the key advantage of the SHTC model proposed in the present paper is its natural ability to describe moving *fluids* and *solids* in an electromagnetic field within the *same* PDE system and thus allows the simulation of magnetized fluids *and* solids within the *same* computer code, while implementations based on classical theories such as NSF and VRMHD only apply to fluids and are *not* able to describe the motion and deformation of elastic solids;
- a numerical method applied to first order hyperbolic PDEs can achieve higher order of accuracy than for high-order PDEs on the same discrete stencil; in particular, in first order hyperbolic models the same order of accuracy for the solution and the stresses and other fluxes is easily achieved, while in parabolic models the dissipative fluxes are based on the derivatives of the state vector, and thus in general one order of accuracy is lost if the stencil of the scheme is not properly extended;
- first order systems are less sensitive to the quality of computational grids and boundary singularities;
- no severe parabolic time step restriction $\Delta t \sim \Delta x^2$ arises for explicit discretizations of first order hyperbolic systems and therefore numerical schemes with an explicit time stepping can be used. This allows not only for a straightforward and efficient parallelization, but can even lead to *faster* simulations with the enlarged SHTC system compared to conventional parabolic models, in particular in the context of explicit discontinuous Galerkin finite element schemes, see the examples provided in [42];
- the possibility of an easy and filter-less visualization of complex flows with the help of the distortion tensor, see [42].

For recent work on hyperbolic reformulations of the steady viscous and resistive MHD equations and time dependent convection–diffusion equations based on standard Maxwell–Cattaneo relaxation, see the papers of Nishikawa et al. [100,101, 89,90,11] and Montecinos and Toro [95,94,135]. These approaches, however, were motivated by computational reasons, while our hyperbolic theory was motivated by the construction of a consistent physical theory first. In particular, the mentioned hyperbolic approaches are attributed to the Maxwell–Cattaneo-type models discussed in Section 1.3 because the gradients of the fields (stress, heat flux) are used as extra state variables, and thus such approaches may suffer from the same physical inconsistencies as discussed in Section 1.3. Models of a similar nature are also used in non-equilibrium gas dynamics. See the following section where we discuss other differences between this sort of models and our approach.

1.6. Beyond conventional continuum theories

After many discussions following the publication of paper I, the authors believe that it is necessary to stress that the unified hyperbolic theory proposed in [110,42] was never thought to be an *extension* of the conventional parabolic Navier–Stokes–Fourier (NSF) theory like it was intended in the Maxwell–Cattaneo approach. It should be rather considered as a completely independent model based on different principles. For example, the constitutive laws (Newton's law of viscosity and Fourier's law of heat conduction) of the NSF theory entirely rely on the *steady state assumption* by completely ignoring the history (even short) of how such a steady state was reached. Such a steady state assumption is not used in our hyperbolic theory, neither explicitly nor implicitly, and thus it should be regarded as a genuinely transient model. In fact, in order to use our model one may *not even know* about the existence of the famous transport laws of Newton and Fourier. Nevertheless, solutions corresponding to Newtonian flows and Fourier heat conduction are realizable in our theory in the long wave-length approximation (or in the stiff relaxation limit) as discussed above and was shown in [42], paper I, through a formal asymptotic expansion up to first order terms in the different relaxation times appearing in the model.

Therefore, one may consider the possibility that the parabolic NSF theory with its steady state assumption is just a particular realization of the more general hyperbolic model [110,42]. This also becomes transparent after recalling that our hyperbolic theory also includes solid mechanics (nonlinear elastic and elasto-plastic solids) as a particular case, see paper I. Clearly, the non-Newtonian liquids fall in between the Newtonian-like and solid-like behavior and hence can also be modeled with our approach via the dependence of the relaxation time on the state parameters. This is however the subject of an ongoing research.

Eventually, there is an apparent similarity between the extended structure (if compared with the Euler equations) of our hyperbolic model and the macroscopic models in non-equilibrium gas dynamics derived with the help of the method of moments [138] from the gas kinetic theory of Boltzmann. Nevertheless, on the mathematical side, there are more differences than similarities between these approaches, and a straightforward comparison of the solutions is not a trivial task. For example, it is not acceptable in the SHTC formalism that the fluxes serve as state variables, but only density-like quantities are admissible, while in the method of moments, the moments of the distribution function are constructed in a such a way that the macroscopic fields have the meaning of fluxes, such as stress tensor, heat flux, etc. Another remarkable difference is the fact that the method of moments serves as a method to derive macroscopic equations for gas flows solely, while

the application of our model is not restricted to gas dynamics only, but it includes elasto-plastic solids and liquids as well, which are not described by the kinetic gas theory of Boltzmann. Nevertheless, a detailed comparison of the approaches in the gas dynamics setting may lead to a better understanding and a further improvement of the theory and deserves a detailed investigation in the future. For now, we only note that both approaches give the same low-order terms in the expansion in the so-called Knudsen number (relaxation time in our case) corresponding to the NSF theory, while the higher order terms, as always, depend on the choice of the closure, which in our case corresponds to the choice of the scalar functions, the total energy potential (to be convex to guarantee the symmetric hyperbolicity) and the relaxation times.

1.7. Outline of the paper

The rest of the paper is structured as follows. In the first part, we concentrate on the mathematical principles of the SHTC formalism. In particular, Section 2 is dedicated to the departure point of the SHTC formalism, namely the Lagrangian system of master equations, while Section 3 contains the Eulerian formulation of the master system after the change of the Lagrangian variables into Eulerian ones. In Section 3.3, we then propose a total energy potential which serves as the closure of the governing equations. In Section 4, we summarize the Eulerian system of governing PDEs which shall be used later for the numerical simulation in Section 7. In Section 5, we demonstrate via a formal asymptotic analysis the relation of the proposed hyperbolic model to the ideal magnetohydrodynamics (MHD) and viscous and resistive magnetohydrodynamics (VRMHD) equations. Here, we also partially repeat the results of paper I for completeness. Section 6 briefly describes the family of ADER methods employed in this paper. Eventually, the proposed energy potential and the Eulerian system of governing PDEs are used in Section 7 where we give extensive numerical evidence of the applicability of the model to a wide range of electromagnetic flows. Some concluding remarks and an outlook to future work is given in Section 8.

In the rest of the paper we use the Einstein summation convention over repeated indices.

2. SHTC formalism and the master system

The hyperbolic dissipative theory discussed in this paper relies on the SHTC formalism. The development of the formalism started in 1961 after it was observed by Godunov [61,62] that some systems of conservation laws admitting an *extra conservation law* also admit an interesting parametrization

$$\frac{\partial M_{p_i}}{\partial t} + \frac{\partial N^j_{p_i}}{\partial y_j} = 0 \tag{3}$$

which allows to rewrite the governing equations in a *symmetric form*

$$M_{p_i p_k} \frac{\partial p_k}{\partial t} + N^j_{p_i p_k} \frac{\partial p_k}{\partial y_j} = 0, \tag{4}$$

where t is the time, y_j are the spatial coordinates, p_k is the vector of state variables, $M(p_i)$ and $N^j(p_i)$ are the scalar potentials of the state variables. Here and in the rest of the paper, a potential with the state variables in the subscript should be understood as the partial derivatives of the potential with respect to these state variables. Thus, for example, M_{p_k}, $N^j_{p_k}$, $M_{p_i p_k}$ and $N^j_{p_i p_k}$ in (3)–(4) should be understood as the first and second partial derivatives of the potentials M and N^j with respect to the state variables p_i, e.g. $M_{p_k} = \partial M / \partial p_k$, $M_{p_i p_k} = \partial^2 M / (\partial p_i \partial p_k)$, etc.

In this parametrization, the extra conservation law has always the following form

$$\frac{\partial (p_i M_{p_i} - M)}{\partial t} + \frac{\partial (p_i N^j_{p_i} - N^j)}{\partial y_j} = 0 \tag{5}$$

and, in fact, it is just a straightforward consequence of the governing equations (3) and can be obtained as a *linear combination* of these equations. Indeed, (5) can be obtained as a sum of the equations (3) multiplied by the corresponding factors p_i.

If the potential $M(p_i)$ is a strictly convex function of the state variables then the symmetric matrix $M_{p_i p_k}$ is positive definite and (4) becomes a *symmetric hyperbolic* system of equations [55].

Usually, the *generating potential* M has the meaning of the generalized pressure while its Legendre transformation $p_i M_{p_i} - M$ has the meaning of the total energy and thus, (5) is the total energy conservation law.[3] Hence, the observation of Godunov establishes the very important connection between the well-posedness of the equations of mathematical physics and thermodynamics.

[3] Note that the potentials N^j have no apparent physical meaning and play no role in the later developments of the SHTC formalism.

It was understood later on the example of the ideal MHD equations [63] that the original observation of Godunov [61] relates only to conservation laws written in the *Lagrangian* frame, which indeed admits a fully *conservative* formulation,[4] while the time evolution equations in the Eulerian frame have a more complicated structure, except for the compressible Euler equations of ideal fluids.

The structure of the Eulerian equations and its relation to the fully conservative structure of the equations in Lagrangian form was revealed in a series of papers by Godunov and Romenski [69,70,65,71,119,120,72]. In particular, in [65], based on the group representation theory [59], a rather general form of first order PDEs with the following properties was proposed:

- PDEs are invariant under rotations
- PDEs are compatible with an extra conservation law
- PDEs are generated by only one potential like M
- PDEs are symmetric hyperbolic
- PDEs are conservative and generated by invariant differential operators only, such as div, grad and curl.

One may naturally question how this class of PDEs, which shall be referred to as the *master system*, relates to the models that describe continuum mechanics and whether it is too restrictive to deal with dissipative processes such as viscous momentum transfer, heat transfer, resistive MHD, etc., typically described by second order parabolic equations. First, it is important to emphasize that invariance under orthogonal transformations and the existence of an extra conservation law, which is typically the total energy conservation, are compulsory requirements for continuum mechanics models. Second, as shown recently [110,42], there is no physical reason imposing that the dissipative transport processes such as viscous momentum transfer or heat conduction should be exclusively modeled by the second order parabolic diffusion theory, but they can also be very successfully modeled by a more general framework based on first order hyperbolic equations with relaxation source terms. Third, after analysis of a rather large number of particular examples of continuum models [69–71,119,120], it was shown that many models fall into the class of SHTC systems. Among them are the compressible Euler equations of ideal fluids, the ideal MHD equations, the equations of nonlinear elasto-plasticity, the electrodynamics of moving media, a model describing superfluid helium, the equations governing compressible multi-phase flows, elastic superconductors, and finally also the unified first order hyperbolic formulation for fluid and solid mechanics introduced in [110,42]. In this paper, we show that also the viscous and resistive MHD equations can be cast into the form of a first order SHTC system.

The starting point of the SHTC formalism is a sub-system of the Lagrangian conservation laws given in eqs. (1) of [65], which will be refereed to as the *master system* from now on. The final governing PDEs written in the Eulerian frame will then be the result of the following system of Lagrangian master equations:

$$\frac{\mathrm{d}M_{v_i}}{\mathrm{d}t} - \frac{\partial P_{ij}}{\partial y_j} = 0, \tag{6a}$$

$$\frac{\mathrm{d}M_{P_{ij}}}{\mathrm{d}t} - \frac{\partial v_i}{\partial y_j} = 0, \tag{6b}$$

$$\frac{\mathrm{d}M_{d_i}}{\mathrm{d}t} - \varepsilon_{ijk}\frac{\partial b_k}{\partial y_j} = 0, \tag{6c}$$

$$\frac{\mathrm{d}M_{b_i}}{\mathrm{d}t} + \varepsilon_{ijk}\frac{\partial d_k}{\partial y_j} = 0. \tag{6d}$$

Here, v_i is the velocity of the matter, P_{ij} is the stress tensor, while d_i and b_i are some vectors describing the electric and magnetic fields, respectively.

In contrast to the classical parabolic theory of dissipative processes, the governing equations in our approach are all *first order* hyperbolic PDEs and the dissipative processes will *not* be modeled by *differential terms*, but *exclusively* via *algebraic relaxation source terms*, which will be specified later in the Eulerian case. This has the *important consequence* that the structure of the differential terms and the type of the PDE is the *same* in both, the dissipative as well as in the non-dissipative case. We recall, that if the dissipation is excluded in the classical second order parabolic diffusion theory, this then changes not only the structure of the PDEs, but also their *type*.

Because of this fact, within the SHTC formalism we can study the structure of the governing equations by restricting our considerations to the non-dissipative case only. We also note that if the dissipation source terms are switched off, then the model describes an elastic medium, see [110,42].

[4] In this paper, under fully conservative form of the equations we understand not only the divergence form of the equations, i.e. generated by the divergence differential operator, but rather that there are no space derivatives multiplied by unknown functions, while algebraic production source terms can be present.

2.1. Variational nature of the field equations in a moving elastic medium

It is well known that many equations of mathematical physics can be derived as the Euler–Lagrange equations obtained by the minimization of a Lagrangian. As an example, one can consider the nonlinear elasticity equations in Lagrangian coordinates [73]. The classical Maxwell equations of electrodynamics can also be derived by the minimization of a Lagrangian with the use of the gauge theory [58]. It turns out that the coupling of these two physical objects in a single Lagrangian gives us a straightforward way to derive the equations for the electromagnetic field in a moving medium. We start by introducing two vector potentials and a scalar potential:

$$\boldsymbol{x} = [x_i(t, \boldsymbol{y})], \quad \boldsymbol{a} = [a_i(t, \boldsymbol{y})], \quad \varphi(t, \boldsymbol{y}), \tag{7}$$

so that

$$\hat{v}_i = \frac{\partial x_i}{\partial t}, \quad \hat{F}_{ij} = \frac{\partial x_i}{\partial y_j}, \tag{8}$$

$$\hat{e}_i = -\frac{\partial a_i}{\partial t} - \frac{\partial \varphi}{\partial y_i}, \quad \hat{h}_i = \varepsilon_{ijk}\frac{\partial a_k}{\partial y_j}, \tag{9}$$

Here, t is time, $\boldsymbol{y} = [y_i]$ and $\boldsymbol{x} = [x_i]$ are the Lagrangian and Eulerian spatial coordinates respectively, while $\boldsymbol{a}$ and φ are the conventional electromagnetic potentials.

Then, we define the action integral

$$\mathcal{L} = \int \Lambda d\boldsymbol{y} dt, \tag{10}$$

where $\Lambda = \Lambda(\hat{v}_i, \hat{F}_{ij}, \hat{e}_i, \hat{h}_i)$ is the Lagrangian.

First variation of $\mathcal{L}$ gives us the Euler–Lagrange equations

$$\frac{\partial \Lambda_{\hat{v}_i}}{\partial t} + \frac{\partial \Lambda_{\hat{F}_{ij}}}{\partial y_j} = 0, \tag{11}$$

$$\frac{\partial \Lambda_{\hat{e}_i}}{\partial t} + \varepsilon_{ijk}\frac{\partial \Lambda_{\hat{h}_k}}{\partial y_j} = 0, \tag{12}$$

$$\frac{\partial \Lambda_{\hat{e}_j}}{\partial y_j} = 0. \tag{13}$$

To this system, the following compatibility constraints should be added (they are trivial consequences of the definitions (8) and (9))

$$\frac{\partial \hat{F}_{ij}}{\partial t} - \frac{\partial \hat{v}_i}{\partial y_j} = 0\,, \quad \frac{\partial \hat{F}_{ij}}{\partial y_k} - \frac{\partial \hat{F}_{ik}}{\partial y_j} = 0\,, \tag{14}$$

$$\frac{\partial \hat{h}_i}{\partial t} + \varepsilon_{ijk}\frac{\partial \hat{e}_k}{\partial y_j} = 0\,, \quad \frac{\partial \hat{h}_j}{\partial y_j} = 0\,. \tag{15}$$

In order to rewrite equations (11)–(15) in the form of system (6), let us introduce the potential U as a partial Legendre transformation of the Lagrangian Λ

$$\begin{aligned} \mathrm{d}U = \mathrm{d}(\hat{v}_i\Lambda_{\hat{v}_i} + \hat{e}_i\Lambda_{\hat{e}_i} - \Lambda) = \hat{v}_i\mathrm{d}\Lambda_{\hat{v}_i} + \hat{e}_i\mathrm{d}\Lambda_{\hat{e}_i} - \Lambda_{\hat{F}_{ij}}\mathrm{d}\hat{F}_{ij} - \Lambda_{\hat{h}_i}\mathrm{d}\hat{h}_i = \\ \hat{v}_i\mathrm{d}\Lambda_{\hat{v}_i} + \hat{e}_i\mathrm{d}\Lambda_{\hat{e}_i} + \Lambda_{\hat{F}_{ij}}\mathrm{d}(-\hat{F}_{ij}) + \Lambda_{\hat{h}_i}\mathrm{d}(-\hat{h}_i). \end{aligned} \tag{16}$$

Hence, denoting $m_i = \Lambda_{\hat{v}_i}$, $e_i = \Lambda_{\hat{e}_i}$, $F_{ij} = -\hat{F}_{ij}$, $h_i = -\hat{h}_i$, we get the thermodynamic identity

$$\mathrm{d}U = U_{m_i}\mathrm{d}m_i + U_{F_{ij}}\mathrm{d}F_{ij} + U_{e_i}\mathrm{d}e_i + U_{h_i}\mathrm{d}h_i.$$

Eventually, in terms of the variables

$$\mathbf{q} = (m_i, F_{ij}, e_i, h_i) \tag{17}$$

and the potential $U = U(\mathbf{q})$, equations (11), (12), $(14)_1$ and $(15)_1$ become

$$\frac{\mathrm{d}m_i}{\mathrm{d}t} - \frac{\partial U_{F_{ij}}}{\partial y_j} = 0, \tag{18a}$$

$$\frac{\mathrm{d}F_{ij}}{\mathrm{d}t} - \frac{\partial U_{m_i}}{\partial y_j} = 0, \tag{18b}$$

$$\frac{\mathrm{d}e_i}{\mathrm{d}t} - \varepsilon_{ijk}\frac{\partial U_{h_k}}{\partial y_j} = 0, \tag{18c}$$

$$\frac{\mathrm{d}h_i}{\mathrm{d}t} + \varepsilon_{ijk}\frac{\partial U_{e_k}}{\partial y_j} = 0, \tag{18d}$$

which should be supplemented by stationary constraints (13), $(14)_2$ and $(15)_2$ which now read as

$$\frac{\partial F_{ij}}{\partial y_k} - \frac{\partial F_{ik}}{\partial y_j} = 0, \qquad \frac{\partial e_i}{\partial y_i} = 0, \qquad \frac{\partial h_i}{\partial y_i} = 0. \tag{19}$$

System (18) is, in fact, identical to (6). In order to see this, one needs to introduce fluxes as new (*conjugate*) state variables

$$\mathbf{p} = (U_{m_i}, U_{F_{ij}}, U_{e_i}, U_{h_i}), \tag{20}$$

which we denote as

$$\begin{aligned} v_i &= U_{m_i}, \;\; P_{ij} = U_{F_{ij}}, \\ d_i &= U_{e_i}, \quad b_i = U_{h_i}, \end{aligned} \tag{21}$$

and a new potential $M(\mathbf{p})$ as a Legendre transform of $U(\mathbf{q})$, i.e.

$$M = m_i U_{m_i} + F_{ij} U_{F_{ij}} + e_i U_{e_i} + h_i U_{h_i} - U, \tag{22}$$

or briefly

$$M(\mathbf{p}) = \mathbf{q}\cdot\mathbf{p} - U(\mathbf{q}). \tag{23}$$

After that, system (18) transforms exactly to (6), while the constraints (19) read as

$$\frac{\partial M_{P_{ij}}}{\partial y_k} - \frac{\partial M_{P_{ik}}}{\partial y_j} = 0, \qquad \frac{\partial M_{d_i}}{\partial y_i} = 0, \qquad \frac{\partial M_{b_i}}{\partial y_i} = 0. \tag{24}$$

One may clearly note a similarity between the equations (6c)–(6d) (or (18c)–(18d)) and the Maxwell equations. However, because no assumptions about the Lagrangian Λ, and thus, about the potentials $U(\mathbf{q})$ and $M(\mathbf{p})$ have been made yet, these equations should be considered as a *nonlinear generalization* of the Maxwell equations, e.g. see [28,126,1].

We note that equations (6a)–(6b) and (6c)–(6d) (or (18a)–(18b) and (18c)–(18d)) are not independent as it may seem. They are coupled via the dependence of the potential $M(\mathbf{p})$ (or $U(\mathbf{q})$) on all the state variables (17). This coupling will emerge in a more transparent way when we shall consider these equations in the Eulerian frame in Section 3.

2.2. Properties of the master system

2.2.1. Energy conservation

A central role in the system formulation is played by the thermodynamic potential

$$U = U(m_i, F_{ij}, e_i, h_i), \tag{25}$$

or its dual

$$M = M(v_i, P_{ij}, d_i, b_i) \tag{26}$$

as one of them generates the fluxes in (18), while the other generates the density fields in (6). The potential U typically has the meaning of the total energy density of the system, while M has the meaning of a pressure.

In addition, solutions of the system (18) satisfy an extra conservation law

$$\frac{\mathrm{d}U}{\mathrm{d}t} - \frac{\partial}{\partial y_j}\left(U_{m_i}U_{F_{ij}} + \varepsilon_{ijk}U_{e_i}U_{h_k}\right) = 0 \tag{27}$$

which should be interpreted as the total energy conservation. In terms of the dual potential M and dual state variables (21) it reads as

$$\frac{\mathrm{d}}{\mathrm{d}t}\left(v_i M_{v_i} + P_{ij}M_{P_{ij}} + d_i M_{d_i} + b_i M_{b_i} - M\right) - \frac{\partial}{\partial y_j}\left(v_i P_{ij} + \varepsilon_{ijk} d_i b_k\right) = 0. \tag{28}$$

The energy conservation law (27) is not independent but a consequence of all the equations (18). Indeed, if we multiply each equation in (18) by a corresponding factor and sum up the result, we obtain equation (27) identically:

$$U_{m_i} \cdot (18a) + U_{F_{ij}} \cdot (18b) + U_{e_i} \cdot (18c) + U_{h_i} \cdot (18d) \equiv (27). \tag{29}$$

The same is true for (28) and (6).

2.2.2. Possible interpretation of the state variables

Usually, the derivation of a model begins with the choice of state variables. In the context of classical hydrodynamics, the answer is universal. The state variables are the classical hydrodynamic fields such as mass, momentum, entropy, or total energy. In any case which is beyond the inviscid hydrodynamics settings, the choice of extra state variables is not universal. In the SHTC formalism, we however follow a different strategy, which consists of two stages. In the first stage, the governing equations are formulated before any choice of extra state variables has been made. The structure of the governing PDEs is a consequence of the five fundamental requirements formulated earlier in this section. The physical meaning of the state variables becomes clear at the second stage, when we try to compare a solution to the model with specific experimental observations. At this stage, we simultaneously clarify the meaning of the state variables and look for an appropriate energy potential which can be seen also as the choice of the constitutive relations in the classical continuum mechanics. For the proposed model, this strategy is realized in Section 3.3.

Thus, in this section, we give only approximate interpretations of the state variables while their precise meanings will be given in Section 3.3. As stated above, the space variables $\boldsymbol{y} = [y_i]$ can be treated as the Lagrangian coordinates which are connected to the Eulerian coordinates $\boldsymbol{x}(t) = [x_i(t)]$ measured relative to a laboratory frame by the equality $y_i = x_i(0)$. It is also implied that $v_i = \frac{\mathrm{d}x_i}{\mathrm{d}t}$ in (6) is the velocity of the matter relative to the laboratory frame, while $m_i = M_{v_i}$ in (18) has a meaning of a generalized momentum density which may include contributions from other physical processes and in general depends on the specification of the potential M, or U. As it will be shown in Section 3.3, m_i couples the material momentum and *electromagnetic momentum* (Poynting vector). The tensorial variable $F_{ij} = \frac{\partial x_i}{\partial y_j}$ is the deformation gradient, e_i and h_i are the electric and magnetic fields, respectively. However, the exact meaning of the fields e_i and h_i will be clarified later in Section 3 when we shall distinguish among different reference frames.

2.2.3. Symmetric hyperbolicity

System (6) can be rewritten in a symmetric quasilinear from

$$\mathbb{M}\frac{\partial \mathbf{p}}{\partial t} + \mathbb{N}_j \frac{\partial \mathbf{p}}{\partial y_j} = 0, \tag{30}$$

with the symmetric matrix $\mathbb{M}(\mathbf{p}) = M_{\mathbf{pp}} = [\partial^2 M / \partial p_i \partial p_j]$ and *constant* symmetric matrices $\mathbb{N}_j$ consisting only of 1, −1 and zeros. Moreover, system (6) is symmetric hyperbolic if $M(\mathbf{p})$ is convex. In other words, the Cauchy problem for (6) (as well as for (18)) is automatically well posed locally in time for smooth initial data [29]. We recall that the convexity of $M(\mathbf{p})$ is equivalent to the convexity of $U(\mathbf{q})$ due to the properties of the Legendre transformation.

2.2.4. $\mathbf{q}$ *and* $\mathbf{p}$*-type state variables*

We emphasize the very distinct nature of the variables $\mathbf{q}$ and $\mathbf{p}$. The variables $\mathbf{q}$ appear in the time derivative and have the meaning of densities (volume averaged quantities). We thus shall refer to components of $\mathbf{q}$ as *density fields*. On the other hand, the variables $\mathbf{p}$ appear as fluxes in the master system (18) (or (6)), and thus will be referred to as *flux fields* (surface defined quantities), see also the discussion in [109]. In the SHTC formalism, the potential $M(\mathbf{p})$ (the generalized pressure) and the flux fields $\mathbf{p}$ are conjugate quantities to the potential $U(\mathbf{q})$ (total energy density) and the density fields $\mathbf{q}$, i.e. they are connected by the following identities

$$p_i = U_{q_i}, \qquad q_i = M_{p_i} \tag{31}$$

and

$$M = q_i U_{q_i} - U, \qquad U = p_i M_{p_i} - M. \tag{32}$$

Thus, it follows from (31) that if we want the nonlinear change of variables (31) to be a one-to-one map, one should require that the potentials $U(\mathbf{q})$ and $M(\mathbf{p})$ be convex functions because

$$M_{\mathbf{pp}} = \frac{\partial \mathbf{q}}{\partial \mathbf{p}} = \left[\frac{\partial \mathbf{p}}{\partial \mathbf{q}}\right]^{-1} = U_{\mathbf{qq}}. \tag{33}$$

2.2.5. Stationary constraints

Solutions to system (18) satisfy some stationary conservation laws that are compatible with system (18) and conditioned by the structure of the flux terms:

$$\frac{\partial F_{ij}}{\partial y_k} - \frac{\partial F_{ik}}{\partial y_j} = 0, \quad \frac{\partial e_k}{\partial y_k} = 0, \quad \frac{\partial h_k}{\partial y_k} = 0. \tag{34}$$

These stationary laws hold for every $t > 0$ if they are valid at $t = 0$, and thus should be considered as the constraints on the initial data. Indeed, applying the divergence operator, for instance, to equations (18d) we obtain

$$\frac{\partial}{\partial t}\left(\frac{\partial h_k}{\partial y_k}\right) = 0, \tag{35}$$

which yields the third equation in (34) if it was fulfilled at the initial time. The other laws can be obtained in a similar way. As we shall discuss later on the example of the Eulerian equations, the situation is rather different in the Eulerian setting, and the stationary constraints like (34) are not separate but an intrinsic part of the structure of the governing equations written in the Eulerian frame.

2.2.6. Complimentary structure

We also note a *complimentary* structure of equations (18) and (6), i.e. the PDEs are split into pairs. In each pair, a variable appearing in the time derivative, say u_i in (18a), then appears in the flux of the complimentary equation as U_{u_i} in (18b). Thus, u_i and F_{ij} are complimentary variables, as well as e_i and h_i. This means, that a physical process should be always presented at least by two state variables and hence by two PDEs in the SHTC formalism. One may note a close relation of such a complimentary structure of the SHTC formalism and the odd and even parity of the state variables with respect to the time-reversal transformation in the context of the GENERIC (general equation of nonequilibrium reversible–irreversible coupling) formalism discussed in [106].

3. Master system in the Eulerian frame

In this section, we formulate a system of governing equations describing motion of a heat conducting deformable medium (fluid or solid) in the electromagnetic field in the Eulerian frame. This system is obtained as a direct consequence of the master system (18) by means of the Lagrange-to-Euler change of variables: $\boldsymbol{y} \to \boldsymbol{x}$. This transformation is a nontrivial task, and the details are given in Appendix B for the electromagnetic field equations and in Appendix C for the momentum conservation law while the details about the derivation of the other equations can be found in the Appendix in [109] or in [65]. We give the Eulerian formulations using both density fields $\mathbf{q}$ and flux fields $\mathbf{p}$. As we shall see, the Eulerian equations do not have such a simple structure as the Lagrangian equations. Nevertheless, we stress that none of the differential terms was prescribed "*by hand*", but all of them are a direct consequence of the $\boldsymbol{y} \to \boldsymbol{x}$ variable transformation solely.

3.1. $(\mathcal{E}, \mathbf{q})$-formulation

The main system of governing equations studied in this paper is formulated in terms of $\mathbf{q}$-type state variables (density fields, see Section 2.2.4)

$$\mathbf{q} = (\rho, \mathbf{m}, \boldsymbol{A}, \mathbf{e}, \mathbf{h}, \mathbf{w}, \sigma), \tag{36}$$

and the total energy density $\mathcal{E}(\mathbf{q}) = w^{-1}U$, where U is the Lagrangian total energy density introduced in Section 2, ρ is the mass density, $\sigma = \rho s$ is the entropy density, s is the specific entropy, $\mathbf{m} = [m_i]$ is a generalized momentum density which couples the ordinary matter momentum density, $\rho\mathbf{v}$, with the electromagnetic momentum density, i.e. the Poynting vector. The exact expression for $\mathbf{m}$ will be given later. Matrix $\boldsymbol{A} = [A_{ik}]$ is the distortion field[5] (see Paper I), $\mathbf{e} = [e_i]$ and $\mathbf{h} = [h_i]$ are the vector fields which relate to the electro-magnetic fields and will be specified later, $\mathbf{w} = \rho\mathbf{J}$ is the thermal impulse density (see Paper I), which can be interpreted as an average momentum density of the heat carriers. The velocity of the medium, $\mathbf{v}$, is not a primary state variable and should be computed from the generalized momentum $\mathbf{m}$, but also, according to the SHTC formalism, the velocity and the generalized momentum relate to each other as $v_i = \mathcal{E}_{m_i}$ (see (21) and the discussion below). In the Eulerian coordinates x_k, the system of governing equations reads as

$$\frac{\partial \rho}{\partial t} + \frac{\partial (\rho v_k)}{\partial x_k} = 0, \tag{37a}$$

$$\frac{\partial m_i}{\partial t} + \frac{\partial}{\partial x_k}\left(m_i v_k + \delta_{ik}\left(\rho\mathcal{E}_\rho + \sigma\mathcal{E}_\sigma + m_l\mathcal{E}_{m_l} + e_l\mathcal{E}_{e_l} + h_l\mathcal{E}_{h_l} - \mathcal{E}\right) + A_{li}\mathcal{E}_{A_{lk}} - e_k\mathcal{E}_{e_i} - h_k\mathcal{E}_{h_i}\right) = 0, \tag{37b}$$

$$\frac{\partial A_{ik}}{\partial t} + \frac{\partial (A_{il} v_l)}{\partial x_k} + v_j\left(\frac{\partial A_{ik}}{\partial x_j} - \frac{\partial A_{ij}}{\partial x_k}\right) = -\frac{\mathcal{E}_{A_{ik}}}{\rho\,\theta_1(\tau_1)}, \tag{37c}$$

[5] Rigorously speaking, $\boldsymbol{A}$ is not a tensor field of rank 2, since it transforms like a tensor of rank 1 with respect to a change of coordinates. Thus, we shall avoid to call it the distortion tensor, but instead call it simply the distortion field.

$$\frac{\partial e_i}{\partial t} + \frac{\partial \left(e_i v_k - v_i e_k - \varepsilon_{ikl} \mathcal{E}_{h_l} \right)}{\partial x_k} + v_i \frac{\partial e_k}{\partial x_k} = - \frac{\mathcal{E}_{e_i}}{\eta}, \tag{37d}$$

$$\frac{\partial h_i}{\partial t} + \frac{\partial \left(h_i v_k - v_i h_k + \varepsilon_{ikl} \mathcal{E}_{e_l} \right)}{\partial x_k} + v_i \frac{\partial h_k}{\partial x_k} = 0, \tag{37e}$$

$$\frac{\partial w_i}{\partial t} + \frac{\partial \left(w_i v_k + \mathcal{E}_\sigma \delta_{ik} \right)}{\partial x_k} = - \frac{\rho \, \mathcal{E}_{w_i}}{\theta_2(\tau_2)}, \tag{37f}$$

$$\frac{\partial \sigma}{\partial t} + \frac{\partial \left(\sigma v_k + \mathcal{E}_{w_k} \right)}{\partial x_k} = \frac{1}{\mathcal{E}_\sigma} \left(\frac{1}{\rho \theta_1} \mathcal{E}_{A_{ik}} \mathcal{E}_{A_{ik}} + \frac{\rho}{\theta_2} \mathcal{E}_{w_i} \mathcal{E}_{w_i} + \frac{1}{\eta} \mathcal{E}_{e_i} \mathcal{E}_{e_i} \right) \geq 0. \tag{37g}$$

The energy conservation law

$$\frac{\partial \mathcal{E}}{\partial t} + \frac{\partial}{\partial x_k} \Big(v_k \mathcal{E} + v_i \left[\left(\rho \mathcal{E}_\rho + \sigma \mathcal{E}_\sigma + m_l \mathcal{E}_{m_l} + e_l \mathcal{E}_{e_l} + h_l \mathcal{E}_{h_l} - \mathcal{E} \right) \delta_{ik} + A_{li} \mathcal{E}_{A_{lk}} - e_k \mathcal{E}_{e_i} - h_k \mathcal{E}_{h_i} \right] + \varepsilon_{ijk} \mathcal{E}_{e_i} \mathcal{E}_{h_j} + \mathcal{E}_\sigma \mathcal{E}_{w_k} \Big) = 0 \tag{38}$$

is a consequence of equations (37), i.e. it can be obtained by means of the summation rule (29). We emphasize that in the numerical computations shown later in Section 4, we solve the energy equation (38) instead of the entropy equation (37g), but from the point of view of the model formulation, the entropy should be considered among the vector of unknowns because it is the complementary variable to the thermal impulse $\mathbf{w} = \rho \mathbf{J}$, see the remark in Section 2.2.6 and Paper I.

All equations in system (37) except the continuity equation[6] (37a) and the heat conduction equation[7] (37f)–(37g) originate from the Lagrangian equations with the structure (18). The momentum equation and the distortion equation are derived from the pair (18a)–(18b), the electromagnetic field equations (37d)–(37e) are derived from the pair (18c)–(18d).

The energy conservation law (38) is the consequence of equations (37), since it can be obtained as a linear combination of all equations (37) with coefficients introduced in the following section. As in the Lagrangian frame, these coefficients (multipliers) are the thermodynamically conjugate state variables and have the meaning of fluxes.

As discussed in [110,42], the distortion field $\boldsymbol{A}$ describes deformability and orientation of the continuum particles which we assume to have a finite (non-zero) length scale. Macroscopic flow is naturally considered as the process of continuum particles rearrangements in the SHTC model. Because of the rearrangements of particles, the field $\boldsymbol{A}$ is not integrable in the sense that it does not relate Eulerian and Lagrangian coordinates of the continuum. As a result, the field $\boldsymbol{A}$ is local and it relates to the deformation gradient $\boldsymbol{F}$ introduced in Section 2.1 only via

$$\det(\boldsymbol{F}) = 1 / \det(\boldsymbol{A}). \tag{39}$$

However, if we consider a particular case of system (37) when the dissipation term in the right hand side of (37c) is absent, which corresponds to an elastic solid (e.g. see the last numerical example in Paper I), then we have that $\boldsymbol{A} = \boldsymbol{F}^{-1}$.

For simplicity, we use the same notations m_i, e_i and h_i for the generalized momentum, electric and magnetic fields in both the Lagrangian and the Eulerian framework. However, these fields are different, see Appendix B. For example, if we denote by $\mathbf{m}_L$, $\mathbf{e}_L$ and $\mathbf{h}_L$ the Lagrangian fields, i.e. exactly those fields which are used in equations (18a), (18c) and (18d), then they are related to $\mathbf{m}$, $\mathbf{e}$ and $\mathbf{h}$ appearing in the Eulerian equations (37b), (37d) and (37e) as

$$\mathbf{m}_L = w \, \mathbf{m}, \quad \mathbf{e}_L = w \boldsymbol{F}^{-1} \mathbf{e}, \quad \mathbf{h}_L = w \boldsymbol{F}^{-1} \mathbf{h}, \tag{40}$$

where $w = \det(\boldsymbol{F}) = 1 / \det(\boldsymbol{A})$, and $\boldsymbol{F}$ is the deformation gradient introduced in Section 2.1. Subsequently, the Lagrangian total energy density U relates to the Eulerian total energy density $\mathcal{E}$ as

$$w^{-1} U(\mathbf{m}_L, \boldsymbol{F}, \mathbf{e}_L, \mathbf{h}_L) = w^{-1} U(w \, \mathbf{m}, \boldsymbol{F}, w \boldsymbol{F}^{-1} \mathbf{e}, w \boldsymbol{F}^{-1} \mathbf{h}) = \mathcal{E}(\rho, \mathbf{m}, \boldsymbol{F}, \mathbf{e}, \mathbf{h}). \tag{41}$$

Here, for brevity, we omit other state variables. For example, if we denote by $\boldsymbol{\Sigma} = [\Sigma_{ij}]$ all the terms in the momentum flux (37b) except the advective term $m_i v_k$, it can be shown (e.g. see [65] or Appendix in [109]) that, after the Lagrange-to-Euler transformation, the Lagrangian momentum flux $U_{F_{ij}}$, see (18a), transforms to the Eulerian momentum flux $\Sigma_{ik} = \rho F_{kj} U_{F_{ij}}$ which in turn, because of the change of the state variables like (40), expands as

$$\Sigma_{ik} = -\delta_{ik} P - A_{li} \mathcal{E}_{A_{lk}} + e_k \mathcal{E}_{e_i} + h_k \mathcal{E}_{h_i}, \tag{42}$$

where the scalar

[6] The continuity equation is, in fact, a consequence of the distortion equation (37c), e.g. see [72,109], but it is convenient to consider density as an independent state variable with the compatibility constraint $\rho = \rho_0 \det(\boldsymbol{A})$.

[7] A different form of the hyperbolic heat conduction is possible, see system (38) in [119], which is fully compatible with the SHTC formalism in the sense that its Lagrangian equations belong to the master system [65]. However, both forms are consistent in the Fourier approximation and because we do not consider non-Fourier heat conduction we follow the hyperbolic heat conduction formulation from Paper I in this study. The detailed comparison of the heat conduction (37f)–(37g) and [119] is the subject of an ongoing research and will be presented somewhere else.

$$P = \rho \mathcal{E}_\rho + m_l \mathcal{E}_{m_l} + e_l \mathcal{E}_{e_l} + h_l \mathcal{E}_{h_l} - \mathcal{E} \tag{43}$$

is the *generalized pressure* which includes the hydrodynamic pressure and electromagnetic pressure. Nevertheless, P is not a *total pressure*[8] in the media given by the trace Σ_{ii} of the total stress tensor $\mathbf{\Sigma} = [\Sigma_{ik}]$ and the rest of the terms in (42) may also contribute to the total pressure Σ_{ii}.

In (42), we also use that $\partial w / \partial F_{ij} = w F^{-1}_{ji}$, $\partial F^{-1}_{jk} / \partial F_{il} = -F^{-1}_{ji} F^{-1}_{lk}$ and that $\rho = \rho_0 w^{-1}$, where ρ_0 is the reference mass density and F^{-1}_{ij} are the entries of the inverse deformation gradient $\boldsymbol{F}^{-1}$ (should not be confused with $1/F_{ij}$). It is important to emphasize that the *structure* of (42) does not depend on the specification of the total energy, but it is only conditioned by the structure of the governing equations.

Note that strictly speaking it is not correct to call $\mathbf{\Sigma}$ the stress tensor because, classically, by the stress tensor the non-advective flux of the *matter momentum* conservation law is understood, while equation (37b) is the *conservation law* for the *matter-field* momentum $\mathbf{m}$. Nevertheless, for brevity, $\mathbf{\Sigma}$ shall be referred to as the stress tensor in the rest of the paper. Recall that the matter momentum $\rho \mathbf{v}$ is not a conservative quantity in the case of a medium moving in an electromagnetic field. In general, the question of definition of the force acting on a matter moving in an electromagnetic field seems to have no universally accepted solution and several forms of the stress tensor are known [51,88,34]. It is thus necessary to emphasize that the form of the momentum flux (37b), quite abstract yet, is fully determined by the structure of the fluxes of the entire system (37) and, at this moment, it does not depend on the physical settings. The only remaining degree of freedom to fulfill experimental observations is to specify the total energy potential $\mathcal{E}$ and define a proper meaning of the state variables which then completely determine the force acting on the matter moving in an electromagnetic field. An example of such a potential and state variables will be given in Section 3.3.

We now make a very important remark about the divergence terms, $\frac{\partial e_k}{\partial x_k}$ and $\frac{\partial h_k}{\partial x_k}$, in equations (37d) and (37e) as they have a clear physical meaning of electric and magnetic (hypothetical though) charge, respectively. It is necessary to emphasize that these terms are not added by hand, but they emerge during the Lagrange-to-Euler change of variables, see Appendix B. Moreover, as can be checked by taking the divergence of Eqs. (37d) and (37e), the following formal relations hold

$$\frac{\partial R}{\partial t} + \frac{\partial (v_i R + \mathcal{J}_i)}{\partial x_i} = 0, \qquad \frac{\partial Q}{\partial t} + \frac{\partial (v_i Q + K_i)}{\partial x_i} = 0, \tag{44}$$

where $R = \frac{\partial e_i}{\partial x_i}$ and $\mathcal{J}_i = \frac{1}{\eta} E_{e_i}$ are the volume electric charge and the electric current, while $Q = \frac{\partial h_i}{\partial x_i}$ and $K_i \equiv 0$ are, at least formally, the analogous magnetic charge and magnetic current. Because it is assumed that $K_i \equiv 0$, it follows from $(44)_2$ that $Q = \partial h_i / \partial x_i \equiv 0$ if it was so at the initial moment of time. Nevertheless, we stress that the term $\partial h_i / \partial x_i$ should not be dropped out from the equation (37e) because, first, this would destroy the Galilean invariance of the system[9] and, secondly, such a system will be not compatible with the energy conservation.

3.2. $(L, \mathbf{p})$-formulation and symmetric hyperbolicity

In the previous section, the governing equations were formulated in terms of the state variables $\mathbf{q}$ and the total energy potential $\mathcal{E}(\mathbf{q})$. In this section, we also provide another, dual, formulation in terms of $\mathbf{p}$-type state variables (flux fields) and a potential L whose physical meaning is, in fact, identical to the generalized pressure (43). This formulation is not used for the numerical solution, but allows to emphasize an exceptional role of the generating potentials L and $\mathcal{E}$ in our formalism.

If we introduce the new vector of state variables

$$\mathbf{p} = (r, v_i, \alpha_{ik}, d_i, b_i, \eta_k, T) \tag{45}$$

as the following partial derivatives of the total energy density $\mathcal{E} = \rho E$ with respect to the conservative state variables $\mathbf{q}$, where

$$r = \mathcal{E}_\rho, \qquad v_i = \mathcal{E}_{m_i}, \qquad \alpha_{ik} = \mathcal{E}_{A_{ik}}, \qquad d_i = \mathcal{E}_{e_i}, \qquad b_i = \mathcal{E}_{h_i}, \qquad \eta_k = \mathcal{E}_{w_k}, \qquad T = \mathcal{E}_\sigma,$$

and a new potential $L(\mathbf{p}) = \mathbf{q} \cdot \mathbf{p} - \mathcal{E} = r\rho + v_i m_i + \alpha_{ij} A_{ik} + d_i e_i + b_i h_i + \eta_i w_i - \mathcal{E}$ as the Legendre transformation of $\mathcal{E}$ then system (37) can be rewritten as (see details in [72,119,120,109])

$$\frac{\partial L_r}{\partial t} + \frac{\partial [(v_k L)_r]}{\partial x_k} = 0, \tag{46a}$$

$$\frac{\partial L_{v_i}}{\partial t} + \frac{\partial}{\partial x_k} \left[(v_k L)_{v_i} + \alpha_{mk} L_{\alpha_{mi}} - \delta_{ik} \alpha_{mn} L_{\alpha_{mn}} - d_i L_{d_k} - b_i L_{b_k} \right] = 0, \tag{46b}$$

[8] We emphasize, however, that the definition of the pressure plays no role in the model formulation and introduced merely for convenience.

[9] One may show that if the terms such as $\partial h_i / \partial x_i$ are dropped out from the system than a non-physical characteristic appears with a 0 velocity instead of $v \pm c$ which apparently violates the Galilean invariance [112]. Here, v is the velocity of the media and c is some wave propagation speed.

$$\frac{\partial L_{\alpha_{ik}}}{\partial t} + \frac{\partial [(v_m L)_{\alpha_{im}}]}{\partial x_k} + \varepsilon_{klj}\varepsilon_{lmn} v_j \frac{\partial L_{\alpha_{in}}}{\partial x_m} = -\frac{1}{\rho\theta_1}\alpha_{ik}, \tag{46c}$$

$$\frac{\partial L_{d_i}}{\partial t} + \frac{\partial [(v_k L)_{d_i} - v_i L_{d_k} - \varepsilon_{ikl} b_l]}{\partial x_k} + v_i \frac{\partial L_{d_k}}{\partial x_k} = -\frac{1}{\eta} d_i, \tag{46d}$$

$$\frac{\partial L_{b_i}}{\partial t} + \frac{\partial [(v_k L)_{b_i} - v_i L_{b_k} + \varepsilon_{ikl} d_l]}{\partial x_k} + v_i \frac{\partial L_{b_k}}{\partial x_k} = 0, \tag{46e}$$

$$\frac{\partial L_{\eta_i}}{\partial t} + \frac{\partial [(v_k L)_{\eta_i} + \delta_{ik} T]}{\partial x_k} = -\frac{\rho}{\theta_2}\eta_i, \tag{46f}$$

$$\frac{\partial L_T}{\partial t} + \frac{\partial [(v_k L)_T + \eta_k]}{\partial x_k} = \frac{1}{T}\left(\frac{1}{\rho\theta_1}\alpha_{ik}\alpha_{ik} + \frac{\rho}{\theta_2}\eta_i\eta_i + \frac{1}{\eta} d_i d_i\right). \tag{46g}$$

In terms of the potential L, the symmetric Cauchy stress tensor Σ_{ik} reads

$$\Sigma_{ik} = -\delta_{ik}\left(L - \alpha_{mn} L_{\alpha_{mn}}\right) - \alpha_{mk} L_{\alpha_{mi}} + d_i L_{d_k} + b_i L_{b_k}. \tag{47}$$

As in the Lagrangian framework, the parametrization of the governing equations in terms of the flux fields $\mathbf{p}$ and generating potential $L(\mathbf{p})$ allows to rewrite the system in a symmetric quasilinear form. Moreover, if L is a convex potential, then the system (46) is *symmetric hyperbolic*, since it can be written as

$$\boldsymbol{\mathcal{M}}(\mathbf{p})\frac{\partial \mathbf{p}}{\partial t} + \boldsymbol{\mathcal{H}}_k(\mathbf{p})\frac{\partial \mathbf{p}}{\partial x_k} = \boldsymbol{\mathcal{S}}(\mathbf{p}), \tag{48}$$

with $\boldsymbol{\mathcal{M}}^{\mathrm{T}} = \boldsymbol{\mathcal{M}} = L_{\mathbf{pp}} > 0$, $\boldsymbol{\mathcal{H}}_k^{\mathrm{T}} = \boldsymbol{\mathcal{H}}_k$ and $\boldsymbol{\mathcal{S}}$ being the vector of the algebraic source terms, i.e. those terms on the right hand side of (46). This was discussed many times in [69,70,119,71,119] and we omit these details.

3.3. Closure relation and the choice of state variables

As we have seen in the previous sections and Paper I, the total energy potential $\mathcal{E}(\mathbf{q})$ or its dual potential $L(\mathbf{p})$ has the meaning of a *generating potential*, and in order to close system (37) or (46), one needs to specify one of these potentials (the other one then can be obtained as the Legendre transformation). In this section, we provide a particular example for the energy $\mathcal{E}$ which completely defines equations (37) and which then will be used in the numerical part of the paper. Of course, other specifications of the energy $\mathcal{E}$ are possible.

One should however note that there is still no universally accepted set of equations describing the motion of a deformable dielectric medium in electromagnetic fields, and we do not have a reference system of PDEs to compare with. At the same time, we note that the resulting equations are not in contradiction with the existing theories, e.g. [83,60,88,51] but rather generalize them.

The SHTC formalism described above and in the papers [65,69,70,119,120,72] gives us the information about the general structure of the macroscopic time evolution equations, while the question of the choice of the state variables remains unaddressed. However, we are interested only in those state variables whose time evolution equations can be cast into the forms (37) or (46). In this section we introduce such state variables for the electromagnetic field.

After the choice of the state variables has been done, another nontrivial task is to specify the generating potentials $\mathcal{E}$ or L. According to the SHTC formalism, such potentials should be convex functions of the chosen state variables and depend on these variables only through their invariants. In general, these potentials should be derived from microscopic theories such as nonequilibrium statistical physics, kinetic theory, etc. To the best of our knowledge, there were no successful attempts to derive such potentials from microscopic theories for such a general case considered here. In this section, we complete the model formulation by specifying state variables and the potential $\mathcal{E} = \rho E$.

We assume the following additive decomposition of the total energy

$$\mathcal{E}(\rho, \mathbf{m}, \boldsymbol{A}, \mathbf{e}, \mathbf{h}, \mathbf{J}, s) = \mathcal{E}_{\mathrm{micro}}(\rho, s) + \mathcal{E}_{\mathrm{meso}}(\boldsymbol{A}, \mathbf{J}) + \mathcal{E}_{\mathrm{macro}}(\mathbf{m}, \mathbf{e}, \mathbf{h}). \tag{49}$$

These three terms are refereed to as the part of the total energy distributed on the microscale ($\mathcal{E}_{\mathrm{micro}}$ is the kinetic energy of the molecular motion), on the mesoscale which is the scale of the continuum particles, $\mathcal{E}_{\mathrm{meso}}$, and on the observable macroscale represented by $\mathcal{E}_{\mathrm{macro}}$. The first two terms were specified in Paper I, while the third term, macroscopic energy, was represented by the macroscopic kinetic energy. In the presence of the electromagnetic field, the macroscopic energy carries also the contribution of the electromagnetic field.

In this paper, we use the same expressions for the energies $\mathcal{E}_{\mathrm{micro}}$ and $\mathcal{E}_{\mathrm{meso}}$ as specified in [110] and Paper I. Moreover, for the rest of this section, we ignore the dissipative effects and thus we assume that $\mathcal{E}_{\mathrm{meso}} = 0$ as it has no influence on the specification of the energy $\mathcal{E}_{\mathrm{macro}}$. We are now in position to specify the macroscopic part $\mathcal{E}_{\mathrm{macro}}(\mathbf{m}, \mathbf{e}, \mathbf{h})$ of the total energy and to give a certain meaning to the electromagnetic fields $\mathbf{e}$ and $\mathbf{h}$ and to the generalized momentum $\mathbf{m}$. The following strategy will be used. Because no exact physical meaning is assigned yet to the fields $\mathbf{m}$, $\mathbf{e}$ and $\mathbf{h}$, we cannot construct the

potential $\mathcal{E}_{\text{macro}}(\mathbf{m},\mathbf{e},\mathbf{h})$ directly. However, as usual, the flux fields $\mathbf{v}$, $\mathbf{d}$ and $\mathbf{b}$ have more intuitive meaning[10] and thus we first construct the dual potential $L(r,\mathbf{v},\mathbf{d},\mathbf{b})$ and then, according to the SHTC formalism, we define density fields and the potential $\mathcal{E}$ as

$$\rho = L_r, \qquad m_i = L_{v_i}, \qquad e_i = L_{d_i}, \qquad h_i = L_{b_i}, \qquad \mathcal{E} = rL_r + v_i L_{v_i} + d_i L_{d_i} + b_i L_{b_i} - L. \tag{50}$$

Following the paper [119] and the discussion made in Appendix A, we define the potential L (for brevity, we also assume that the medium is isentropic and omit entropy in this section) as the following function

$$L(r,\mathbf{v},\mathbf{d},\mathbf{b}) = \rho^2 e_\rho + \frac{1}{2}\left(\epsilon' d_i d_i + \mu' b_i b_i\right) + \epsilon'\mu'\,\varepsilon_{ijk} v_i d_j b_k, \tag{51}$$

or

$$L(r,\mathbf{v},\mathbf{d},\mathbf{b}) = \rho^2 e_\rho + \frac{1}{2}\left(\epsilon'\mathbf{d}^2 + \mu'\mathbf{b}^2\right) + \epsilon'\mu'\,\mathbf{v}\cdot(\mathbf{d}\times\mathbf{b})$$

of the state variables

$$\mathbf{p} = (r,\mathbf{v},\mathbf{d},\mathbf{b}), \tag{52}$$

where $e = \rho^{-1}\mathcal{E}_{\text{micro}}$ is the specific internal energy, $r = e + \rho e_\rho - v_i v_i/2$ is a scalar state variable dual to the density (see $(50)_1$), $\mathbf{v}$ is the velocity of the medium, $\mu' = \mu_0\mu_r$ denotes the magnetic permeability (we use μ' throughout this paper, to avoid confusion with the fluid viscosity μ, which is also used later) and $\epsilon' = \epsilon_0\epsilon_r$ is the electric permittivity of the continuum. As usual, μ_0 and ϵ_0 are respectively the permeability and the permittivity of vacuum, while ϵ_r and μ_r are dimensionless parameters that depend on the material. We furthermore use the standard relation between the speed of light in the medium c, the magnetic permeability and the electric permittivity of the medium:

$$c^2 = \frac{1}{\epsilon'\mu'}. \tag{53}$$

Eventually, the fields $\mathbf{d} = [d_i]$ and $\mathbf{b} = [b_i]$ are the electric and magnetic fields in the *comoving* frame[11] with velocity $\mathbf{v}$, which are related to the electric field $\mathbf{E} = [E_i]$ and the magnetic field $\mathbf{B} = [B_i]$ in the *laboratory frame* by

$$\mathbf{d} = [E_i + \quad \varepsilon_{ijk} v_j B_k] = \mathbf{E} + \mathbf{v}\times\mathbf{B}, \tag{54}$$

$$\mathbf{b} = \frac{1}{\mu'}[B_i - \frac{1}{c^2}\varepsilon_{ijk} v_j E_k] = \frac{1}{\mu'}\left(\mathbf{B} - \frac{1}{c^2}\mathbf{v}\times\mathbf{E}\right). \tag{55}$$

The motivation for this choice of the potential L is in the field equations for a slowly moving medium (see §76 of [83] and [88]) obtained under the assumption of small $\mathbf{v}^2/c^2$ ratios. To show that the equations from [83,88] are indeed recovered in our formalism, one needs to put the partial derivatives $L_{d_i} = \partial L/\partial d_i$ and $L_{b_i} = \partial L/\partial b_i$

$$\mathbf{e} = [L_{d_i}] = [\epsilon' d_i - \epsilon'\mu'\,\varepsilon_{ijk} v_j b_k] = \epsilon'\mathbf{d} - \frac{1}{c^2}\mathbf{v}\times\mathbf{b}, \tag{56}$$

$$\mathbf{h} = [L_{b_i}] = [\mu' b_i + \epsilon'\mu'\,\varepsilon_{ijk} v_j d_k] = \mu'\mathbf{b} + \frac{1}{c^2}\mathbf{v}\times\mathbf{d}, \tag{57}$$

into the equations (46d) and (46e).

According to the momentum equation (46b), the field-medium momentum density $\rho\mathbf{u} = \mathbf{m} = [m_i]$ is defined as the partial derivative of L with respect to $\mathbf{v}$

$$\mathbf{m} = [L_{v_i}] = [\rho v_i + \epsilon'\mu'\,\varepsilon_{ijk} d_j b_k] = \rho\mathbf{v} + \frac{1}{c^2}\mathbf{d}\times\mathbf{b}, \tag{58}$$

which includes the Poynting vector. Here, one needs to take into account that the potential L is not a fully explicit function of unknowns (52). Namely, the hydrodynamic pressure $\rho^2 e_\rho$ is the implicit part, and to compute the derivative L_{v_i} one needs also to express $\rho^2 e_\rho$ in terms of $r = e + \rho e_\rho - v_i v_i/2$, v_i, d_i and b_i, e.g. see [72].

Note that fields $\mathbf{e}$ and $\mathbf{h}$ can be obtained from the electric and magnetic fields $\mathbf{E}$ and $\mathbf{B}$ in the Eulerian frame as

[10] This, however, should not be a reason to use flux fields as the state variables because usually time evolution equations for the flux fields are highly complex and, which is more important, have no apparent structure.

[11] We note that it is necessary to distinguish a comoving frame from the Lagrangian frame of reference used in Section 2.1. Both frames move with the matter, however the distance between two points in the comoving frame changes in time (because it is measured with respect to the Laboratory frame) while it is constant in the Lagrangian frame (because the distance is measured with respect to the reference frame itself). That is why the transformation of fields between the comoving and the Laboratory frame involves only the velocity, like in (54) and (55), but it involves the deformation gradient $F_{ij} = \frac{\partial x_i}{\partial y_j}$ in the other case, see (40).

$$\mathbf{e} = \epsilon' \left(\mathbf{E} + \frac{1}{c^2} \mathbf{v} \times (\mathbf{v} \times \mathbf{E}) \right), \tag{59}$$

$$\mathbf{h} = \mathbf{B} + \frac{1}{c^2} \mathbf{v} \times (\mathbf{v} \times \mathbf{B}). \tag{60}$$

An apparent difference between the fields $(\mathbf{d}, \mathbf{b})$ and $(\mathbf{e}, \mathbf{h})$ is that each of the fields $(\mathbf{d}, \mathbf{b})$ depends on both $\mathbf{E}$ and $\mathbf{B}$ while the fields $(\mathbf{e}, \mathbf{h})$ depend on either $\mathbf{E}$ or $\mathbf{B}$.

The unknown functions (52) belong to the **p**-type state variables (flux fields) in our classification, while the energy potential $\mathcal{E}$ depends on **q**-type state variables (density fields) which are ρ, $\mathbf{m}$, $\mathbf{e}$ and $\mathbf{h}$. Therefore, to complete the formulation of the model, we need to find the expression for $\mathcal{E}(\rho, \mathbf{m}, \mathbf{e}, \mathbf{h})$.

According to the SHTC formalism, total energy density $\mathcal{E}(\rho, \mathbf{m}, \mathbf{e}, \mathbf{h})$ is the Legendre transformation of $L(r, \mathbf{v}, \mathbf{d}, \mathbf{b})$:

$$\mathcal{E} = rL_r + v_i L_{v_i} + d_i L_{d_i} + b_i L_{b_i} - L = (e + \rho e_\rho - v_i v_i/2)\rho + v_i m_i + d_i e_i + b_i h_i - L. \tag{61}$$

It appears that to express $\mathcal{E} = \rho E$ explicitly in terms of ρ, $\mathbf{m}$, $\mathbf{e}$ and $\mathbf{h}$ only is a nontrivial task. However, using formulas (58), (56) and (57), it can be easily expressed in terms of the dual variables $\mathbf{v}$, $\mathbf{d}$ and $\mathbf{b}$ as

$$\mathcal{E}(\rho, \mathbf{v}, \mathbf{d}, \mathbf{b}) = \rho e + \frac{1}{2} \left(\rho \mathbf{v}^2 + \epsilon' \mathbf{d}^2 + \mu' \mathbf{b}^2 \right) + 2\epsilon'\mu' \begin{vmatrix} v_1 & d_1 & b_1 \\ v_2 & d_2 & b_2 \\ v_3 & d_3 & b_3 \end{vmatrix}, \tag{62}$$

Moreover, because we restrict ourselves to flows for which $\mathbf{v}^2/c^2 \ll 1$ is small and terms of the order c^{-4} can be ignored, then an approximate expression for $\mathcal{E}$ can be obtained in terms of ρ, $\mathbf{m}$, $\mathbf{e}$ and $\mathbf{h}$. Under such assumptions, $\mathcal{E}$ can be approximated as

$$\mathcal{E}(\rho, \mathbf{m}, \mathbf{e}, \mathbf{h}) = \rho e + \frac{1}{2} \left(\frac{1}{\rho} \mathbf{m}^2 + \frac{1}{\epsilon'} \mathbf{e}^2 + \frac{1}{\mu'} \mathbf{h}^2 \right) - \frac{1}{2\rho} \begin{vmatrix} m_1 & e_1 & h_1 \\ m_2 & e_2 & h_2 \\ m_3 & e_3 & h_3 \end{vmatrix}. \tag{63}$$

When compared with (49) then ρe is $\mathcal{E}_{\text{micro}}$ and the rest of the terms in (63) are $\mathcal{E}_{\text{macro}}$, while we recall that $\mathcal{E}_{\text{meso}}$ was omitted in this section. Therefore, system (37) together with the energy potential (63) supplemented by $\mathcal{E}_{meso}$ from Paper I form the closed system of PDEs.

Note that (62) can be also rewritten in terms of $\mathbf{v}$, $\mathbf{E}$ and $\mathbf{B}$ as

$$\mathcal{E} = \rho e + \frac{1}{2} \left(\rho \mathbf{v}^2 + \epsilon' \mathbf{E}^2 + \frac{1}{\mu'} \mathbf{B}^2 \right), \tag{64}$$

where we again ignore quadratic terms in $\mathbf{v}/c$ and terms of the order of c^{-4}. Remark that the determinant term is not present in $\mathcal{E}$ if the fields $\mathbf{E}$ and $\mathbf{B}$ are used.

We accomplish the model formulation by giving an explicit formula for the total stress tensor $\boldsymbol{\Sigma}$ in the case of an inviscid medium moving in the electromagnetic field. Note that this expression for the stress tensor is, of course, the result of a particular definition of the energy potential (63). Thus, using formulas (63) and (42), one can write (42) as

$$\boldsymbol{\Sigma}(\rho, \mathbf{m}, \mathbf{e}, \mathbf{h}) = -P\mathbf{I} - \frac{1}{\rho} \mathbf{m} \otimes \mathbf{m} + \frac{1}{\epsilon'} \mathbf{e} \otimes \mathbf{e} + \frac{1}{\mu'} \mathbf{h} \otimes \mathbf{h} + \frac{1}{\rho} \mathbf{m} \otimes (\mathbf{e} \times \mathbf{h}), \tag{65}$$

$$P = p + \frac{1}{2} \left(\frac{1}{\epsilon'} \mathbf{e}^2 + \frac{1}{\mu'} \mathbf{h}^2 \right). \tag{66}$$

where $\otimes$ means the dyadic product, $\mathbf{I}$ is the identity tensor, $p = \rho^2 e_\rho$ is the matter pressure.

If required, the stress tensor can be expressed in terms of $\mathbf{v}$, $\mathbf{d}$ and $\mathbf{b}$ using formulas (47) and (51) as

$$\boldsymbol{\Sigma}(\rho, \mathbf{v}, \mathbf{d}, \mathbf{b}) = -P\mathbf{I} + \epsilon' \mathbf{d} \otimes \mathbf{d} + \mu' \mathbf{b} \otimes \mathbf{b} + \epsilon'\mu' [\mathbf{b} \otimes (\mathbf{v} \times \mathbf{d}) - \mathbf{d} \otimes (\mathbf{v} \times \mathbf{b})], \tag{67}$$

$$P = L = p + \frac{1}{2} \left(\epsilon' \mathbf{d}^2 + \mu' \mathbf{b}^2 \right) + \epsilon'\mu' \mathbf{v} \cdot (\mathbf{d} \times \mathbf{b}). \tag{68}$$

Eventually, for the slowly moving media, the above formulas are equivalent to the following one written in terms of $\mathbf{v}$, $\mathbf{E}$ and $\mathbf{B}$

$$\boldsymbol{\Sigma}(\rho, \mathbf{v}, \mathbf{E}, \mathbf{B}) = -P\mathbf{I} + \epsilon' \mathbf{E} \otimes \mathbf{E} + \frac{1}{\mu'} \mathbf{B} \otimes \mathbf{B}, \tag{69}$$

$$P = p + \frac{1}{2} \left(\epsilon' \mathbf{E}^2 + \frac{1}{\mu'} \mathbf{B}^2 \right). \tag{70}$$

We recall that the scalar P is introduced merely for convenience and should not be understood as the total pressure $\text{tr}\boldsymbol{\Sigma}$, trace of the stress tensor, but just as a part of it.

4. The mathematical model for the numerical solution

The form of the equations adopted for the numerical simulations is obtained from system (37) closed by (63) by dropping the terms of the order $\mathbf{v}^2/c^2$ and by expressing the contributions to the momentum and total energy equation in conventional form, i.e. by using the fluid pressure, the electro-magnetic pressure, the viscous stress tensor and the Maxwell stress tensor. From $\mathbf{v}^2/c^2 \ll 1$ it also follows that $e_i = E_i/(\mu' c^2) = \epsilon' E_i = D_i$ and $h_i = B_i$, see also Appendix A. In this notations, the relations between $\mathbf{v}$, $\mathbf{d}$, $\mathbf{b}$ and $\mathbf{m}$, $\mathbf{D}$, $\mathbf{B}$ read as (see (55), (54) and (58))

$$\mathbf{d} = \frac{1}{\epsilon'}\mathbf{D} + \mathbf{v} \times \mathbf{B}, \tag{71}$$

$$\mathbf{b} = \frac{1}{\mu'}\mathbf{B} - \mathbf{v} \times \mathbf{D}, \tag{72}$$

and

$$\mathbf{m} = \rho\mathbf{v} + \epsilon'\mu'\,\mathbf{d} \times \mathbf{b} = \rho\mathbf{v} + \mathbf{D} \times \mathbf{B} - \mu'\mathbf{D} \times (\mathbf{v} \times \mathbf{D}) - \epsilon'\mathbf{B} \times (\mathbf{v} \times \mathbf{B}). \tag{73}$$

Furthermore, the compatibility condition $\nabla \cdot \mathbf{B} = 0$ in general holds exactly only at the continuous level. Within a numerical method, discretization errors can lead to a violation of this constraint, which is a well-known problem in computational electro-magnetics. Therefore, in this paper the divergence constraint on the magnetic field is imposed by making use of the hyperbolic generalized Lagrangian multiplier (GLM) approach of Dedner et al. [31], which introduces an evolution equation for an *additional auxiliary field* variable φ with associated propagation speed c_h, that is supposed to propagate errors in the $\nabla \cdot \mathbf{B} = 0$ constraint out of the computational domain. However, it has to be pointed out that there are also very important and widely-used numerical methods that guarantee the divergence condition *exactly* even at the discrete level by using a proper discretization of the equations on *staggered* grids, see for example the Yee scheme [141] for the time domain Maxwell equations and its extension to the MHD equations proposed by Balsara and Spicer in [4]. For very recent developments concerning exactly divergence-free high order schemes, see [5,7,6]. We also note that within this paper, we do not take any measures to enforce the compatibility conditions on the distortion $\boldsymbol{A}$ or on the electric field $\mathbf{D}$. After that, system (37) reads as

$$\frac{\partial \rho}{\partial t} + \frac{\partial \rho v_k}{\partial x_k} = 0, \tag{74a}$$

$$\frac{\partial m_i}{\partial t} + \frac{\partial \left(m_i v_k + p\delta_{ik} - \sigma_{ik} + \beta_{ik}\right)}{\partial x_k} = 0, \tag{74b}$$

$$\frac{\partial A_{ik}}{\partial t} + \frac{\partial A_{in} v_n}{\partial x_k} + v_j\left(\frac{\partial A_{ik}}{\partial x_j} - \frac{\partial A_{ij}}{\partial x_k}\right) = -\frac{\psi_{ik}}{\theta_1(\tau_1)}, \tag{74c}$$

$$\frac{\partial (\rho J_i)}{\partial t} + \frac{\partial \left(\rho J_i v_k + T\delta_{ik}\right)}{\partial x_k} = -\frac{\rho H_i}{\theta_2(\tau_2)}, \tag{74d}$$

$$\frac{\partial D_i}{\partial t} + \frac{\partial \left(v_k D_i - v_i D_k - \varepsilon_{ikl} b_l\right)}{\partial x_k} + v_i \frac{\partial D_k}{\partial x_k} = -\frac{1}{\eta} d_i, \tag{74e}$$

$$\frac{\partial B_i}{\partial t} + \frac{\partial \left(v_k B_i - v_i B_k + \varepsilon_{ikl} d_l + \varphi\delta_{ik}\right)}{\partial x_k} + v_i \frac{\partial B_k}{\partial x_k} = 0, \tag{74f}$$

$$\frac{\partial (\rho E)}{\partial t} + \frac{\partial \left(v_k \rho E + v_i[p\delta_{ik} - \sigma_{ik} + \beta_{ik}] + \varepsilon_{ijk} d_i b_j + q_k\right)}{\partial x_k} = 0, \tag{74g}$$

$$\frac{\partial \varphi}{\partial t} + \frac{\partial \left(c_h^2 B_k\right)}{\partial x_k} = 0, \tag{74h}$$

where ε_{ijk} is the three dimensional Levi-Civita tensor. Neglecting the presence of the artificial scalar φ, the entropy production equation is given according to (37g) by

$$\frac{\partial (\rho s)}{\partial t} + \frac{\partial \left(\rho s v_k + H_k\right)}{\partial x_k} = \frac{\rho}{\theta_1(\tau_1) T}\psi_{ik}\psi_{ik} + \frac{\rho}{\theta_2(\tau_2) T} H_i H_i + \frac{1}{\eta T} d_i d_i \geq 0. \tag{75}$$

In the following, we will refer to the above model given by (74a)–(75) also as the Godunov–Peshkov–Romenski (GPR) model. These equations are the mass conservation (74a), the momentum conservation (74b), the time evolution for the distortion (74c), the time evolution equations for the electric and magnetic field (74e) and (74f), the evolution equations for the thermal impulse (74d) and the entropy (75) as well as the total energy conservation law given by (74g). The PDE governing the time evolution of the thermal impulse (74d) looks formally very similar to the momentum equation (74b), where the temperature T takes the role of the pressure p. Due to this similarity, it will also be called the *thermal momentum equation* in the following.

Recall that the system (74)–(75) is an overdetermined system of PDEs which has one more equation than the number of unknowns. In the formulation of the SHTC formalism, see Section 2.1 and 3, the energy potential plays an exceptional role and its time evolution is considered as an extra conservation law which is a consequence of the rest of the governing equations. However, from the numerical viewpoint, it is convenient to consider the total energy among the unknowns and the entropy law as an extra equation. This means that the entropy equation (75) is not discretized and that the entropy is found on each time instant $t = t^{n+1}$ as the solution to the nonlinear algebraic equation $E(\rho^{n+1}, s, v^{n+1}, \boldsymbol{A}^{n+1}, \mathbf{J}^{n+1}, \mathbf{D}^{n+1}, \mathbf{B}^{n+1}) = E^{n+1}$.

According to the definitions made in the previous sections of this paper, $[A_{ik}] = \boldsymbol{A}$ is the distortion, $[J_i] = \mathbf{J}$ is the thermal impulse vector, s is the entropy, $\mathcal{E} = \rho E = \rho E(\rho, s, \mathbf{v}, \boldsymbol{A}, \mathbf{J}, \mathbf{D}, \mathbf{B})$ is the total energy density (specified below), $p = \rho^2 E_\rho$ is the fluid pressure, δ_{ik} is the Kronecker delta and $[\sigma_{ik}] = \boldsymbol{\sigma} = [-A_{mi}(\rho E)_{A_{mk}}]$ is the symmetric stress tensor. Because we are interested in flows for which the ratio $\mathbf{v}^2/c^2 \ll 1$ is small (Newtonian limit), the Maxwell stress reduces to (see (69)–(70))

$$\boldsymbol{\beta} = \frac{1}{2}\left(\frac{1}{\epsilon'}\mathbf{D}^2 + \frac{1}{\mu'}\mathbf{B}^2\right)\mathbf{I} - \frac{1}{\epsilon'}\mathbf{D}\otimes\mathbf{D} - \frac{1}{\mu'}\mathbf{B}\otimes\mathbf{B}. \tag{76}$$

Moreover, $T = E_s = (\rho E)_{\rho s}$ is the temperature, $[q_k] = \mathbf{q} = [E_s E_{J_k}]$ is the heat flux vector; $\theta_1 = \theta_1(\tau_1) > 0$ and $\theta_2 = \theta_2(\tau_2) > 0$ are positive scalar functions, which will be specified below, and which depend on the strain dissipation time $\tau_1 > 0$ and on the thermal impulse relaxation time $\tau_2 > 0$. The parameter $\eta > 0$ is the electric resistivity of the medium. All the relaxation parameters τ_1, τ_2 and η in general may depend on the state parameters, however, in this paper we consider them to be constant. The viscous stress tensor and the heat flux vector are directly related to the dissipative terms on the right hand side via $\boldsymbol{\sigma} = -\rho \boldsymbol{A}^T \boldsymbol{\psi}$ and $\mathbf{q} = T\,\mathbf{H}$.

The first two non-conventional dissipative terms ψ_{ik} and H_i on the right hand side of the evolution equations for $\boldsymbol{A}$, $\mathbf{J}$, E_i and s are given by $[\psi_{ik}] = \boldsymbol{\psi} = [E_{A_{ik}}]$ and $[H_i] = \mathbf{H} = [E_{J_i}]$, respectively. The algebraic source term on the right-hand side of equation (74c) describes the shear strain dissipation due to material element rearrangements, see [110] for a detailed discussion. The source term in (74d) describes the relaxation of the thermal impulse due to heat exchange between material elements, while the one in the governing equations for the electric field (74e) is the well-known law of Ohm [102].

We stress that in the GPR model (74a)–(75) derived within the SHTC framework, *all* dissipative processes have the *same* structure and take the form of algebraic relaxation source terms. The structure of these terms is a *result* of the SHTC formalism, in order to guarantee energy conservation and consistency with the second principle of thermodynamics, see also [42].

As a result of this observation, it is very interesting to note that the dissipative term $-\frac{1}{\eta}d_i$ in the PDE for the *electric field* is given by the well-known *Ohm law* [102] discovered in 1826, which already *has* a suitable structure that directly fits into the SHTC framework. It is a question of mere philosophical nature, but from the viewpoint of hyperbolic thermodynamically compatible systems, it seems that a mathematically more consistent and perhaps even more profound insight into the physics of dissipative processes has first been discovered in the equations of electro-dynamics rather than in the classical standard laws of dissipative transport processes, such as the Newtonian law for viscous fluids and the Fourier law for heat transfer. The latter lead to *parabolic* differential terms in the governing equations, while Ohm's law in the Maxwell equations does *not* generate parabolic terms.

As detailed in the previous sections, E_ρ, E_s, $E_{A_{ik}}$ and E_{J_i} should be understood as the partial derivatives $\partial E/\partial\rho$, $\partial E/\partial s$, $\partial E/\partial A_{ik}$ and $\partial E/\partial J_i$; they are the so-called *energy gradients in the state space* or the *thermodynamic forces*.

One can clearly see that in order to close the system, it is necessary to specify the total energy potential $\rho E(\rho, s, \mathbf{v}, \boldsymbol{A}, \mathbf{J}, \mathbf{d}, \mathbf{b})$. This potential then generates all the constitutive fluxes (*i.e.* non-advective fluxes) and source terms by means of its partial derivatives with respect to the state variables. Hence, the energy specification is one of the key steps in the model formulation.

The total energy density (i.e. energy per unit volume) ρE is the sum of four terms, i.e.

$$\rho E(\rho, s, \mathbf{v}, \boldsymbol{A}, \mathbf{J}, \mathbf{d}, \mathbf{b}) = \rho E_{\rm int}(\rho, s) + \rho E_{\rm mes}(\boldsymbol{A}, \mathbf{J}) + \rho E_{\rm kin}(\mathbf{v}) + \mathcal{E}_{\rm em}(\mathbf{d}, \mathbf{b}), \tag{77}$$

where

- $E_{\rm int}$ is the specific (i.e. per unit mass) internal energy, which depends on the equation of state chosen, and which in the rest of the paper we assume to be that of an ideal gas

$$E_{\rm int}(\rho, s) = \frac{c_0^2}{\gamma(\gamma-1)}, \quad c_0^2 = \gamma\rho^{\gamma-1}e^{s/c_V}, \tag{78}$$

or the stiffened gas equation of state

$$E_{\rm int}(\rho, s) = \frac{c_0^2}{\gamma(\gamma-1)}\left(\frac{\rho}{\rho_0}\right)^{\gamma-1} e^{s/c_V} + \frac{\rho_0 c_0^2 - \gamma p_0}{\gamma\rho}, \quad c_0^2 = const. \tag{79}$$

In both cases, c_0 has the meaning of the adiabatic sound speed, c_V is the specific heat capacity at constant volume, γ is the ratio of the specific heats, *i.e.* $\gamma = c_P/c_V$, if c_P is the specific heat capacity at constant pressure. In (79), ρ_0 is the reference mass density, p_0 is the reference (atmospheric) pressure.

- $E_{\rm mes}$ is the specific energy density at the mesoscale level

$$E_{\rm mes}(\boldsymbol{A},\mathbf{J}) = \frac{c_s^2}{4} G_{ij}^{\rm TF} G_{ij}^{\rm TF} + \frac{\alpha^2}{2} J_i J_i, \tag{80}$$

with

$$[G_{ij}^{\rm TF}] = \mathrm{dev}(\mathbf{G}) = \mathbf{G} - \frac{1}{3}\mathrm{tr}(\mathbf{G})\mathbf{I}, \qquad \text{and} \qquad \mathbf{G} = \boldsymbol{A}^{\rm T}\boldsymbol{A}. \tag{81}$$

Here, $[G_{ij}^{\rm TF}] = \mathrm{dev}(\mathbf{G})$ is the deviator, or the *trace-free* part, of the tensor $\mathbf{G} = \boldsymbol{A}^{\rm T}\boldsymbol{A}$ and $\mathrm{tr}(\mathbf{G}) = G_{ii}$ is its trace, $\mathbf{I}$ is the unit tensor and c_s is the characteristic velocity of propagation of transverse perturbations. In the following we shall refer to it as the *shear sound velocity*.

- $E_{\rm kin} = \frac{1}{2} v_i v_i$ is the specific kinetic energy and, finally
- $\mathcal{E}_{\rm em}$ is the energy density of the electromagnetic field, which is given by (see (62))

$$\mathcal{E}_{\rm em}(\mathbf{d},\mathbf{b}) = \frac{1}{2}\left(\epsilon'\mathbf{d}^2 + \mu'\mathbf{b}^2\right) + 2\epsilon'\mu'\mathbf{v}\cdot(\mathbf{d}\times\mathbf{b}), \tag{82}$$

or by the following approximate relation in terms of quantities in the laboratory frame (see (64))

$$\mathcal{E}_{\rm em}(\mathbf{D},\mathbf{B}) = \frac{1}{2}\left(\frac{1}{\epsilon'}\mathbf{D}^2 + \frac{1}{\mu'}\mathbf{B}^2\right). \tag{83}$$

In our implementation, we have used (82), since it uses less assumptions.

After the total energy potential has been specified, one can write all fluxes and source terms in an explicit form. Thus, for the energy $E_{\rm mes}(\boldsymbol{A},\mathbf{J})$ given by (80), we have $\boldsymbol{\psi} = E_{\boldsymbol{A}} = c_s^2 \boldsymbol{A}\,\mathrm{dev}(\mathbf{G})$, hence the shear stresses are

$$\boldsymbol{\sigma} = -\rho \boldsymbol{A}^{\rm T}\boldsymbol{\psi} = -\rho \boldsymbol{A}^{\rm T} E_{\boldsymbol{A}} = -\rho c_s^2 \mathbf{G}\,\mathrm{dev}(\mathbf{G}), \tag{84}$$

and the strain dissipation source term is

$$-\frac{\boldsymbol{\psi}}{\theta_1(\tau_1)} = -\frac{E_{\boldsymbol{A}}}{\theta_1(\tau_1)} = -\frac{3}{\tau_1}|\boldsymbol{A}|^{\frac{5}{3}}\,\boldsymbol{A}\,\mathrm{dev}(\mathbf{G}), \tag{85}$$

where we have chosen $\theta_1(\tau_1) = \tau_1 c_s^2/3\,|\boldsymbol{A}|^{-\frac{5}{3}}$, with $|\boldsymbol{A}| = \det(\boldsymbol{A}) > 0$ the determinant of $\boldsymbol{A}$ and τ_1 being the strain relaxation time, or, in other words, the time scale that characterizes how long a continuum particle is connected with its neighbor elements before rearrangement.[12] Note, that the determinant of $\boldsymbol{A}$ must satisfy the *constraint*

$$|\boldsymbol{A}| = \frac{\rho}{\rho_0}, \tag{86}$$

where ρ_0 is the density at a reference configuration, see [110]. Furthermore, from the energy potential $E_{\rm mes}(\boldsymbol{A},\mathbf{J})$ the heat flux vector follows with $E_{\mathbf{J}} = \alpha^2\mathbf{J}$ directly as

$$\mathbf{q} = T\,\mathbf{H} = E_s E_{\mathbf{J}} = \alpha^2 T \mathbf{J}. \tag{87}$$

For the thermal impulse relaxation source term, we choose $\theta_2 = \tau_2\alpha^2\frac{\rho}{\rho_0}\frac{T_0}{T}$, and hence

$$-\frac{\rho\mathbf{H}}{\theta_2(\tau_2)} = -\frac{\rho E_{\mathbf{J}}}{\theta_2(\tau_2)} = -\frac{T}{T_0}\frac{\rho_0}{\rho}\frac{\rho\mathbf{J}}{\tau_2}. \tag{88}$$

It contains another characteristic relaxation time τ_2 that is associated to heat conduction.

5. Formal asymptotic analysis and wave speeds

In [42] we have studied in detail the behavior of the GPR model in the stiff relaxation limit $\tau_1 \to 0$ and $\tau_2 \to 0$ without the presence of electro-magnetic forces. Here, we briefly present the main results of this analysis and extend it also to the case when $\eta \to 0$ and $c \to \infty$. In all cases, the employed technique is a formal asymptotic analysis based on the Chapman–Enskog expansion.

[12] Following Frenkel [54], this relaxation time was called particle-settled-life (PSL) time in [110].

5.1. Asymptotic limit of the viscous stress tensor

Here we briefly recall the main results found in [42] when expanding the tensor $\mathbf{G} = \boldsymbol{A}^{\mathrm{T}}\boldsymbol{A}$ in a series of the relaxation parameter τ_1,

$$\mathbf{G} = \mathbf{G}_0 + \tau_1 \mathbf{G}_1 + \tau_1^2 \mathbf{G}_2 + \dots \tag{89}$$

To analyze the stress tensor in the stiff relaxation limit we start from the derivation of an evolution equation for $\mathbf{G}$. Using the definition of $\mathbf{G} = \boldsymbol{A}^{\mathrm{T}}\boldsymbol{A}$ and the product rule, we obtain $\dot{\mathbf{G}} = \boldsymbol{A}^{\mathrm{T}}\dot{\boldsymbol{A}} + \dot{\boldsymbol{A}}^{\mathrm{T}}\boldsymbol{A}$, where the dot denotes the *Lagrangian* or *material* derivative $\dot{\mathbf{G}} = d\mathbf{G}/dt = \partial \mathbf{G}/\partial t + \mathbf{v}\cdot\nabla\mathbf{G}$. Summing up equation (74c) multiplied by $\boldsymbol{A}^{\mathrm{T}}$ from the left and transposing equation (74c) multiplied by $\boldsymbol{A}$ from the right, and using that $\boldsymbol{\sigma} = -\rho \boldsymbol{A}^{\mathrm{T}} E_{\boldsymbol{A}} = -\rho (E_{\boldsymbol{A}})^{\mathrm{T}} \boldsymbol{A} = \boldsymbol{\sigma}^{\mathrm{T}}$ we obtain the sought evolution equation under the following form:

$$\dot{\mathbf{G}} = -\left(\mathbf{G}\nabla\mathbf{v} + \nabla\mathbf{v}^{\mathrm{T}}\mathbf{G}\right) + \frac{2}{\rho\,\theta_1}\,\boldsymbol{\sigma}, \tag{90}$$

where $\nabla\mathbf{v}$ is the velocity gradient. As in [42] we define $\theta_1 = \tau_1 |\boldsymbol{A}|^{-\frac{5}{3}} c_s^2/3 = \tau_1 |\mathbf{G}|^{-\frac{5}{6}} c_s^2/3$. With $E_{\boldsymbol{A}} = c_s^2 \boldsymbol{A}\,\mathrm{dev}(\mathbf{G})$ and after inserting (89) into (90) and collecting terms of the same power in τ_1 one has

$$\tau_1^{-1} \underbrace{\left(6|\mathbf{G}|^{\frac{5}{6}}\mathbf{G}\,\mathrm{dev}(\mathbf{G}_0)\right)}_{0} + \tau_1^{0} \underbrace{\left(\frac{\mathrm{d}\mathbf{G}_0}{\mathrm{d}t} + \dots\right)}_{0} + \dots = 0. \tag{91}$$

Relation (91) holds for any τ_1, hence the coefficients which multiply powers of τ_1 must be equal to zero. Since $\rho = \rho_0 |\boldsymbol{A}| = \rho_0 |\mathbf{G}|^{\frac{1}{2}} > 0$ we have $|\mathbf{G}| > 0$, which means that $\mathbf{G}$ is invertible. Thus, the leading order term (τ_1^{-1}) in (91), yields

$$\mathrm{dev}\,(\mathbf{G}_0) = 0, \quad \Rightarrow \quad \mathbf{G}_0 - \frac{1}{3}\,\mathrm{tr}\,(\mathbf{G}_0)\,\mathbf{I} = 0, \quad \Rightarrow \mathbf{G}_0 = \frac{1}{3}\,\mathrm{tr}\,(\mathbf{G}_0)\,\mathbf{I}. \tag{92}$$

Introducing the definition $g := \frac{1}{3}\,\mathrm{tr}\,(\mathbf{G}_0)$ and neglecting higher order terms, we obtain

$$\mathbf{G} = g\mathbf{I} + \tau_1 \mathbf{G}_1 = \boldsymbol{A}^{\mathrm{T}}\boldsymbol{A}, \tag{93}$$

i.e. in the stiff limit $\tau_1 \ll 1$, the distortion matrix $\boldsymbol{A}$ tends to an *orthogonal matrix*. The coefficient g can be easily computed from the determinant of $\mathbf{G}$ and the compatibility condition $\rho = \rho_0 |\boldsymbol{A}|$ as $g = |\mathbf{G}|^{\frac{1}{3}} = |\boldsymbol{A}|^{\frac{2}{3}} = (\rho/\rho_0)^{\frac{2}{3}}$. Retaining only the leading term $\mathbf{G}_0$ in the expansion (89) we get $\mathbf{G} = \mathbf{G}_0 = g\mathbf{I}$ and thus $\sigma = -\rho c_s^2 \mathbf{G}_0\,\mathrm{dev}(\mathbf{G}_0) = 0$, hence as zeroth order approximation one retrieves the *inviscid* case in the limit $\tau_1 \to 0$.

To get a first order approximation of the viscous stress tensor $\boldsymbol{\sigma}$ in terms of τ_1 one needs to expand the stress tensor (84) in a series of τ_1. With $\mathbf{G} = g\mathbf{I} + \tau_1\mathbf{G}_1$ one has that $\rho = \rho_0 |\boldsymbol{A}| = \rho_0 |g\mathbf{I} + \tau_1\mathbf{G}_1|^{\frac{1}{2}} = \rho_0 (g^{3/2} + \frac{\tau_1}{2} g^{1/2}\,\mathrm{tr}(\mathbf{G}_1) + \mathcal{O}(\tau_1^2))$ and $\mathrm{dev}(\mathbf{G}) = \mathrm{dev}(g\mathbf{I} + \tau_1\mathbf{G}_1) = \tau_1\,\mathrm{dev}(\mathbf{G}_1)$. Then, the viscous stress tensor can be written as

$$\boldsymbol{\sigma} = -\rho c_s^2 \mathbf{G}\,\mathrm{dev}(\mathbf{G}) = -\rho_0 c_s^2 \left(g^{3/2} + \frac{\tau_1}{2} g^{1/2}\,\mathrm{tr}(\mathbf{G}_1)\right)(g\mathbf{I} + \tau_1\mathbf{G}_1)\,\tau_1\,\mathrm{dev}(\mathbf{G}_1). \tag{94}$$

Retaining only the leading terms τ_1 yields the simple expression

$$\boldsymbol{\sigma} = -\tau_1 \rho_0 c_s^2 g^{5/2}\,\mathrm{dev}(\mathbf{G}_1). \tag{95}$$

After applying the "dev" operator to (90) one gets the following evolution equation for $\mathrm{dev}(\mathbf{G})$:

$$\frac{\mathrm{d}}{\mathrm{d}t}\,\mathrm{dev}(\mathbf{G}) + \mathbf{G}\nabla\mathbf{v} + \nabla\mathbf{v}^{\mathrm{T}}\mathbf{G} - \frac{1}{3}\,\mathrm{tr}(\mathbf{G}\nabla\mathbf{v} + \nabla\mathbf{v}^{\mathrm{T}}\mathbf{G})\mathbf{I} = -\frac{6}{\tau_1}|\mathbf{G}|^{5/6}\,\mathrm{dev}(\mathbf{G}\,\mathrm{dev}(\mathbf{G})). \tag{96}$$

Inserting (89) into (96) and recalling from (92) that $\mathrm{dev}\,\mathbf{G}_0 = 0$, one gets the following relation for the leading order terms (τ_1^0):

$$\mathbf{G}_0\nabla\mathbf{v} + \nabla\mathbf{v}^{\mathrm{T}}\mathbf{G}_0 - \frac{2}{3}\,\mathrm{tr}(\mathbf{G}_0\nabla\mathbf{v})\mathbf{I} = -6|\mathbf{G}_0|^{7/6}\,\mathrm{dev}(\mathbf{G}_1).$$

Since $\mathbf{G}_0 = g\mathbf{I}$, the last relation can be rewritten as

$$g\left(\nabla\mathbf{v} + \nabla\mathbf{v}^{\mathrm{T}} - \frac{2}{3}\,\mathrm{tr}(\nabla\mathbf{v})\mathbf{I}\right) = -6\,g^{7/2}\,\mathrm{dev}(\mathbf{G}_1). \tag{97}$$

After inserting (97) into (95) one obtains the following final expression for the first order approximation of the viscous stress tensor in terms of τ_1:

$$\boldsymbol{\sigma} = \frac{1}{6}\tau_1\rho_0 c_s^2\left(\nabla\mathbf{v} + \nabla\mathbf{v}^T - \frac{2}{3}\,\mathrm{tr}(\nabla\mathbf{v})\mathbf{I}\right) := \mu\left(\nabla\mathbf{v} + \nabla\mathbf{v}^T - \frac{2}{3}(\nabla\cdot\mathbf{v})\mathbf{I}\right), \tag{98}$$

This is nothing else than the classical viscous stress tensor that is known from the compressible Navier–Stokes equations (using Stokes' hypothesis), where the dynamic viscosity coefficient is given in terms of the relaxation time τ_1 and the shear sound speed c_s as

$$\mu = \frac{1}{6}\tau_1\rho_0 c_s^2, \tag{99}$$

see [110,42]. For a comment on the possible experimental measurement of τ_1 and c_s see [42]. We stress at this point that the usual form of the viscous stress tensor of the compressible Navier–Stokes equations is a result of the model, which is obtained by the mere choice of a quadratic energy potential in terms of $\mathbf{G}^{TF}$. The special choice of θ_1 was only made to produce a *constant* viscosity coefficient μ. More general relations of μ (say, e.g., the well-known law of Sutherland) can be obtained by a suitable choice of θ_1.

5.2. Asymptotic limit of the heat flux

In [42] a formal asymptotic analysis was also carried out for the heat flux $\mathbf{q} = E_S E_{\mathbf{J}} = \alpha^2 T\mathbf{J}$. The Chapman–Enskog expansion of the thermal impulse vector $\mathbf{J}$ in terms of the small relaxation parameter $\tau_2 \ll 1$ reads

$$\mathbf{J} = \mathbf{J}_0 + \tau_2\mathbf{J}_1 + \tau_2^2\mathbf{J}_2 + \dots \tag{100}$$

With $\theta_2 = \tau_2\alpha^2\frac{\rho}{\rho_0}\frac{T_0}{T}$ the PDE (74d) for $\mathbf{J}$ becomes:

$$\frac{\partial\rho\mathbf{J}}{\partial t} + \nabla\cdot(\rho\mathbf{J}\otimes\mathbf{u}) + \nabla T = -\frac{1}{\tau_2}\frac{T}{T_0}\frac{\rho_0}{\rho}\rho\mathbf{J}. \tag{101}$$

Inserting (100) into (101) and proceeding with the collection of the τ_2 terms as in the previous section yields

$$\tau_2^{-1}\underbrace{\left(\frac{T}{T_0}\frac{\rho_0}{\rho}\rho\mathbf{J}_0\right)}_{0} + \tau_2^{0}\underbrace{\left(\frac{\partial\rho\mathbf{J}_0}{\partial t} + \nabla\cdot(\rho\mathbf{J}_0\otimes\mathbf{u}) + \nabla T + \frac{T}{T_0}\frac{\rho_0}{\rho}\rho\mathbf{J}_1\right)}_{0} + \dots = 0. \tag{102}$$

As a consequence one obtains the following relations for the first two terms in the expansion of $\mathbf{J}$:

$$\mathbf{J}_0 = 0, \qquad \text{and} \qquad \mathbf{J}_1 = -\frac{T_0}{T\rho_0}\nabla T. \tag{103}$$

As a result of (100) and (103) the heat flux vector $\mathbf{q} = \alpha^2 T\mathbf{J}$ becomes for small relaxation times $\tau_2 \ll 1$

$$\mathbf{q} = \alpha^2 T\mathbf{J} = -\alpha^2\tau_2\frac{T_0}{\rho_0}\nabla T := -\kappa\nabla T, \tag{104}$$

which is the familiar form of the Fourier heat flux with heat conduction coefficient $\kappa = \alpha^2\tau_2\frac{T_0}{\rho_0}$.

5.3. Asymptotic limit of the electro-magnetic stresses

In this paper the extended GPR model (74a)–(74g) also accounts for the presence of electro-magnetic forces and effects. We therefore analyze the model in the stiff relaxation limit for $\eta \to 0$ and $c \to \infty$. From (55) and (58) we immediately obtain $\mathbf{b} \to \frac{1}{\mu'}\mathbf{B}$ and $\mathbf{u} \to \mathbf{v}$ for $c \to \infty$. Furthermore, the governing PDE system for the electric field reduces for $c \to \infty$ to the simple relation

$$-\frac{1}{\mu'}\nabla\times\mathbf{B} = -\frac{1}{\eta}\mathbf{d}. \tag{105}$$

A Chapman–Enskog expansion of $\mathbf{d}$ in terms of the small parameter η reads

$$\mathbf{d} = \mathbf{d}_0 + \eta\mathbf{d}_1 + \eta^2\mathbf{d}_2 + \dots \tag{106}$$

and thus eqn. (105) becomes

$$\eta^{-1}(\mathbf{d}_0) + \eta^0\left(\mathbf{d}_1 - \frac{1}{\mu'}\nabla\times\mathbf{B}\right) + \dots = 0. \tag{107}$$

Since the above equation must be valid for any η, we set all coefficients multiplying terms with η to zero and get as a result

$$\mathbf{d}_0 = 0, \qquad \text{and} \qquad \mathbf{d}_1 = \frac{1}{\mu'} \nabla \times \mathbf{B}. \tag{108}$$

From $\mathbf{d}_0 = 0$ and (54) follows immediately that at leading zeroth order the electric field behaves as $\mathbf{E} = -\mathbf{v} \times \mathbf{B}$, which is a well known relation for the ideal MHD equations. It also means that in the comoving frame, the electric field vanishes. Inserting (108) into the PDE for the magnetic field (74f) we obtain

$$\frac{\partial B_i}{\partial t} + \frac{\partial}{\partial x_k} \left(v_k B_i - v_i B_k \right) + v_i \frac{\partial B_k}{\partial x_k} = -\frac{\eta}{\mu'} \frac{\partial}{\partial x_k} \varepsilon_{ikl} \frac{\partial}{\partial x_m} \varepsilon_{lmp} B_p, \tag{109}$$

i.e. we obtain the classical dissipative term of the type $-\frac{\eta}{\mu'} \nabla \times (\nabla \times \mathbf{B}) = \frac{\eta}{\mu'} \nabla \cdot \left(\nabla \mathbf{B} - \nabla \mathbf{B}^T \right)$ that is present in the viscous and resistive MHD equations [140,37]. For $\eta \ll 1$ and $c \to \infty$ the flux term $\varepsilon_{ijk} d_i b_j$ in the energy equation (74g) becomes up to first order terms in η

$$\mathbf{d} \times \mathbf{b} = \frac{\eta}{(\mu')^2} \nabla \times (\mathbf{B} \times \mathbf{B}) = -\frac{\eta}{(\mu')^2} \mathbf{B}^T \left(\nabla \mathbf{B} - \nabla \mathbf{B}^T \right), \tag{110}$$

see [140,37]. Finally, the Maxwell stress tensor $\boldsymbol{\beta}$ reduces to

$$\boldsymbol{\beta} = \frac{1}{\mu'} \left(\frac{1}{2} \mathbf{B}^2 \mathbf{I} - \mathbf{B} \otimes \mathbf{B} \right), \tag{111}$$

which is the usual relation for the ideal MHD equations.

5.4. Asymptotically reduced limit system

Combining the results of the previous sections, we get the following asymptotically reduced system (i.e. if only first order terms are kept in the formal series expansions (89), (100) and (106)) for the quantities ρ, $\rho \mathbf{u} \to \rho \mathbf{v}$, ρE and $\mathbf{B}$, in the stiff relaxation limit when $\eta \to 0$, $\tau_1 \to 0$ and $\tau_2 \to 0$:

$$\frac{\partial}{\partial t} \begin{pmatrix} \rho \\ \rho \mathbf{v} \\ \rho E \\ \mathbf{B} \\ \varphi \end{pmatrix} + \nabla \cdot \begin{pmatrix} \rho \mathbf{v} \\ \rho \mathbf{v} \otimes \mathbf{v} + p \mathbf{I} - \boldsymbol{\sigma} + \boldsymbol{\beta} \\ \mathbf{v}^T \left((\rho E + p) \mathbf{I} - \boldsymbol{\sigma} + \boldsymbol{\beta} \right) + \mathbf{q} - \frac{\eta}{(\mu')^2} \mathbf{B}^T \left(\nabla \mathbf{B} - \nabla \mathbf{B}^T \right) \\ \mathbf{B} \otimes \mathbf{v} - \mathbf{v} \otimes \mathbf{B} - \frac{\eta}{\mu'} \left(\nabla \mathbf{B} - \nabla \mathbf{B}^T \right) + \varphi \mathbf{I} \\ c_h^2 \mathbf{B} \end{pmatrix} = 0, \tag{112}$$

with the viscous shear stress tensor of the fluid

$$\boldsymbol{\sigma} = \mu \left(\nabla \mathbf{v} + \nabla \mathbf{v}^T - \frac{2}{3} \nabla \cdot \mathbf{v} \right), \qquad \text{with} \qquad \mu = \frac{1}{6} \tau_1 c_s^2 \rho_0, \tag{113}$$

the heat flux

$$\mathbf{q} = -\kappa \nabla T, \qquad \text{with} \qquad \kappa = \tau_2 \alpha^2 \frac{T_0}{\rho_0}, \tag{114}$$

and the Maxwell stress tensor of the electro-magnetic forces

$$\boldsymbol{\beta} = \frac{1}{\mu'} \left(\frac{1}{2} \mathbf{B}^2 \mathbf{I} - \mathbf{B} \otimes \mathbf{B} \right). \tag{115}$$

The above system (112) is the classical viscous and resistive MHD system based on conventional parabolic terms for the description of dissipative momentum and heat transfer. In this system, also the electric resistivity of the medium is modeled by parabolic terms, which is in contrast to the original Maxwell equations. Because system (112) is one of the principal models that will be compared with the new hyperbolic model (74) in Section 7, it is therefore useful to compare these PDE systems in terms of the number of equations. As we discussed in Section 1.5, there are 23 time evolution equations that have to be solved in the SHTC formalism (we ignore here field φ which is only added for computational reasons in both approaches) and 8 PDEs to be solved in the classical second order parabolic approach. Thus, the flow is represented by 13 fields $(\rho, \mathbf{m}, \boldsymbol{A})$ in (74) while it is represented by 4 fields $(\rho, \rho \mathbf{v})$ in (112). The electrodynamics is represented by 6 fields $(\mathbf{D}, \mathbf{B})$ in (74) and by 3 fields $\mathbf{B}$ in (112). Eventually, the heat transfer is represented by four fields $(s, \mathbf{J})$ in (74) and by one field, the energy E, in (112).

5.5. Characteristic velocities for the inviscid case

The approximate Riemann solvers used later in this paper only require extremal wave speed estimates, since we employ the simple Rusanov or local Lax–Friedrichs flux [123]. This means that the full eigenvalue decomposition of the coefficient matrices of the quasi-linear form of (74) is not needed. The same holds true if centered fluxes such as the FORCE method of Toro and Billet is used, see [133,134,41]. However, it is in general always useful to know the characteristic speeds in order to better understand the characteristic structure of a considered hyperbolic model. Unfortunately, to find analytical formulas for the characteristic speeds when all fields are present in (74) is a very difficult task and *numerical* linear algebra algorithms have to be used. However, even to obtain formulas for a simplified inviscid and non-heat conducting case might be useful for direct comparison with, for example, ideal MHD equations. We thus consider system (74) in a one-dimensional case, along the axis x_1 (we also ignore equation (74h)) without the equations for the distortion field and thermal impulse. The following formulas for the characteristic velocities can be obtained

$$\lambda_{1,2,3,4} = \frac{1}{\sqrt{\epsilon'\mu'}} = \pm c, \qquad \lambda_{5,6,7,8,9} = v_1, \qquad \lambda_{10,11} = \frac{Zv_1 - X \pm \sqrt{4Z(Xv_1+Y) + (Zv_1 - X)^2}}{2Z}, \tag{116}$$

where

$$\begin{aligned} X = \rho \Big[& \epsilon' B_1 \left(\rho - \epsilon' \mathbf{B}^2\right) \mathbf{B}\cdot\mathbf{v} + \mu D_1 \left(\rho - \mu' \mathbf{D}^2\right) \mathbf{D}\cdot\mathbf{v} + \\ & \rho v_1 \left(\rho - 3\left(\mu' \mathbf{D}^2 - \epsilon' \mathbf{B}^2\right) + \frac{2}{\rho}\left(\mu'^2 \left(\mathbf{D}^2\right)^2 + \epsilon'^2 \left(\mathbf{B}^2\right)^2\right)\right) + \\ & \left(\rho - \mu' \mathbf{D}^2 - \epsilon' \mathbf{B}^2\right) P_1 \Big] - \epsilon\mu' \Big(\rho \left(B_1 \mathbf{D}\cdot\mathbf{v} + D_1 \mathbf{B}\cdot\mathbf{v}\right) \mathbf{D}\cdot\mathbf{B} - 4\rho v_1 \mathbf{B}^2 \mathbf{D}^2 - \\ & \mathbf{P}^2 \left(\left(\rho - 2\epsilon' \mathbf{B}^2 - 2\mu' \mathbf{D}^2\right) v_1 + P_1\right)\Big), \end{aligned}$$

$$\begin{aligned} Y = & -\rho c_0^2 \Big[\rho^2 + \epsilon'^2 B_1^2 \mathbf{B}^2 + \mu'^2 D_1^2 \mathbf{D}^2 - \epsilon' \rho \left(B_1^2 + \mathbf{B}^2\right) - \mu' \rho \left(D_1^2 + \mathbf{D}^2\right) \\ & + \epsilon'\mu' \left(B_1^2 D_1^2 - (\mathbf{B}\cdot\mathbf{D} - B_1 D_1)^2 + \mathbf{B}^2 \mathbf{D}^2\right)\Big], \end{aligned}$$

$$\begin{aligned} Z = -\rho \Big[& \rho^2 - 2\epsilon'\rho\mathbf{B}^2 - 2\mu'\rho\mathbf{D}^2 + \epsilon'^2 \left(\mathbf{B}^2\right)^2 + \mu'^2 \left(\mathbf{D}^2\right)^2 \Big) + \epsilon'\mu' \Big(\rho \left((\mathbf{D}\cdot\mathbf{B})^2 - 3\mathbf{B}^2\mathbf{D}^2\right) + \\ & \left(\mu'\mathbf{D}^2 + \epsilon'\mathbf{B}^2\right) \left(\mathbf{B}^2\mathbf{D}^2 - (\mathbf{D}\cdot\mathbf{B})^2\right)\Big], \end{aligned}$$

and $\mathbf{P} = [P_i] = \mathbf{D}\times\mathbf{B}$.

One may note that the characteristic speeds (116) are apparently different from those of the ideal MHD equations. For example, there is no light characteristics in the MHD equations such as $\lambda_{1,2,3,4}$ above. These velocities correspond to the electric and magnetic fields and indicate that the field equations are not Galilean invariant,[13] exactly as the Maxwell equations, while the MHD equations are Galilean invariant [112]. In addition, if the fields $\mathbf{D}$ and $\mathbf{B}$ are genuinely independent like in our case then there are no two pairs of the so-called fast and slow magneto-sonic waves [117], but instead we have only one pair of waves with velocities $\lambda_{10,11}$. Note that speeds $\lambda_{10,11}$ are not symmetric with respect to v_1 in the presence of electro-magnetic fields. If however $\mathbf{D} = \mathbf{B} = (0,0,0)$ then $\lambda_{10,11} = v_1 \pm c_0$. As in the whole system (74), the velocity vector and the electro-magnetic fields are strongly entangled in $\lambda_{10,11}$.

As discussed in [42,97,96], the characteristic speeds of the non-dissipative part of a hyperbolic relaxation model are not the real sound speeds but the high frequency limits of the sound speeds due to the dispersion of sound waves while the characteristic speeds of the ideal MHD equations should be obtained in our model as the low frequency limits, exactly as the classical adiabatic sound speed of the Euler equation is recovered in the low frequency limit of our SHTC model, as it is shown in [42]. The detailed dispersion analysis of the model is however beyond the scopes of this study and will be presented somewhere else.

6. The numerical scheme

As in Paper I, the governing equations of the SHTC formulation of the GPR model can be written as a nonlinear system of hyperbolic PDEs with non-conservative products and stiff source terms:

[13] To be more precise, the field equations of our model are not invariant under translations of the space but they are still rotationally invariant [65].

$$\frac{\partial \mathbf{Q}}{\partial t} + \nabla \cdot \mathbf{F}(\mathbf{Q}) + \mathcal{B}(\mathbf{Q}) \cdot \nabla \mathbf{Q} = \mathbf{S}(\mathbf{Q}), \tag{117}$$

where $\mathbf{Q} = \mathbf{Q}(\mathbf{x}, t)$ is the state vector, $\mathbf{F}(\mathbf{Q}) = (\mathbf{F}^1, \mathbf{F}^2, \mathbf{F}^3)$ is the nonlinear flux tensor expressing the conservative part of the PDE system, while $\mathbf{S}(\mathbf{Q})$ contains the potentially stiff algebraic relaxation source terms and $\mathcal{B}(\mathbf{Q}) \cdot \nabla \mathbf{Q}$ is a purely non-conservative term. The explicit expressions for $\mathbf{Q}$, $\mathbf{F}(\mathbf{Q})$ and $\mathbf{S}(\mathbf{Q})$ are directly obvious from (74).

The matrix $\mathcal{B}(\mathbf{Q})$ consists of zeros and only components of the velocity vector v_i and accommodates the terms

$$v_j \left(\frac{\partial A_{ik}}{\partial x_j} - \frac{\partial A_{ij}}{\partial x_k} \right), \qquad v_i \frac{\partial D_k}{\partial x_k}, \qquad v_i \frac{\partial B_k}{\partial x_k} \tag{118}$$

on the left hand side of the equations (74c), (74e) and (74f).

The exact expressions for the elastic stress σ_{ik} and Maxwell stress β_{ik} are given by (84) and (76), while the expressions for the pressure $p = \rho^2 E_\rho$ and the temperature $T = E_s$ depend on the choice of the internal energy given by (78) or (79). The relaxation times $\tau_1 > 0$ and $\tau_2 > 0$ and the resistivity $\eta > 0$ are assumed to be constant of the order $\sim 10^{-3}$ in most of the numerical examples. The shear sound speed $c_s < c_0$ and the adiabatic sound speed c_0 were typically taken of the order of ~ 1, while the speed of light ~ 10.

The system (117) can also be written in quasilinear form as

$$\frac{\partial \mathbf{Q}}{\partial t} + \mathcal{A}(\mathbf{Q}) \cdot \nabla \mathbf{Q} = \mathbf{S}(\mathbf{Q}), \tag{119}$$

where $\mathcal{A}(\mathbf{Q}) = \partial \mathbf{F}(\mathbf{Q}) / \partial \mathbf{Q} + \mathcal{B}(\mathbf{Q})$ includes both the Jacobian of the conservative flux, as well as the non-conservative product.

We choose to solve the PDE system (117) by using high order one-step ADER-DG methods, which evolve in time the degrees of freedom with respect to a given basis, rather than the point values or the cell averages of the solution, like in finite difference or in finite volume methods. Our description of the numerical scheme is limited to the most relevant aspects, while all the details can be found in [36,46,75,8,48,145,144]. At the generic time t^n, the numerical solution of the PDE is represented within each cell T_i by polynomials of maximum degree $N \geq 0$, namely

$$\mathbf{u}_h(\mathbf{x}, t^n) = \sum_{l=0}^{\mathcal{N}} \Phi_l(\mathbf{x}) \hat{\mathbf{u}}_l^n = \Phi_l(\mathbf{x}) \hat{\mathbf{u}}_l^n, \qquad \mathbf{x} \in T_i, \tag{120}$$

where the coefficients $\hat{\mathbf{u}}_l^n$ are sometimes called the *degrees of freedom*. The functions $\Phi_l(\mathbf{x})$ form a nodal basis, which is given by the Lagrange interpolation polynomials passing through the Gauss–Legendre quadrature nodes associated with element T_i, see [127]. The symbol $\mathcal{N}$ denotes the number of degrees of freedom per element and is given by $\mathcal{N} = (N+1)^d$ for tensor-product elements in d space dimensions.

6.1. The discontinuous Galerkin scheme

A fully discrete one-step ADER-DG scheme [36,48] is obtained after multiplying the governing PDE (117) by test functions Φ_k identical to the spatial basis functions of Eq. (120). After that, we integrate over the space–time control volume $T_i \times [t^n; t^{n+1}]$. Following the idea of path-conservative schemes, see [24,104,39,41], one obtains:

$$\begin{aligned} &\left(\int_{T_i} \Phi_k \Phi_l d\mathbf{x} \right) \left(\hat{\mathbf{u}}_l^{n+1} - \hat{\mathbf{u}}_l^n \right) + \int_{t^n}^{t^{n+1}} \int_{\partial T_i} \Phi_k \, \mathcal{D}_h^- \left(\mathbf{q}_h^-, \mathbf{q}_h^+ \right) \cdot \mathbf{n} \, dS dt \\ &+ \int_{t^n}^{t^{n+1}} \int_{T_i \setminus \partial T_i} \Phi_k \left(\nabla \cdot \mathbf{F}(\mathbf{q}_h) + \mathcal{B}(\mathbf{q}_h) \cdot \nabla \mathbf{q}_h \right) d\mathbf{x} dt = \int_{t^n}^{t^{n+1}} \int_{T_i} \Phi_k \mathbf{S}(\mathbf{q}_h) d\mathbf{x} dt, \end{aligned} \tag{121}$$

where $\mathbf{n}$ is the outward pointing unit normal vector on the surface ∂T_i of element T_i. There are a couple of aspects worth mentioning in the above expression. First of all, we used the symbol $\mathbf{q}_h$ to denote a *predictor* state available at any intermediate time between t^n and t^{n+1} and with the same spatial accuracy of the initial DG polynomial. The calculation of $\mathbf{q}_h$ is briefly described in the next Section. Second, the element mass matrix appears in the first integral of (121), the second term is a Riemann solver (written in terms of fluctuations) that accounts for the jump in the discrete solution at element boundaries and the third term takes into account the smooth part of the non-conservative product, while the fourth term (the one on the right hand side) accounts for the presence of the algebraic source terms. Third, due to the presence of non-conservative products, the jumps of $\mathbf{q}_h$ across element boundaries are taken into account in the framework of path-conservative schemes put forward by Castro and Parés in the finite volume context [24,104] and extended to discontinuous Galerkin schemes in [116,39,41]. Finally, as for the choice of the Riemann solver, in this paper we have used the simple Rusanov method [123] (also called the local Lax Friedrichs method), although any other kind of Riemann solver could

be adopted in principle, in particular the centered FORCE flux, which does *not even* need extremal wave speed estimates, see [133,134,41], or the recent generalizations of the Osher–Solomon flux proposed in [43,44,23], or the extension of the HLLEM method [50] recently forwarded in [38]. In all the latter Riemann solvers, it is sufficient to use a *numerical* eigenvector decomposition of the matrix $\mathcal{A}$, which can be achieved with standard numerical linear algebra packages. In terms of fluctuations our path-conservative Rusanov method simply reads

$$\mathcal{D}_h^- \left(\mathbf{q}_h^-, \mathbf{q}_h^+\right) \cdot \mathbf{n} = \frac{1}{2}\left(\mathbf{F}(\mathbf{q}_h^+) - \mathbf{F}(\mathbf{q}_h^+)\right) \cdot \mathbf{n} + \frac{1}{2}\tilde{\mathcal{B}}_n \left(\mathbf{q}_h^+ - \mathbf{q}_h^-\right) - \frac{1}{2} s_{\max} \left(\mathbf{q}_h^+ - \mathbf{q}_h^-\right), \tag{122}$$

where $s_{\max}$ is an extremal wave speed estimate for the largest eigenvalue of $\mathcal{A}(\mathbf{q}_h^-) \cdot \mathbf{n}$ and $\mathcal{A}(\mathbf{q}_h^+) \cdot \mathbf{n}$ and the matrix $\tilde{\mathcal{B}}_n$ has been calculated according to [24,104,39,41,44] as the path integral

$$\tilde{\mathcal{B}}_n = \int_0^1 \mathcal{B}\left(\boldsymbol{\psi}(\mathbf{q}_h^-, \mathbf{q}_h^+, s)\right) \cdot \mathbf{n}\, ds, \tag{123}$$

along the simple straight line segment path

$$\boldsymbol{\psi} = \boldsymbol{\psi}\left(\mathbf{q}_h^-, \mathbf{q}_h^+, s\right) = \mathbf{q}_h^- + s\left(\mathbf{q}_h^+ - \mathbf{q}_h^-\right), \qquad \text{with} \qquad 0 \le s \le 1. \tag{124}$$

The path integral in (123) has been computed *numerically* via Gauss quadrature, as suggested in [41,44,43]. Since the SHTC model presented in this paper explicitly includes the speed of light c as propagation speed, we simply set $s_{\max} = c$, assuming that all other wave speeds are bounded by c from above. The ADER-DG method described above refers to the *unlimited* scheme. In the presence of discontinuities, a proper nonlinear limiting strategy is needed. Here, we use the *a posteriori* finite volume subcell limiter proposed in [48,145,144], which is based on the MOOD framework developed in [27,32,33].

6.2. Local space–time predictor

The computation of the *predictor* state $\mathbf{q}_h$ is obtained after resorting to an element-local weak formulation of the governing PDE in space–time, see [40,36,75,46,8,48,145,144]. Since this procedure is performed locally for each computational element, irrespective of neighbouring elements, no Riemann problem is implied in that. To simplify notation, we define

$$\langle f, g \rangle = \int_{t^n}^{t^{n+1}} \int_{T_i} f(\mathbf{x}, t) g(\mathbf{x}, t)\, d\mathbf{x}\, dt, \qquad [f, g]^t = \int_{T_i} f(\mathbf{x}, t) g(\mathbf{x}, t)\, d\mathbf{x}, \tag{125}$$

which denote the scalar products of two functions f and g over the space–time element $T_i \times \left[t^n; t^{n+1}\right]$ and over the spatial element T_i at time t, respectively. The discrete representation of $\mathbf{q}_h$ in element $T_i \times [t^n, t^{n+1}]$ is assumed to have the following form

$$\mathbf{q}_h = \mathbf{q}_h(\mathbf{x}, t) = \sum_l \theta_l(\mathbf{x}, t) \hat{\mathbf{q}}_{l,i}^n := \theta_l \hat{\mathbf{q}}_{l,i}^n, \tag{126}$$

where it is important to stress that $\theta_l(\mathbf{x}, t)$ is now a space–time basis function, of degree N. At this point we multiply (117) with a space–time test function $\theta_k = \theta_k(\mathbf{x}, t)$ and subsequently integrate over the space–time control volume $T_i \times \left[t^n; t^{n+1}\right]$. Replacing for $\mathbf{q}_h$, the following weak formulation of the PDE is obtained:

$$\left\langle \theta_k, \frac{\partial \mathbf{q}_h}{\partial t} \right\rangle + \langle \theta_k, \nabla \cdot \mathbf{F}(\mathbf{q}_h) + \mathcal{B}(\mathbf{q}_h) \cdot \nabla \mathbf{q}_h \rangle = \langle \theta_k, \mathbf{S}(\mathbf{q}_h) \rangle. \tag{127}$$

After integration by parts in time of the first term, eqn. (127) reads

$$[\theta_k, \mathbf{q}_h]^{t^{n+1}} - \left[\theta_k, \mathbf{u}_h(\mathbf{x}, t^n)\right]^{t^n} - \left\langle \frac{\partial}{\partial t}\theta_k, \mathbf{q}_h \right\rangle + \langle \theta_k, \nabla \cdot \mathbf{F}(\mathbf{q}_h) + \mathcal{B}(\mathbf{q}_h) \cdot \nabla \mathbf{q}_h \rangle = \langle \theta_k, \mathbf{S}(\mathbf{q}_h) \rangle. \tag{128}$$

Eq. (128) represents a nonlinear system to be solved in the unknown expansion coefficients $\hat{\mathbf{q}}_{l,i}^n$. We recall that, unlike the original ADER approach based on the Cauchy–Kowalevski procedure, the discontinuous Galerkin predictor just described remains valid even in the presence of stiff source terms, as it has been done for various physical systems in [46,75,143,45,42] and as it is the case for the equations considered in this paper. Since the space–time predictor method above is locally *implicit*, we restrict our time step Δt only based on a standard CFL-type stability condition for explicit DG schemes based on the maximum wave speed and not in terms of the relaxation times τ_1, τ_2 and the resistivity η, i.e.

$$\Delta t < \frac{1}{(2N+1)} \frac{1}{\frac{c}{\Delta x_1} + \frac{c}{\Delta x_2} + \frac{c}{\Delta x_3}}, \tag{129}$$

where Δx_i are the mesh spacings in coordinate direction x_i and we have again assumed that the maximum wave speed is the speed of light c and the term $(2N+1)$ is typical for high order explicit DG schemes. For more details on the time step restriction of explicit ADER-DG schemes, see [113,36].

7. Numerical results

In this section on numerical results, we will assume that the magnetic permeability of the medium is $\mu' = 1$ for all test problems, and only the speed of light c is explicitly specified. If not stated otherwise, the ideal gas equation of state (EOS) is used. Within this section, we will specify the standard material parameters that are conventionally used in continuum mechanics, i.e. the fluid viscosity μ and the heat conduction coefficient κ. Together with the associated wave speeds c_s (shear sound speed) and α (heat propagation wave speed), one can calculate the corresponding characteristic times τ_1 and τ_2 used in the GRP model according to the results (99) and (104) given by the formal asymptotic analysis presented in Section 5. Note that the model parameter η is already a well-known quantity, namely the electric resistivity of the medium used in the Ohm law. Also, remark that the wave speeds c_s and α can be measured in the experiments on propagation of high frequency sound waves as discussed in paper I. The associated relaxation times τ_1 and τ_2 however might be extremely small, of the order of nanoseconds, and the use of such values would put the model into extremely stiff conditions. Thus we stress that if one is interested in simulating Newtonian flows with Fourier heat conduction it is not necessary to use physical values (recovered from an experiment or from a microscopic theory) for the model parameters. Indeed, the asymptotic analysis suggests that if the flow is in local equilibrium (Newton and Fourier transport laws are dominant) the process is not anymore governed by two parameters c_s and τ_1 (or α and τ_2) but by their product, the viscosity $\mu = \frac{1}{6}\rho_0\tau_1 c_s^2$ (or heat conductivity κ). In fact, in such a case, any values for the relaxation time are valid which satisfy two conditions $\tau_1 = 6\mu/(\rho_0 c_s^2)$ and $\tau_1 \ll T$, where T is the characteristic macroscopic time scale (time scale of the problem). If one chooses $\tau_1 \approx T$ then the flow will be viscoelastic with an apparent elastic effect, while if $\tau_1 > T$ then the flow is absent and the medium deforms elastically during the time T. For the non-equilibrium flows when the Navier–Stokes–Fourier approximation does not work, the sound speed c_s and relaxation time τ_1 (or α and τ_2) may not satisfy the relations (99) or (104) and, in fact, may not be constant anymore. In such a case, extra information (experiments) have to be used to define the model parameters.

7.1. Numerical convergence results in the stiff relaxation limit

As shown in the formal asymptotic analysis carried out in [42] and Section 5 of this paper, the governing PDE system (74a)–(74g) relaxes to the classical ideal MHD equations in the case where $c \to \infty$ and when the relaxation times and the resistivity tend to zero, i.e. for $\tau_1 \to 0$, $\tau_2 \to 0$ and $\eta \to 0$. We can use this knowledge in order to design a test case that allows us to verify numerically the order of accuracy of our high order one-step ADER-DG schemes in the stiff relaxation limit of the first order hyperbolic GPR model by comparing against known exact solutions of the ideal MHD system. For that purpose, we use the initial condition proposed by Balsara in [3] that consists of a smooth magnetized vortex. The computational domain used for this test is $\Omega = [-10, +10]^2$ and the initial condition is given by

$$\rho = 1, \qquad u = 1 + \delta u, \qquad v = 1 + \delta v, \qquad w = 0, \qquad p = 1 + \delta p,$$

$$\mathbf{E} = -\mathbf{v} \times \mathbf{B}, \qquad \boldsymbol{A} = \sqrt[3]{\rho}\,\mathbf{I}, \qquad \mathbf{J} = 0,$$

with $r = \sqrt{x^2 + y^2}$, $\epsilon = \frac{1}{2\pi}$ and the perturbations

$$\delta u = -y\epsilon \exp\left(\frac{1}{2}(1-r^2)\right), \quad \delta v = +x\epsilon \exp\left(\frac{1}{2}(1-r^2)\right), \quad \delta p = -\frac{1}{2}\epsilon^2 r^2 \exp(1-r^2),$$

$$B_x = -y\epsilon \exp\left(\frac{1}{2}(1-r^2)\right), \quad B_y = +x\epsilon \exp\left(\frac{1}{2}(1-r^2)\right), \quad B_z = 0.$$

For the governing PDE system, we use the following parameters: $\gamma = 1.4$, $\rho_0 = 1$, $c_s = 0.8$, $\alpha^2 = 0.8$, $c = 100$, $\mu = \kappa = \eta = 10^{-6}$. The speed for the hyperbolic divergence cleaning in the GLM approach [31] is set to $c_h = 2$. The simulations are carried out with a fourth and fifth order accurate ADER-DG scheme until a final simulation time of $t = 0.1$ using a sequence of successively refined meshes. The exact solution of the underlying ideal MHD problem consists in a mere transport of the initial condition translated with velocity $\mathbf{v} = (1, 1, 0)$. This test is very difficult for the GPR model, since the system is run in a very stiff regime and with $c \gg 1$, so that the resulting time step is very small due to the CFL condition. For that reason, only a small final simulation time has been chosen.

The obtained numerical convergence rates are reported in Table 1, where we can observe that the schemes reach their designed order of accuracy even in the stiff relaxation limit, which is a very important property of the numerical method used here.

Table 1
Numerical convergence results for the magnetized vortex obtained with ADER-DG P_3 and P_4 schemes applied to the GPR model ($c_s = 0.8$, $\alpha^2 = 0.8$, $c = 100$) in the stiff relaxation limit ($\mu \ll 1, \kappa \ll 1, \eta \ll 1$). Results are shown for the magnetic field component B_x at a final time of $t = 0.1$. The reference solution is given by the exact solution of the ideal MHD equations.

N_x	$\epsilon(L_1)$	$\epsilon(L_2)$	$\epsilon(L_\infty)$	$\mathcal{O}(L_1)$	$\mathcal{O}(L_2)$	$\mathcal{O}(L_\infty)$
ADER-DG P_3 ($\mu = \kappa = \eta = 10^{-6}$)						
20	2.9646E−03	7.9141E−04	7.0490E−04			
30	3.7070E−04	1.0288E−04	9.3677E−05	5.13	5.03	4.98
40	8.9193E−05	2.4785E−05	2.1279E−05	4.95	4.95	5.15
50	2.9814E−05	8.2723E−06	7.8091E−06	4.91	4.92	4.49
ADER-DG P_4 ($\mu = \kappa = \eta = 10^{-6}$)						
8	2.4129E−02	5.2803E−03	4.2926E−03			
10	6.2946E−03	1.4070E−03	1.0618E−03	6.02	5.93	6.26
12	1.4985E−03	3.2871E−04	2.9132E−04	7.87	7.97	7.09
16	3.1902E−04	7.1927E−05	5.8008E−05	5.38	5.28	5.61

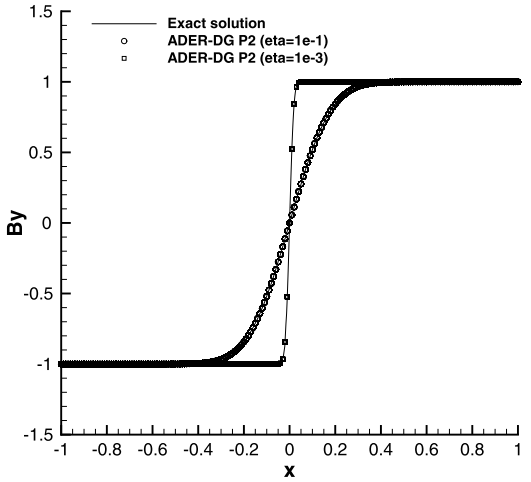

Fig. 1. Current sheet at time $t = 0.1$ simulated for different resistivities ($\eta = 10^{-1}$ and $\eta = 10^{-3}$) with the GPR model using an ADER-DG P_2 scheme.

7.2. Current sheet

Here, we simulate a simple current sheet, see [82,46], in order to verify the correct description of resistive effects by the model. The computational domain is defined as $\Omega = [-1, +1] \times [-0.1, +0.1]$ and the initial condition is given by $\rho = 1$, $\mathbf{v} = 0$, $\boldsymbol{A} = \mathbf{I}$, $\mathbf{J} = 0$, $p = 1$, $B_x = B_z = 0$ and $B_y = \text{sign}(x)$. The parameters for the simulation are $\rho_0 = 1$, $\gamma = 1.4$, $c_s = 0.8$, $\alpha^2 = 0.8$, $c = 10$, $\mu = \kappa = \eta$. In this test, two different values for the resistivity have been used, namely $\eta = 10^{-1}$ and $\eta = 10^{-3}$, respectively. The exact solution for the time evolution of the magnetic field component B_y in the current sheet is given by (see [82,46]):

$$B_y(x,t) = \text{erf}\left(\frac{x}{2\sqrt{\eta t}}\right).$$

A comparison between the exact solution and the numerical solution obtained with an ADER-DG P_2 method on a uniform grid composed of 100×5 grid points for both values of the resistivity is depicted at time $t = 0.1$ in Fig. 1, where an excellent agreement can be observed in both cases.

7.3. Riemann problems

While the previous test cases involved only smooth solutions, the Riemann problems solved in this section contain all different kinds of elementary flow discontinuities. The initial conditions for density, velocity, pressure and magnetic field together with the final simulation time t_e as well as the position of the initial discontinuity x_d are summarized in Table 2, while the initial data for the remaining variables are given by $\boldsymbol{A} = \sqrt[3]{\rho}\,\mathbf{I}$, $\mathbf{J} = 0$ and $\mathbf{E} = -\mathbf{v} \times \mathbf{B}$. The computational domain is $\Omega = [-0.5, +0.5] \times [-0.1, 0.1]$ and is discretized with an ADER-DG P_2 method using an adaptive Cartesian mesh (AMR) with initial resolution on the level zero grid of 100×4 cells. Two levels of refinement are admitted ($\ell_{\max} = 2$) with a refinement factor of $r = 3$ between two adjacent levels. Refinement and recoarsening are based on the density as indicator variable. For more details on the AMR implementation, in particular for high order ADER schemes in combination with

Table 2
Initial states left and right for the density ρ, velocity vector $\mathbf{v} = (u, v, w)$, the pressure p and the magnetic field vector $\mathbf{B} = (B_x, B_y, B_z)$. The final output times, (t_{end}) and the initial position of the discontinuity (x_d) are also given.

Case	ρ	u	v	w	p	B_x	B_y	B_z	t_e, x_d
RP1 L:	1.0	0.0	0.0	0.0	1.0	$\frac{3}{4}$	1	0.0	0.1
R:	0.125	0.0	0.0	0.0	0.1	$\frac{3}{4}$	-1	0.0	0.0
RP2 L:	1.08	1.2	0.01	0.5	0.95	0.564189	1.015541	0.564189	0.2
R:	0.9891	-0.0131	0.0269	0.010037	0.97159	0.564189	1.135262	0.564923	-0.1
RP3 L:	1.0	0.0	0.0	0.0	1.0	1.3	1	0.0	0.16
R:	0.4	0.0	0.0	0.0	0.4	1.3	-1	0.0	0.0

time-accurate local time stepping (LTS), see [47,145]. The model parameters used for the simulation are $\gamma = \frac{5}{3}$, $\rho_0 = 1$, $c_s = 0.8$, $\alpha^2 = 0.8$, $c = 10$ and $\mu = \kappa = \eta = 10^{-4}$, i.e. we are in a rather stiff regime of the model where a comparison with the ideal MHD equations is appropriate. The results obtained with the GPR model for density ρ and the magnetic field component B_y are depicted in Fig. 2 for all three problems, together with the exact solution of the Riemann problem of the ideal MHD equations. Overall, a good agreement can be noted, apart from the compound wave which can be observed in the density for RP1. This phenomenon is visible also in standard finite volume schemes applied to the ideal MHD equations, see e.g. [43].

7.4. MHD rotor problem

Here we solve the well-known MHD rotor problem originally proposed by Balsara and Spicer in [4] and later also used in many other papers on numerical methods for the ideal MHD equations. In this test problem, a rapidly rotating high density fluid (the rotor) is embedded in a low density atmosphere at rest. The fluid pressure and the magnetic field are initially constant everywhere. The rotor produces torsional Alfvén waves which travel into the outer fluid. The computational domain is defined as $\Omega = [-0.5, +0.5]^2$ and we use an ADER-DG P_2 scheme on a uniform Cartesian grid composed of 200×200 elements. The initial density is $\rho = 10$ inside the rotor ($0 \le r \le 0.1$) and $\rho = 1$ for the outer fluid. The velocity in the outer fluid is initially set to zero, while it is given by $\mathbf{v} = \boldsymbol{\omega} \times \mathbf{x}$ inside the rotor, with $\boldsymbol{\omega} = (0, 0, 10)$. The initial pressure is $p = 1$ and the magnetic field vector is set to $\mathbf{B} = (B_0, 0, 0)^T$ in the entire computational domain Ω, with $B_0 = \frac{2.5}{\sqrt{4\pi}}$. As proposed by Balsara and Spicer, a linear taper is applied to the velocity and density field between $0.1 \le r \le 0.105$. The other variables are initially set to $\boldsymbol{A} = \sqrt[3]{\rho}\,\mathbf{I}$, $\mathbf{J} = 0$ and $\mathbf{E} = -\mathbf{v} \times \mathbf{B}$. The speed for the hyperbolic divergence cleaning is set to $c_h = 2$ and the model parameters are $\gamma = 1.4$, $c = 10$, $\alpha^2 = 0.8$, $\rho_0 = 1$, $c_s = 0.8$ and $\mu = \kappa = \eta = 10^{-4}$, which make the system sufficiently stiff so that a comparison with the ideal MHD equations is possible. The results are depicted at time $t = 0.25$ in Fig. 3 for the usual quantities density, pressure, Mach number and magnetic pressure. The results agree qualitatively well with those reported by Balsara and Spicer in [4], as well as those reported in other papers on high order numerical methods for the ideal MHD equations, see e.g. [36,47].

7.5. MHD blast wave problem

The MHD blast wave problem is a very challenging test problem even for numerical schemes applied to the ideal MHD equations. Here, we solve the GPR model (74a)–(74g) in a rather stiff regime so that comparisons with numerical results obtained with the ideal MHD equations are possible. The computational domain is given by $\Omega = [-0.5, +0.5]^2$ and is discretized with an ADER-DG P_2 scheme on a uniform Cartesian grid using 200×200 elements. The initial data are $\rho = 1$, $\mathbf{v} = 0$ and $\mathbf{B} = (B_0, 0, 0)$ with $B_0 = \frac{100}{\sqrt{4\pi}}$. The pressure is set to $p = 1000$ in a small internal circular region ($r < 0.1$) and is $p = 0.1$ elsewhere, hence the pressure jumps over four orders of magnitude in this test problem. Furthermore, the fluid is highly magnetized due to the presence of a very strong magnetic field in the entire domain.

The other variables of the model are initially set to $\boldsymbol{A} = \sqrt[3]{\rho}\,\mathbf{I}$, $\mathbf{J} = 0$ and $\mathbf{E} = -\mathbf{v} \times \mathbf{B}$. The speed for the hyperbolic divergence cleaning is chosen as $c_h = 2$ and the model parameters are given by $\gamma = 1.4$, $c = 10$, $\alpha^2 = 0.8$, $\rho_0 = 1$, $c_s = 0.8$ and $\mu = \kappa = \eta = 10^{-3}$. The computational results are depicted at time $t = 0.01$ in Fig. 4 for the magnetic field component B_x, the fluid pressure p, the density ρ and the color map of the limited cells and unlimited cells in red and blue, respectively. For details on the finite volume subcell limiter, see [48,145,144]. The computational results agree qualitatively with those reported by Balsara and Spicer in [4].

7.6. Inviscid Orszag–Tang vortex system

In this section we study the well-known Orszag–Tang vortex system for the MHD equations [103,30,111], comparing the numerical results of the GPR model with those obtained with the ideal MHD equations. The setup is the one used in [77] and [36]. In both computations, the numerical method and the computational grid used are identical, as well as the initial conditions for the density, velocity, pressure and the magnetic field. The other variables of the GPR model are set to $\boldsymbol{A} = \sqrt[3]{\rho}\,\mathbf{I}$, $\mathbf{J} = 0$ and $\mathbf{E} = -\mathbf{v} \times \mathbf{B}$. The computational domain under consideration is $\Omega = [0, 2\pi]^2$ with four periodic boundary

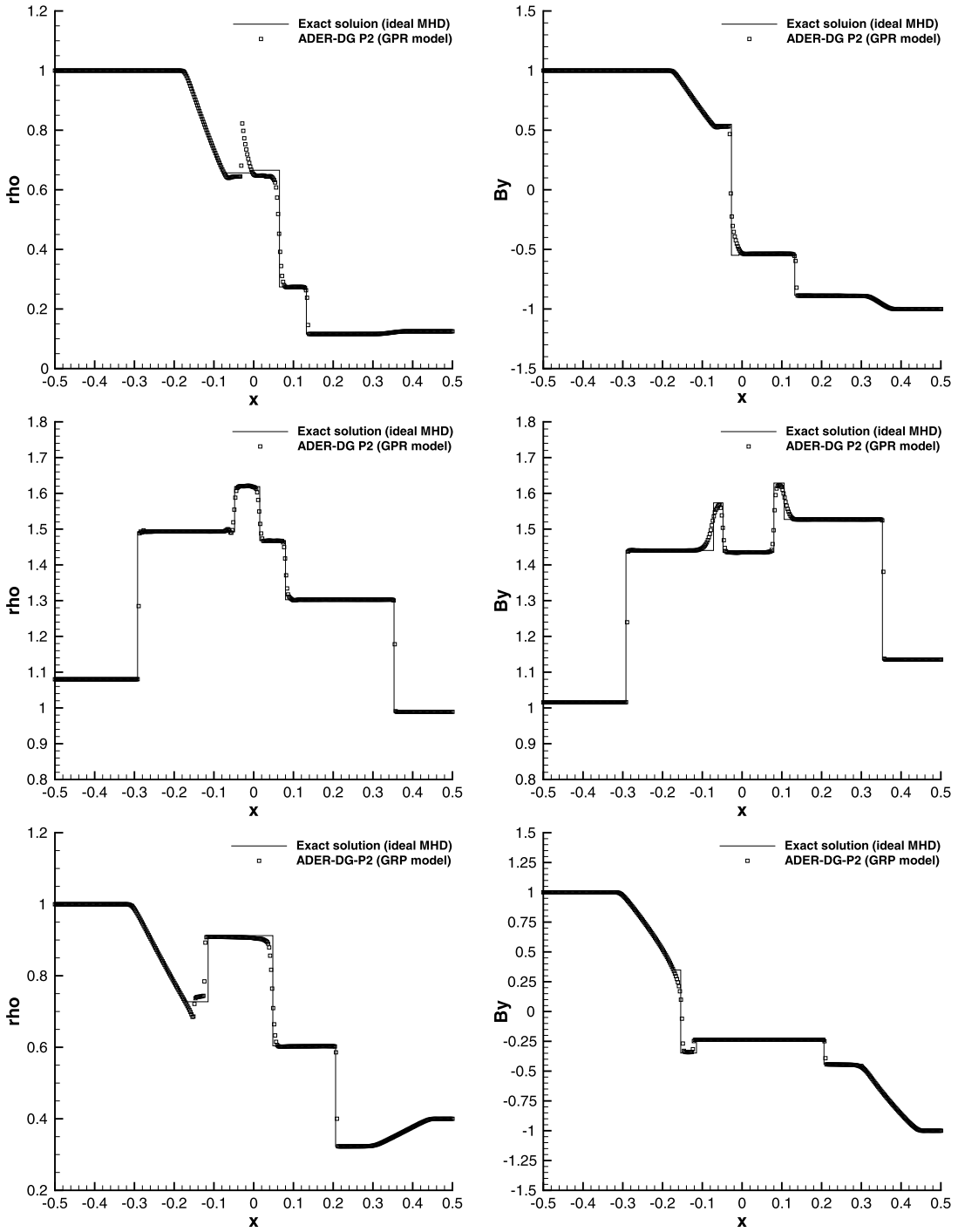

Fig. 2. MHD Riemann problems RP1 (top), RP2 (center) and RP3 (bottom) simulated with the GPR model ($\mu = \kappa = \eta = 10^{-4}$) using an ADER-DG P_2 scheme with AMR and comparison with the exact solution of the ideal MHD equations. The fluid density ρ (left) and the magnetic field component B_y (right) are depicted.

conditions and the initial conditions are given by $\rho = \gamma^2$, $\mathbf{v} = (-\sin(y), \sin(x), 0)$, $p = \gamma$ and $\mathbf{B} = (-\sin(y), \sin(2x), 0)$, with $\gamma = \frac{5}{3}$. The remaining parameters of the GPR model are $c = 10$, $\alpha^2 = 0.8$, $c_s = 0.8$, $c_h = 2$, $\rho_0 = 1$ and $\mu = \kappa = \eta = 10^{-4}$, so that the system is sufficiently stiff in order to allow a comparison with the ideal MHD equations. Simulations are carried out on a uniform Cartesian grid composed of 200×200 elements using an ADER-DG P_2 scheme until a final time of $t = 3$. The comparison between the computational results obtained with the GPR model and the ideal MHD equations is provided in

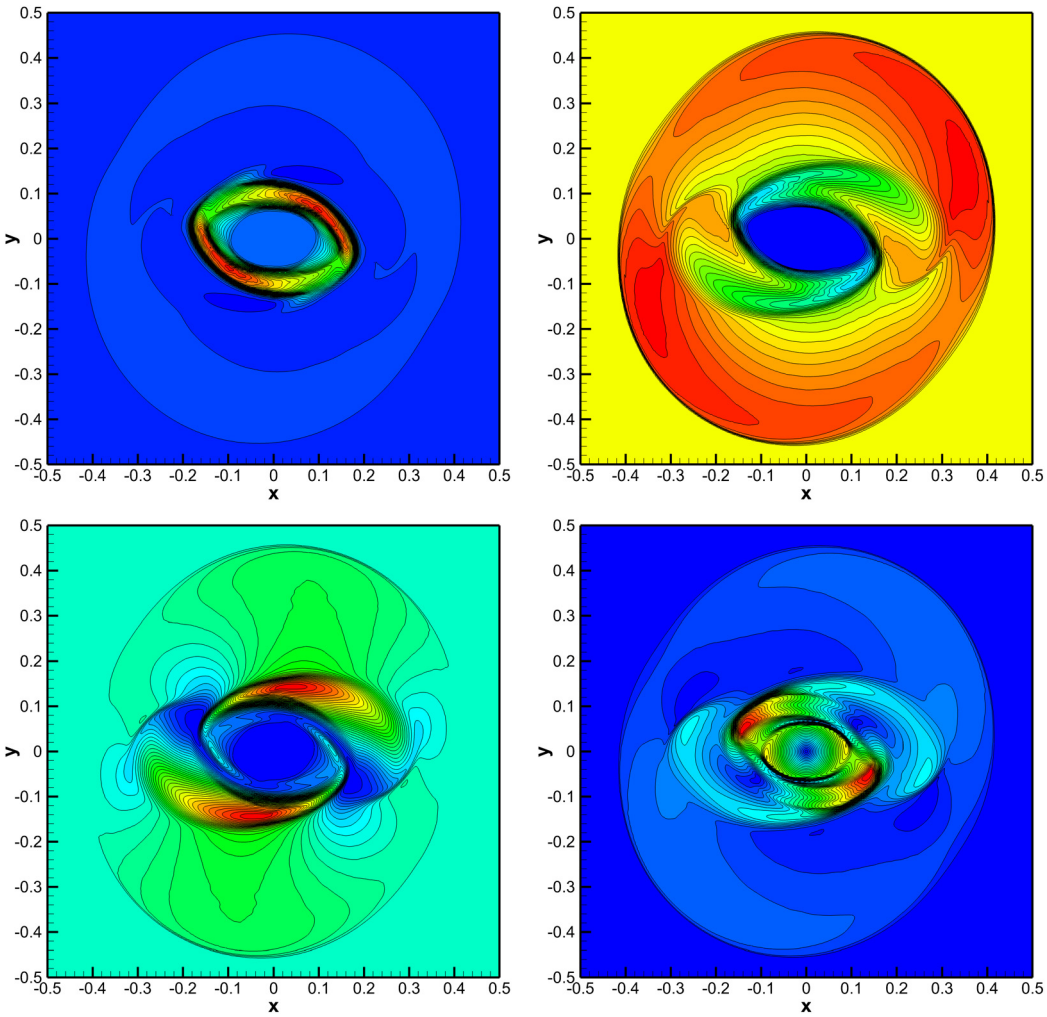

Fig. 3. MHD rotor problem at time $t = 0.25$ simulated with the GPR model ($\mu = \kappa = \eta = 10^{-4}$) using an ADER-DG P_2 scheme. The contours of fluid density ρ (top left), fluid pressure p (top right), magnetic pressure (bottom left) and Mach number (bottom right) are shown.

Fig. 5. A very good agreement between the two solutions can be noted, even for later times when the solution has already developed many small scale structures. We stress that in both cases two completely different PDE systems have been solved.

7.7. Viscous and resistive Orszag–Tang vortex

We now solve the Orszag–Tang vortex system in a highly viscous and resistive regime, where the computational results of the GPR model are compared with those of the *viscous* and *resistive* MHD equations (VRMHD). The computational setup of this test case is taken from [140] and [37]. The computational domain is again $\Omega = [0, 2\pi]^2$ with four periodic boundary conditions and the common initial condition for both models is given this time by $\rho = 1$, $\mathbf{v} = (-\sin(y), \sin(x), 0)$, $\mathbf{B} = (-\sin(y), \sin(2x), 0)$, $p = \frac{15}{4} + \frac{1}{4}\cos(4x) + \frac{4}{5}\cos(2x)\cos(y) - \cos(x)\cos(y) + \frac{1}{4}\cos(2y)$. The ratio of specific heats is set to $\gamma = \frac{5}{3}$. The other variables of the GPR model are set to $\boldsymbol{A} = \mathbf{I}$, $\mathbf{J} = 0$ and $\mathbf{E} = -\mathbf{v} \times \mathbf{B}$. We choose $\mu = \eta = 10^{-2}$ and a Prandtl number of $Pr = 1$ based on the heat capacity at constant volume of $c_v = 1$, leading to a heat conduction coefficient of $\kappa = \gamma\mu$.

For the GPR model, we run the test problem until $t = 2$ with an ADER-DG P_3 scheme on a uniform Cartesian grid composed of 200×200 elements, while the numerical solution of the viscous and resistive MHD equations has been taken directly from [37], where an eighth order P_4P_7 scheme has been used to solve the VRMHD equations on a very coarse unstructured triangular mesh composed of only 990 triangles. The direct comparison between the first order hyperbolic GPR model and the second order hyperbolic–parabolic VRMHD model is provided in Fig. 6, where the velocity streamlines as well as the magnetic field lines are plotted. Overall, we can observe an excellent agreement between the two computational results, which have been obtained by solving two completely different PDE systems and using two different mesh topologies (Cartesian grid versus an unstructured simplex mesh).

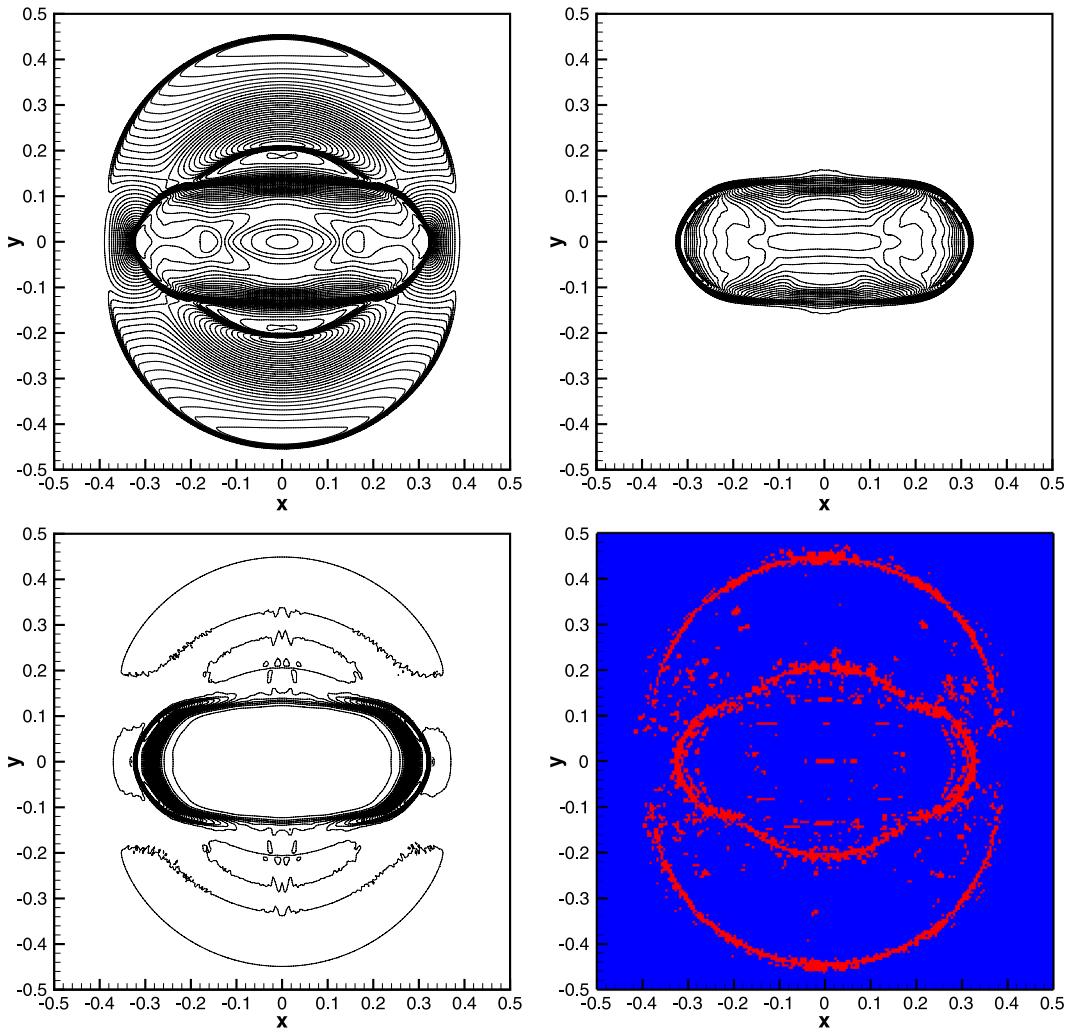

Fig. 4. MHD blast wave problem at time $t = 0.01$ using the GPR model ($\mu = \kappa = \eta = 10^{-3}$) and an ADER-DG P_2 scheme. The contours of the magnetic field component b_x (top left), the fluid pressure p (top right) and the fluid density ρ (bottom left) are shown, together with a map of troubled zones in red that use the subcell finite volume limiter of the ADER-DG P_2 scheme, while unlimited cells are colored in blue (bottom right). (For interpretation of the references to color in this figure legend, the reader is referred to the web version of this article.)

7.8. Kelvin–Helmholtz instability in a viscous and resistive magnetized fluid

This test problem concerns the simulation of the Kelvin–Helmholtz instability in a magnetized fluid. As in the previous test, we solve the problem with the first order hyperbolic GPR model and with the viscous and resistive MHD equations (VRMHD). The setup of the initial conditions of the problem is taken from [37] and references therein: $\rho = 1$, $p = \frac{3}{5}$, $\gamma = \frac{5}{3}$, $\mathbf{v} = (u, v, 0)$ with $u = -\frac{1}{2} U_0 \tanh\left(\frac{y-0.5}{a}\right)$ and $v = \delta v \sin(2\pi x)\sin(\pi y)$. The magnetic field is given by

$$\mathbf{B} = \begin{cases} (B_0, 0, 0), & \text{if} \quad \frac{1}{2} + a < y < 1, \\ (B_0 \sin(\chi), 0, B_0 \cos(\chi)), & \text{if} \quad \frac{1}{2} - a < y < \frac{1}{2} + a, \\ (0, 0, B_0), & \text{if} \quad 0 < y < \frac{1}{2} - a, \end{cases}$$

with $\chi = \frac{\pi}{2} \frac{y-0.5+a}{2a}$, $a = \frac{1}{25}$, $U_0 = 1$, $\delta v = 0.01$ and $B_0 = 0.07$. The computational domain is $\Omega = [0, 1] \times [-1, 1]$ with periodic boundary conditions in the x direction and is discretized with an ADER-DG P_2 scheme using 200×400 elements for both PDE models, i.e. for the first order hyperbolic GPR system and for the viscous and resistive MHD model (VRMHD). The physical parameters are $\mu = \eta = 10^{-3}$, $\kappa = 0$, i.e. heat conduction is neglected in this test. The remaining parameters of the GPR model are set to $c = 2$, $\alpha = 0$, $c_s = 0.8$, $c_h = 2$ and $\rho_0 = 1$. The computational results are shown in Fig. 7, where an

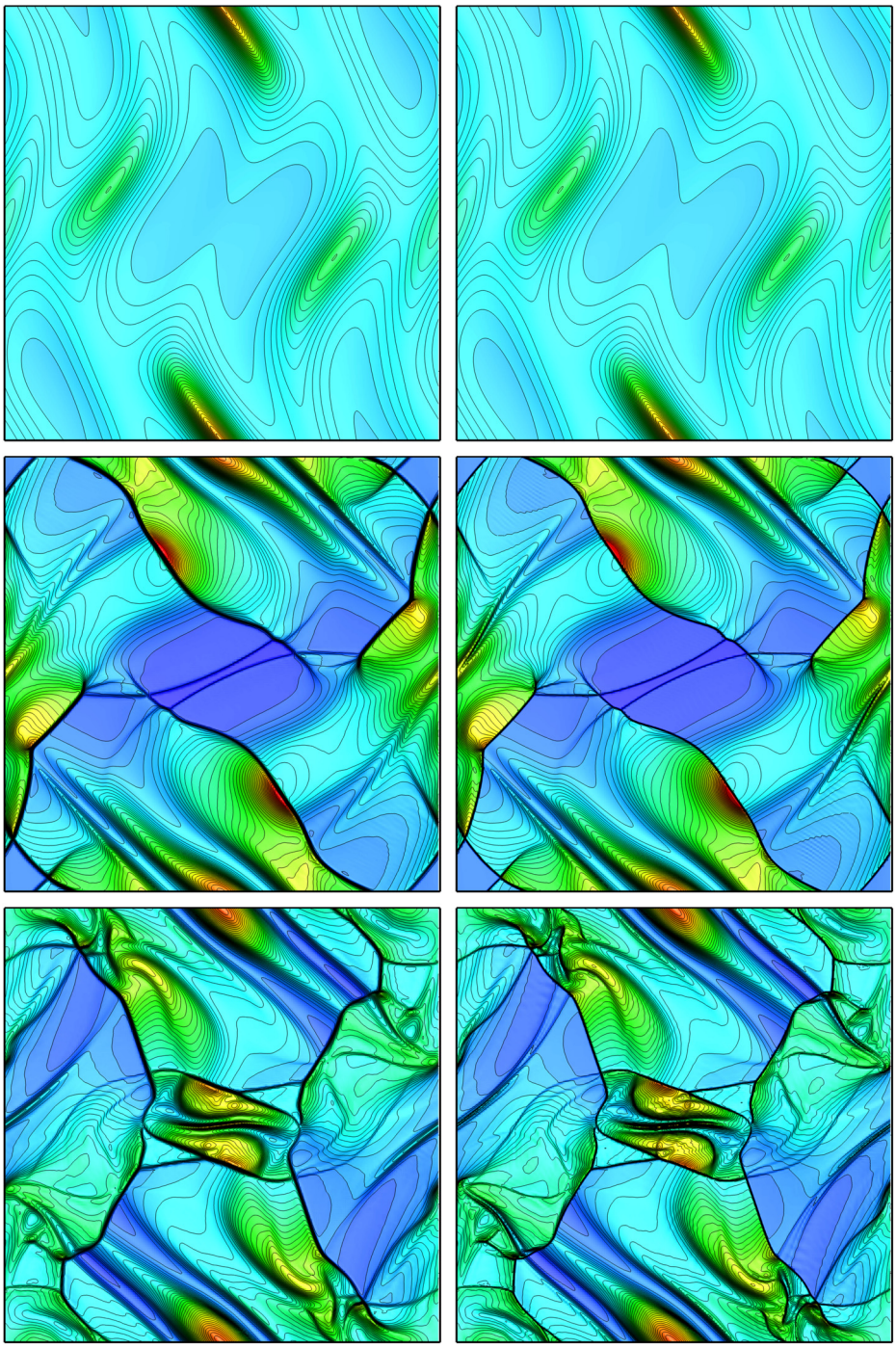

Fig. 5. Orszag–Tang vortex problem at output times $t = 0.5$, $t = 2.0$ and $t = 3.0$ from top to bottom. Left column: GPR model ($\mu = \kappa = \eta = 10^{-4}$). Right column: ideal MHD equations for a direct comparison.

excellent agreement between the GPR results and the VRMHD results can be noted. One can clearly see the development of the so-called cat-eye vortices and the thin filaments connecting the individual vortices. For a detailed discussion of the MHD Kelvin–Helmholtz instability, see [81] and [76]. In Fig. 8 we also show two components of the distortion $\boldsymbol{A}$, which is the key quantity of the GPR model that allows the computation of the stress tensor in the case of both, fluids and solids. As already emphasized in [42], the distortion $\boldsymbol{A}$ is very well suited for flow visualization.

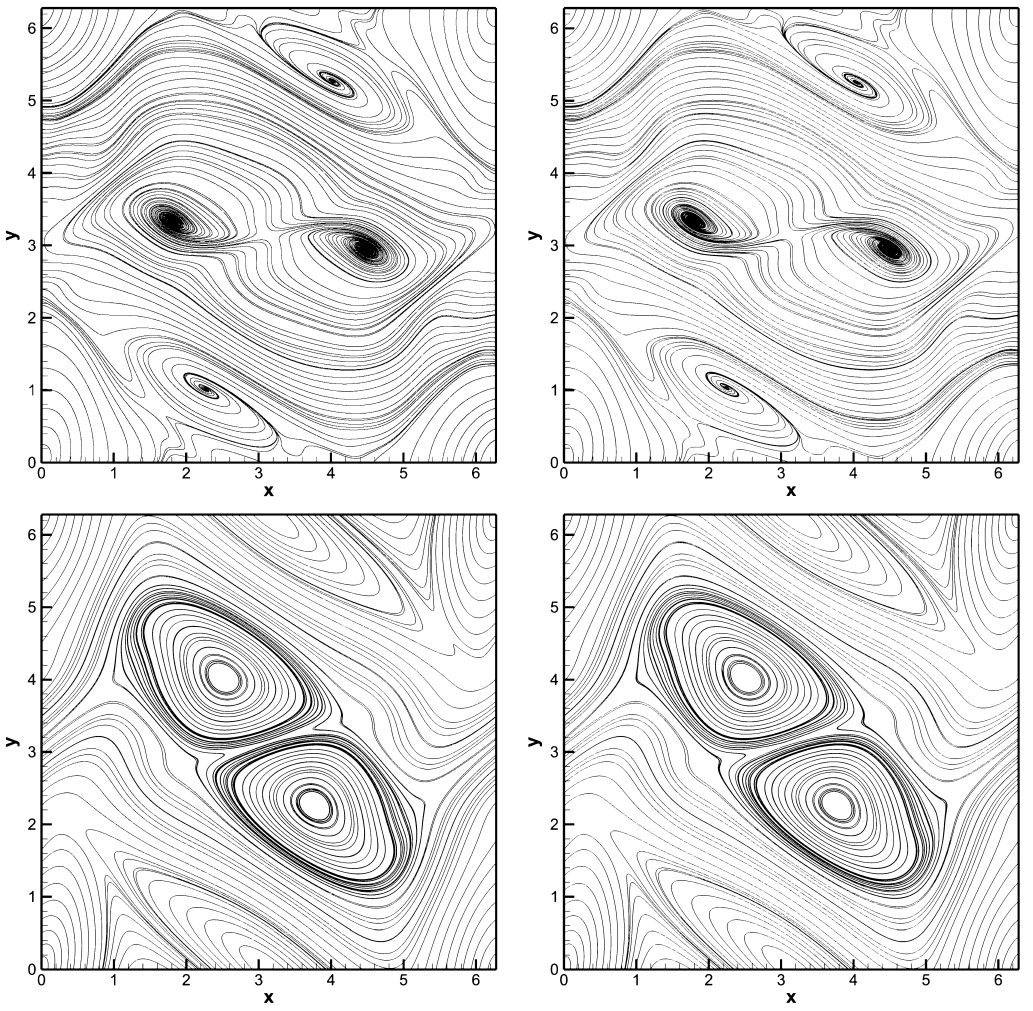

Fig. 6. Viscous Orszag–Tang vortex problem ($\mu = \eta = 10^{-2}$, $Pr = 1$) at time $t = 2.0$. First order hyperbolic GPR model (left) and classical VRMHD equations (right) for direct comparison. Velocity streamlines (top) and magnetic field lines (bottom).

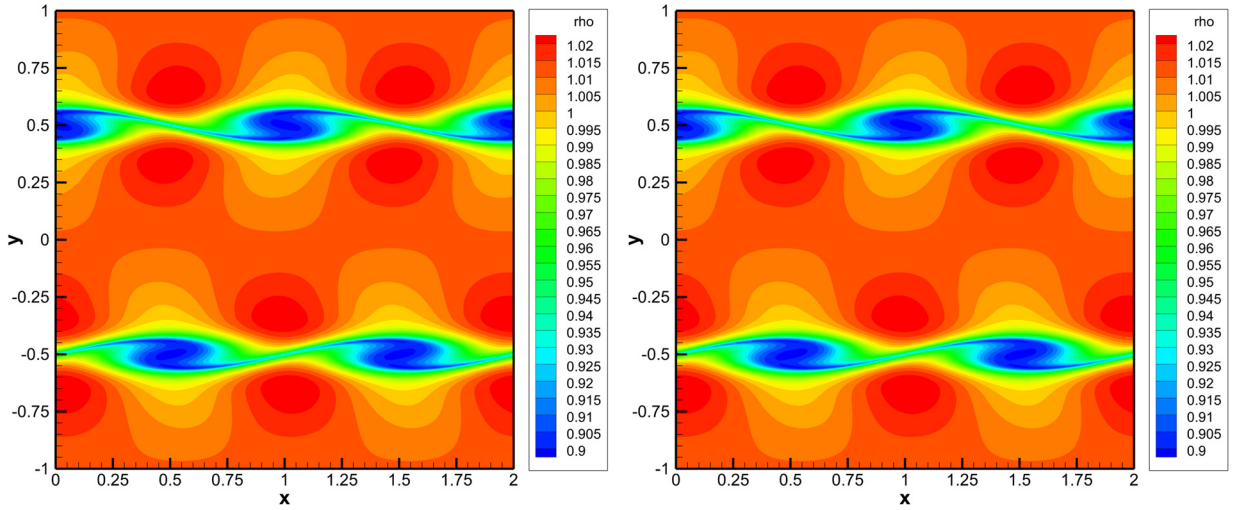

Fig. 7. Kelvin–Helmholtz instability in a viscous and resistive magnetized fluid ($\mu = \eta = 10^{-3}$, $\kappa = 0$) at time $t = 4.0$. Density contours obtained with an ADER-DG P_3 scheme for the first order hyperbolic GPR model (left) and for the VRMHD equations (right).

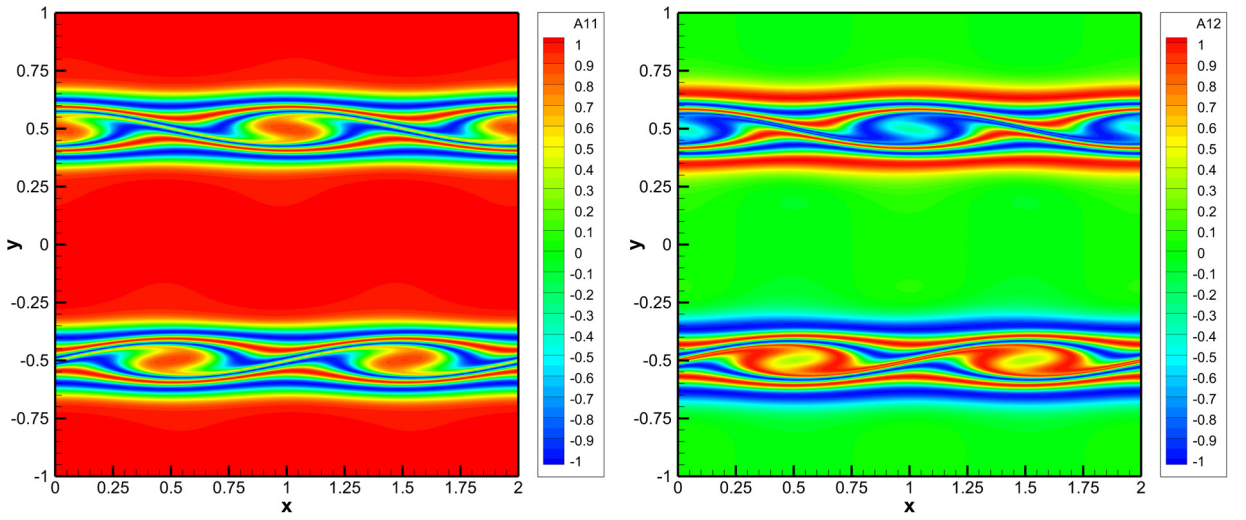

Fig. 8. Kelvin–Helmholtz instability in a viscous and resistive magnetized fluid ($\mu = \eta = 10^{-3}$, $\kappa = 0$) at time $t = 4.0$. Contours of the distortion components A_{11} (left) and A_{12} (right) for the first order hyperbolic GPR model.

7.9. High Lundquist number magnetic reconnection

As next test problem we consider the case of a high Lundquist number magnetic reconnection. Reconnection occurs in unstable current sheets due to the tearing instability that generates so-called plasmoid chains, see e.g. [13,86,125,84]. For investigations of magnetic reconnection in the resistive relativistic case see [143], where high order ADER schemes similar to those employed in the present paper have been used [46].

The computational domain is given by $\Omega = [-25a, 25a] \times [-L/2, L/2]$, where L is the length of the domain, $a = L/S^{1/3}$ is the width of the current sheet and the Lundquist number is $S = Lv_a/\eta$, with the Alfvén speed v_a. The initial condition for the magnetic field is

$$\mathbf{B} = (0, B_0 \tanh(x/a), B_0 \operatorname{sech}(x/a)), \tag{130}$$

with the relation between B_0 and v_a given by $v_a^2 = B_0^2/\rho$. The initial fluid pressure is set to $p = \rho/(\gamma M^2)$, where $M = v_a/c_0$ is the magnetic Mach number and c_0 is the sound speed. For our test we use $\rho = 1$, $v_a = L = 1$, $\gamma = 5/3$, $M = 0.7$ and $S = 10^6$, hence the thickness of the current sheet is $a = 0.01$, while the plasma parameter β is given by $\beta = 2.4$. The instability is triggered by adding a small perturbation to the velocity field of the form

$$u = \varepsilon \tanh\xi \exp(-\xi^2) \cos(ky) \tag{131}$$

$$v = \varepsilon (2\xi \tanh\xi - \operatorname{sech}^2\xi) \exp(-\xi^2) S^{1/2} \sin(ky)/k, \tag{132}$$

where $\varepsilon = 10^{-3}$, $\xi = xS^{1/2}$ and the wave-number is computed from $kL = 2\pi m$, with $m = 10$. Free outflow and periodic boundary conditions are chosen along the x and y direction, respectively. The remaining variables and parameters of the GPR model are set to $\boldsymbol{A} = \sqrt[3]{\rho}\mathbf{I}$, $\mathbf{J} = 0$, $\mathbf{E} = -\mathbf{v} \times \mathbf{B}$, $c = 2$, $c_h = 2$, $\rho_0 = 1$, $c_s = \alpha = 0$, $\mu = \kappa = 0$. Simulations have been carried out until a final time of $t = 5.5$ using an ADER-DG P_2 scheme with *a posteriori* subcell finite volume limiter [48,145, 144] on a uniform Cartesian grid composed of 200×400 elements. In Fig. 9 the computational results for density, magnetic field component B_y and for two components of the distortion $\boldsymbol{A}$ are shown. One can clearly see the formation of a main *reconnection island* or *major plasmoid*, which has the usual form similar to that observed also in other simulations reported in the literature [84,52].

7.10. Scattering of a plane wave

Here, we run the GPR model inside a solid medium at rest in the limit $\tau_1 \to \infty$, $\tau_2 \to \infty$ and $\eta \to \infty$, i.e. without source terms. Hence, one expects to recover the behavior of the classical Maxwell equations concerning electromagnetic wave propagation. We therefore run the following test case twice, once with the full GPR model (74a)–(74g), and once with the standard time domain Maxwell equations in a laboratory frame at rest. For high order ADER-DG schemes applied to the Maxwell equations, see [129]. The computational domain for this test problem is $\Omega = [-2.5, +2.5]^2$ with four periodic boundary conditions. The initial electric and magnetic field vectors are set to $\mathbf{E} = (0, 0, E_0 \sin(kx))$ and $\mathbf{B} = (0, -B_0 \sin(kx), 0)$, with $k = 4\pi$ and $E_0 = B_0 = 0.1$, while the remaining variables of the GPR model are initially set to $\rho = 1$, $p = 1$, $\mathbf{v} = \mathbf{J} = 0$ and $\boldsymbol{A} = \mathbf{I}$. The light speed is set to $c = c_o = 1$ everywhere in Ω, apart from a small cylindrical inclusion of radius $R = 0.25$, where it has been set to $c = c_i = 2$. In order to avoid spurious oscillations, the transition has

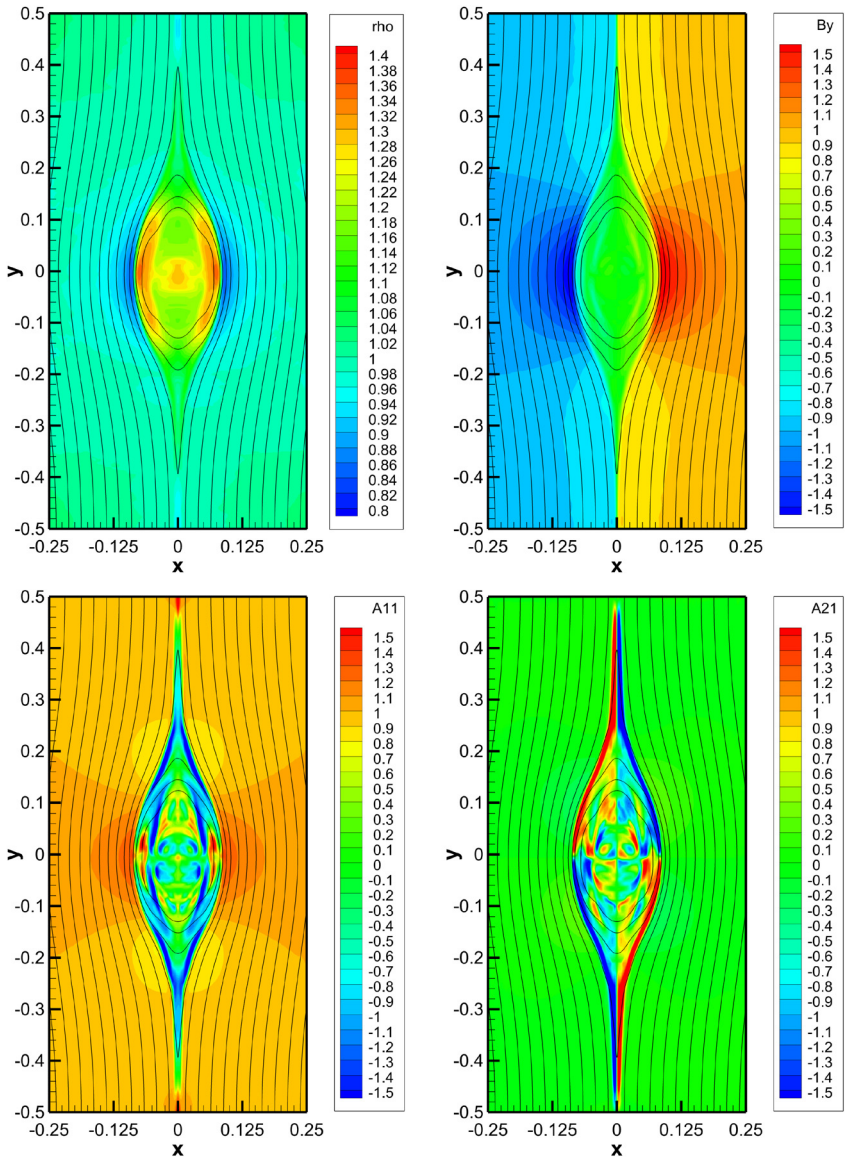

Fig. 9. High Lundquist number magnetic reconnection ($\eta = 10^{-6}$, $\mu = \kappa = 0$) at time $t = 5.5$. Results obtained for the first order hyperbolic GPR model with an ADER-DG P_2 scheme. Density (top left), magnetic field component B_y (top right), distortion components A_{11} (bottom left) and A_{21} (bottom right). The magnetic field lines are also shown.

been smoothed by setting $c(r) = c_i(1-\xi) + c_o\xi$, with $\xi = \frac{1}{2}(1 + \mathrm{erf}((r-R)/\delta))$ and $\delta = 0.05$. The remaining parameters in the GPR model are chosen as $\gamma = 1.4$, $\tau_1 = \tau_2 = \eta = 10^{20}$, $c_h = 2$, $c_s = 0.8$, $\alpha^2 = 0.8$ and $\rho_0 = 1$. The problem is run with an unlimited ADER-DG P_3 scheme on a uniform Cartesian grid composed of 100×100 elements until a final time of $t = 2.0$, so that the scattered waves have not yet reached the boundaries. In Fig. 10, the computational results obtained with the GPR model are compared to those of the standard Maxwell equations. Overall, a very good agreement can be noted between the two different models, both, for the contour plot of B_x that represents the scattered wave field, as well as for the time series recorded in the four observation points $\mathbf{x}_1 = (-1, 0)$, $\mathbf{x}_2 = (+1, 0)$, $\mathbf{x}_3 = (0, -1)$ and $\mathbf{x}_4 = (0, +1)$.

7.11. Comparison of different model regimes

In this last example we explore the behavior of the GPR model in a large range of relaxation parameters, from the regime of a viscous and conducting magnetized fluid (case I, $\tau_1 \ll 1$, $\tau_2 \ll 1$, $\eta \ll 1$) over an electrically conducting elastic solid (case II, $\tau_1 \to \infty$, $\tau_2 \to \infty$, $\eta \ll 1$) to a non-conducting elastic solid (case III, $\tau_1 \to \infty$, $\tau_2 \to \infty$, $\eta \to \infty$). The initial data are essentially the same as for the MHD rotor problem solved in Section 7.4, i.e. density is set to $\rho = 1$ in the ambient fluid and $\rho = 10$ inside the rotor of radius $R = 0.1$, while the initial pressure is constant everywhere $p = 1$. The magnetic field vector

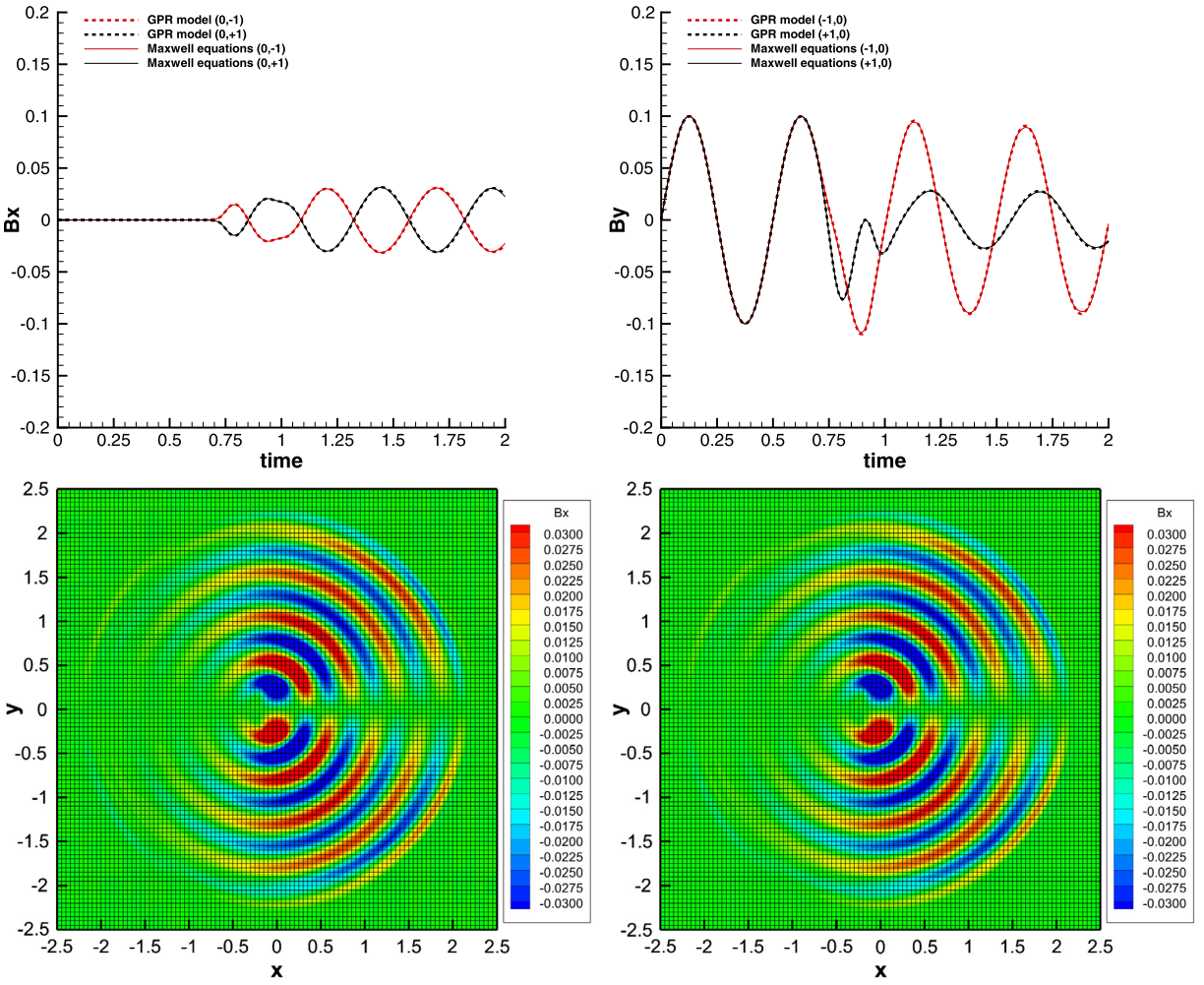

Fig. 10. Scattering of a planar EM wave ($k = 4\pi$) at a cylindrical inclusion of radius $R = 0.25$. The light speed is $c = 1$ in the ambient medium, while it is $c = 2$ inside the inclusion. Comparison of the GPR model with the Maxwell equations using an ADER-DG P_3 scheme. Time series of the magnetic field components B_x (top left) and B_y (top right) registered in four observation points. Contour plot of the magnetic field component B_x at time $t = 2.0$ using the GPR model (bottom left) and the Maxwell equations (bottom right).

Table 3
Relaxation parameters of the GPR model used for the three different cases under consideration ($c_s = 0.8$, $\alpha^2 = 0.8$, $c = 4$).

	Case I (viscous and resistive fluid)	Case II (conducting elastic solid)	Case III (non-conducting elastic solid)
τ_1	10^{-3}	10^{20}	10^{20}
τ_2	10^{-3}	10^{20}	10^{20}
η	10^{-3}	10^{-3}	10^{20}

is set to $\mathbf{B} = (B_0, 0, 0)^T$ in the entire computational domain Ω, with $B_0 = \frac{2.5}{\sqrt{4\pi}}$ and the velocity is zero in the ambient fluid and $\mathbf{v} = \boldsymbol{\omega} \times \mathbf{x}$ inside the rotor, with $\boldsymbol{\omega} = (0, 0, 10)$. In this test we use a light speed of $c = 4$ and the stiffened gas equation of state [42] with $p_0 = 1$. Furthermore, the reference density inside the rotor is chosen as $\rho_0 = 10$ so that the initial condition for the distortion is simply given by $\boldsymbol{A} = \mathbf{I}$. Furthermore, we initially set $\mathbf{J} = 0$ and $\mathbf{E} = -\mathbf{v} \times \mathbf{B}$. The computational domain is $\Omega = [-1.25, +1.25]^2$, covered with a uniform Cartesian grid of 400×400 elements. All simulations are carried out with a third order ADER-WENO finite volume scheme [47] and are run up to a final time of $t = 0.25$. The parameters used for the three cases under consideration are summarized in Table 3.

The computational results are depicted in Fig. 11. We can see that in the case of electrically conducting material $\eta \ll 1$, the magnetic field is tight to the main pressure and shear waves arising in the medium, while in the case of an infinitely resistive or electrically non-conducting solid ($\eta \to \infty$), the electro-magnetic waves travel at the speed of light, independently of the other waves present in the medium. One can also clearly observe the effect of elasticity in the case of an elastic solid,

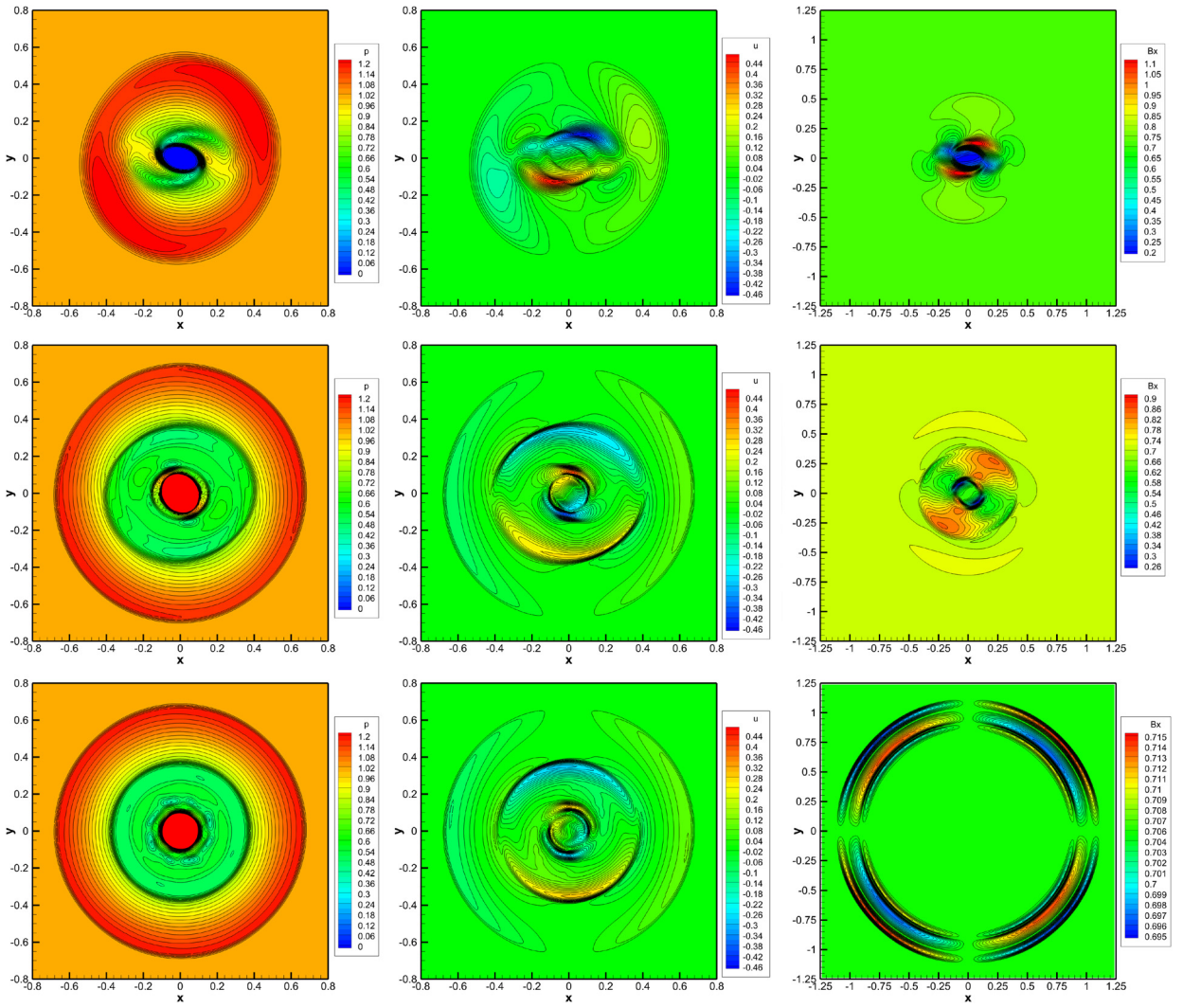

Fig. 11. Rotor problem in different regimes of the relaxation parameters. Case I: viscous and conducting magnetized fluid (top row). Case II: magnetized electrically conducting elastic solid (middle row). Case III: magnetized electrically non-conducting elastic solid (bottom row). The contours of pressure (left column), velocity component u (middle column) and magnetic field component B_x are reported.

since the rotor starts to oscillate and produce shear waves that are not visible in the case of the magnetized fluid, see the middle column of Fig. 11. A similar behavior of the velocity field in elastic bodies has already been observed in [36].

8. Conclusions

We have presented a new unified first order *symmetric hyperbolic* and thermodynamically compatible (SHTC) model for the description of continuous media like fluids and solids interacting with electro-magnetic fields. The theoretical foundations of the model have been shown in great detail, in particular the connection of the final Eulerian form of model to the Euler–Lagrange differential equations associated with the underlying variational principle governed by the minimization of a Lagrangian. In the SHTC framework, the dissipative terms are *not* modeled by classical parabolic differential operators (as for example in the Navier–Stokes or in the viscous and resistive MHD equations), but via *algebraic* relaxation source terms, like the Ohm law in the case of electro-magnetic wave propagation in conducting media. In the SHTC framework, the same idea is also used to model dissipative momentum and heat transfer. The model satisfies the first and second principle of thermodynamics. It has also been shown via formal asymptotic analysis that in the stiff relaxation limit our first order hyperbolic system of PDEs reduces to the classical viscous and resistive MHD equations. A particular feature of the governing PDE system presented in this paper is the fact that all wave speeds remain *finite*, even in the stiff relaxation limit when the relaxation parameters τ_1, τ_2 and η tend to zero. This makes the model a potential candidate for a possible future extension to the more general case of special and general *relativistic* continuum mechanics, in particular for the description of viscous and resistive relativistic fluids, where all propagation speeds in the medium must be necessarily bounded from above by the

speed of light in order to obtain a causal theory. In absence of relaxation source terms ($\tau_1 \to \infty$, $\tau_2 \to \infty$, $\eta \to \infty$), the PDE system proposed in this paper describes the propagation of electromagnetic waves in moving, electrically non-conducting dielectric media.

Future investigations will concern a more detailed study of the coupling between the stress tensor and the electromagnetic field, as it appears, for example, in piezoelectric actuators. For that purpose, the coupling between the distortion and the electro-magnetic field needs to be considered within the generating potential. Further work is also needed concerning the development of new numerical methods which are able to preserve *all* stationary compatibility conditions, i.e. those on the matrix $\boldsymbol{A}$ and on the electro-magnetic fields *exactly* also at the discrete level. Finally, also the introduction of dispersive effects where the speed of propagation of electro-magnetic waves depends on the wave number will be subject to future research.

Acknowledgements

The research presented in this paper has been financed by the European Research Council (ERC) under the European Union's Seventh Framework Programme (FP7/2007–2013) with the research project *STiMulUs*, ERC Grant agreement No. 278267. M.D. and O.Z. have further received funding from the European Union's Horizon 2020 Research and Innovation Programme under the project *ExaHyPE*, grant agreement No. 671698 (call FETHPC-1-2014). E.R. acknowledges a partial support by the Program N15 of the Presidium of RAS, project 121. I.P. acknowledges a partial support by ANR-11-LABX-0040-CIMI within the program ANR-11-IDEX-0002-02 and the Russian Foundation for Basic Research (grant number 16-31-00146).

The authors are grateful to the Leibniz Rechenzentrum (LRZ) for awarding access to the SuperMUC supercomputer based in Munich, Germany and to the HLRS supercomputing center in Stuttgart, Germany, for awarding access to the Hazel Hen supercomputer.

The authors would also like to thank the anonymous referee of the manuscript for his insightful, encouraging and constructive comments that helped to improve the quality of the paper.

We also would like to thank Sergei Konstantinovich Godunov for his groundbreaking and very inspiring seminal ideas that are at the basis of both the theoretical as well as the numerical framework employed in this paper.

Appendix A. Connection of the SHTC model with the Maxwell equations

We start from the Maxwell equations in the **laboratory frame**, which are universally accepted to be true:

$$\frac{\partial \mathbf{D}}{\partial t} - \nabla \times \mathbf{H} = -\mathbf{I} \tag{A.1a}$$

$$\frac{\partial \mathbf{B}}{\partial t} + \nabla \times \mathbf{E} = 0, \tag{A.1b}$$

with the constitutive relations

$$\mathbf{D} = \epsilon' \mathbf{E} \qquad \text{and} \qquad \mathbf{B} = \mu' \mathbf{H}. \tag{A.2}$$

From (A.1) and (A.2) one obtains

$$\frac{\partial}{\partial t}\left(\epsilon' \mathbf{E}\right) - \nabla \times \mathbf{H} = -\mathbf{I} \tag{A.3a}$$

$$\frac{\partial}{\partial t}\left(\mu' \mathbf{H}\right) + \nabla \times \mathbf{E} = 0, \tag{A.3b}$$

Here, $\mu' = \mu_0 \mu_r$ denotes the magnetic permeability of the medium (not to be confounded with the fluid viscosity μ), given as a product of the magnetic permeability of vacuum μ_0 and the relative permeability μ_r. The electric permittivity is denoted by $\epsilon' = \epsilon_0 \epsilon_r$, where ϵ_0 is the electric permittivity of vacuum and ϵ_r is the relative permittivity of the medium. In (A.1) the electric current $\mathbf{I}$ is given by the usual Ohm law

$$\mathbf{I} = \rho_c \mathbf{v} + \sigma \left(\mathbf{E} + \mathbf{v} \times \mathbf{B}\right), \tag{A.4}$$

with the conductivity $\sigma = 1/\eta$ and the resistivity η. The charge density is $\rho_c = \epsilon' \nabla \cdot \mathbf{E}$. We furthermore have the standard relation between the speed of light in the medium c, the magnetic permeability and the electric permittivity of the medium:

$$c^2 = \frac{1}{\epsilon' \mu'}. \tag{A.5}$$

We now make the following change of variables

$$\mathbf{d} = \mathbf{E} + \mathbf{v} \times \mathbf{B}, \tag{A.6a}$$

$$\mathbf{b} = \mathbf{H} - \mathbf{v} \times \mathbf{D} = \mathbf{H} - \frac{\mathbf{v} \times \mathbf{E}}{\mu' c^2} = \frac{1}{\mu'}\left(\mathbf{B} - \frac{\mathbf{v} \times \mathbf{E}}{c^2}\right), \tag{A.6b}$$

where $\mathbf{d}$ and $\mathbf{b}$ denote respectively the electric and the magnetic field in the **comoving frame** K' that moves with velocity $\mathbf{v}$. Substituting (A.6) into (A.1) yields

$$\frac{\partial}{\partial t}\left[\epsilon'\left(\mathbf{d}-\mathbf{v}\times\mathbf{B}\right)\right]-\nabla\times\left(\mathbf{b}+\frac{\mathbf{v}\times\mathbf{E}}{\mu' c^2}\right)=-\sigma\mathbf{d}-\epsilon'\mathbf{v}\nabla\cdot\mathbf{E}, \tag{A.7a}$$

$$\frac{\partial}{\partial t}\left[\mu'\left(\mathbf{b}+\frac{\mathbf{v}\times\mathbf{E}}{\mu' c^2}\right)\right]+\nabla\times\left(\mathbf{d}-\mathbf{v}\times\mathbf{B}\right)=0. \tag{A.7b}$$

We now substitute (A.6) also into the remaining terms of (A.7), hence obtaining

$$\frac{\partial}{\partial t}\left[\epsilon'\left(\mathbf{d}-\mathbf{v}\times\left(\mu'\mathbf{b}+\frac{\mathbf{v}\times\mathbf{E}}{c^2}\right)\right)\right]+\nabla\times\left(-\mathbf{b}-\frac{\mathbf{v}\times\left(\mathbf{d}-\mathbf{v}\times\mathbf{B}\right)}{\mu' c^2}\right)=-\sigma\mathbf{d}-\epsilon'\mathbf{v}\nabla\cdot\mathbf{E}, \tag{A.8a}$$

$$\frac{\partial}{\partial t}\left[\mu'\left(\mathbf{b}+\frac{\mathbf{v}\times\left(\mathbf{d}-\mathbf{v}\times\mathbf{B}\right)}{\mu' c^2}\right)\right]+\nabla\times\left(\mathbf{d}-\mathbf{v}\times\left(\mu'\mathbf{b}+\frac{\mathbf{v}\times\mathbf{E}}{c^2}\right)\right)=0. \tag{A.8b}$$

The above equations are still fully consistent with the relativistic equations; *no assumptions* have been made so far, only a change of variables. The formal structure is still exactly the same as the one of the original Maxwell equations (A.1). We now insert (A.6) once more into the fluxes of (A.8), which yields

$$\frac{\partial}{\partial t}\left[\epsilon'\left(\mathbf{d}-\mathbf{v}\times\left(\mu'\mathbf{b}+\frac{\mathbf{v}\times\mathbf{E}}{c^2}\right)\right)\right]+\nabla\times\left(-\mathbf{b}-\frac{\mathbf{v}\times\left(\mathbf{d}-\mathbf{v}\times\left(\mu'\mathbf{b}+\frac{\mathbf{v}\times\mathbf{E}}{c^2}\right)\right)}{\mu' c^2}\right)=-\sigma\mathbf{d}-\epsilon'\mathbf{v}\nabla\cdot\mathbf{E}, \tag{A.9a}$$

$$\frac{\partial}{\partial t}\left[\mu'\left(\mathbf{b}+\frac{\mathbf{v}\times\left(\mathbf{d}-\mathbf{v}\times\mathbf{B}\right)}{\mu' c^2}\right)\right]+\nabla\times\left(\mathbf{d}-\mathbf{v}\times\left(\mu'\mathbf{b}+\frac{\mathbf{v}\times\left(\mathbf{d}-\mathbf{v}\times\mathbf{B}\right)}{c^2}\right)\right)=0. \tag{A.9b}$$

With the auxiliary variables

$$\mathbf{e}':=\epsilon'\left(\mathbf{d}-\mathbf{v}\times\left(\mu'\mathbf{b}+\frac{\mathbf{v}\times\mathbf{E}}{c^2}\right)\right)=\epsilon'\left(\mathbf{d}-\mu'\mathbf{v}\times\mathbf{b}-\frac{1}{c^2}\mathbf{v}\times\left(\mathbf{v}\times\mathbf{E}\right)\right), \tag{A.10a}$$

$$\mathbf{h}':=\mu'\mathbf{b}+\frac{\mathbf{v}\times\left(\mathbf{d}-\mathbf{v}\times\mathbf{B}\right)}{c^2}=\mu'\mathbf{b}+\frac{\mathbf{v}\times\mathbf{d}}{c^2}-\frac{1}{c^2}\mathbf{v}\times\left(\mathbf{v}\times\mathbf{B}\right), \tag{A.10b}$$

the system (A.9) can be rewritten as

$$\frac{\partial\mathbf{e}'}{\partial t}+\nabla\times\left(-\mathbf{v}\times\mathbf{e}'-\mathbf{b}\right)=-\sigma\mathbf{d}-\epsilon'\mathbf{v}\nabla\cdot\mathbf{E}, \tag{A.11a}$$

$$\frac{\partial\mathbf{h}'}{\partial t}+\nabla\times\left(-\mathbf{v}\times\mathbf{h}'+\mathbf{d}\right)=0. \tag{A.11b}$$

We now assume that $\mathbf{v}^2/c^2\ll 1$, hence we neglect quadratic terms in $\mathbf{v}/c$. This allows us to define the new simplified conserved variables

$$\mathbf{e}:=\epsilon'\mathbf{d}-\epsilon'\mu'\mathbf{v}\times\mathbf{b}\approx\mathbf{e}', \tag{A.12a}$$

$$\mathbf{h}:=\mu'\mathbf{b}+\epsilon'\mu'\mathbf{v}\times\mathbf{d}\approx\mathbf{h}', \tag{A.12b}$$

which yields the following *simplified* system, where we have also used the identity $\nabla\cdot\mathbf{B}=0$ and where again quadratic terms in $\mathbf{v}/c$ have been neglected in the final expressions:

$$\frac{\partial\mathbf{e}}{\partial t}+\nabla\times\left(-\mathbf{v}\times\mathbf{e}-\mathbf{b}\right)+\mathbf{v}\nabla\cdot\mathbf{e}=-\sigma\mathbf{d}, \tag{A.13a}$$

$$\frac{\partial\mathbf{h}}{\partial t}+\nabla\times\left(-\mathbf{v}\times\mathbf{h}+\mathbf{d}\right)+\mathbf{v}\nabla\cdot\mathbf{h}=0. \tag{A.13b}$$

The above system is written in the form given in [119]. Note that compared to [119], the consistency with the Maxwell equations in the laboratory frame requires the following definition of the generating potential for electro-magnetic energy density:

$$L_{em}=\frac{1}{2}\left(\mu'\mathbf{b}^2+\epsilon'\mathbf{d}^2\right)+\epsilon'\mu'\mathbf{v}\cdot\left(\mathbf{d}\times\mathbf{b}\right)=\frac{1}{2}\left(\mu' b_i b_i+\epsilon' d_i d_i\right)+\epsilon'\mu'\,\varepsilon_{ijk}v_i d_j b_k, \tag{A.14}$$

since we must have that

$$e_i=\frac{\partial L_{em}}{\partial d_i}=\epsilon' d_i-\epsilon'\mu'\,\varepsilon_{ijk}v_j b_k, \tag{A.15}$$

$$h_i=\frac{\partial L_{em}}{\partial b_i}=\mu' b_i+\epsilon'\mu'\,\varepsilon_{ijk}v_j d_k. \tag{A.16}$$

Using (A.12) and (A.6) the variables $\mathbf{e}$ and $\mathbf{h}$ can be expressed in terms of the electro-magnetic field quantities in the laboratory frame as follows:

$$\mathbf{e} = \epsilon' \left(\mathbf{E} + \frac{1}{c^2} \mathbf{v} \times \mathbf{v} \times \mathbf{E} \right), \qquad \text{and} \qquad \mathbf{h} = \mu' \mathbf{H} + \frac{1}{c^2} \mathbf{v} \times \mathbf{v} \times \mathbf{E}, \tag{A.17}$$

which together with (A.2) reduces to the simple identities

$$\mathbf{e} = \mathbf{D}, \qquad \text{and} \qquad \mathbf{h} = \mathbf{B}, \tag{A.18}$$

if quadratic terms in $\mathbf{v}/c$ are again neglected in (A.17).

Appendix B. Euler-to-Lagrange field transformation

In this section, we demonstrate how to obtain Eulerian equations (37d)–(37e) for electromagnetic fields e_i and h_i from their Lagrangian counterparts (18c)–(18d). However, it is more convenient to chose the opposite strategy. Namely, we derive the Lagrangian field equations from the Eulerian. Thus, if one likes to get the Lagrange-to-Euler derivation then the calculations should be repeated from the end to the beginning of what follows. Recall that in (18c)–(18d) we use the same notations e_i and h_i for the fields however they are different. As we mentioned earlier and as will be proven in what follows, the Eulerian and Lagrangian fields are related by (40). As discussed in Section 2, in the structure study, we can ignore the algebraic source terms as they are low order terms.

B.1. Auxiliary relations

Here, we summarize the definitions and formulas used in this section. The total deformation gradient $\boldsymbol{F} = [F_{ij}]$, the distortion matrix $\boldsymbol{A} = [A_{ij}]$ and the velocity are defined as

$$F_{ij} = \frac{\partial x_i}{\partial y_j}, \qquad \boldsymbol{A} = \boldsymbol{F}^{-1}, \qquad w = \det(\boldsymbol{F}) = \frac{\rho_0}{\rho}, \qquad v_i = \frac{\mathrm{d}x_i}{\mathrm{d}t}, \tag{B.1}$$

where, as previously, y_j are the Lagrangian coordinates and x_i are the Eulerian ones, ρ and ρ_0 are the actual and the reference mass densities, respectively. The time evolution equation for F_{ij} in the Lagrangian coordinates

$$\frac{\mathrm{d}F_{ij}}{\mathrm{d}t} - \frac{\partial v_i}{\partial y_j} = 0 \tag{B.2}$$

is a trivial consequence of definitions (B.1).

The following standard definitions and formulas are also introduced

$$\boldsymbol{C} = \operatorname{cof}(\boldsymbol{F}) = w \boldsymbol{A}^{\mathrm{T}} = \left[C_{ij} \right], \quad \text{or} \quad A_{ij} = w^{-1} C_{ji}, \tag{B.3}$$

$$\frac{\partial C_{ij}}{\partial y_j} = 0, \qquad \varepsilon_{mjp} \frac{\partial F_{mp}}{\partial y_j} = 0, \tag{B.4}$$

$$\frac{\mathrm{d}w}{\mathrm{d}t} - \frac{\partial w A_{jk} v_k}{\partial y_j} = 0, \text{ or using (B.3) and (B.4):} \quad \frac{\mathrm{d}w}{\mathrm{d}t} - w A_{jk} \frac{\partial v_k}{\partial y_j} = 0, \tag{B.5}$$

$$\varepsilon_{ikl} A_{mi} A_{jk} A_{al} = \varepsilon_{mja} w^{-1}, \tag{B.6}$$

$$C_{km} = \frac{1}{2} \varepsilon_{lnk} \varepsilon_{pqm} F_{lp} F_{nq}, \tag{B.7}$$

$$\varepsilon_{imn} \varepsilon_{jmn} = 2 \delta_{ij}. \tag{B.8}$$

B.2. Transformation of (37d)–(37e) to (18c)–(18d)

We shall transform (37d) into (18c) while (37e) transforms into (18d) analogously. Thus, (37d) is equivalent to

$$\frac{\partial e_i}{\partial t} + v_k \frac{\partial e_i}{\partial x_k} + \frac{\partial v_k}{\partial x_k} e_i - \frac{\partial v_i}{\partial x_k} e_k - \varepsilon_{ikl} \frac{\partial \mathcal{E}_{h_l}}{\partial x_k} = 0. \tag{B.9}$$

Using $\mathrm{d}/\mathrm{d}t = \partial/\partial t + v_k/\partial x_k$ we have

$$\frac{\mathrm{d}e_i}{\mathrm{d}t} + \frac{\partial v_k}{\partial x_k} e_i - \frac{\partial v_i}{\partial x_k} e_k - \varepsilon_{ikl} \frac{\partial \mathcal{E}_{h_l}}{\partial x_k} = 0. \tag{B.10}$$

From (B.1) it follows that $\frac{\partial}{\partial x_k} = A_{jk} \frac{\partial}{\partial y_j}$ and thus we change the variables x_k on y_j

$$\frac{\mathrm{d}e_i}{\mathrm{d}t} + A_{jk}\frac{\partial v_k}{\partial y_j}e_i - A_{jk}\frac{\partial v_i}{\partial y_j}e_k - \varepsilon_{ikl}A_{jk}\frac{\partial \mathcal{E}_{h_l}}{\partial y_j} = 0. \tag{B.11}$$

Applying $(B.5)_2$ to the second term and (B.2) to the third term of the last equation, we have

$$\frac{\mathrm{d}e_i}{\mathrm{d}t} + \frac{1}{w}\frac{\mathrm{d}w}{\mathrm{d}t}e_i - A_{jk}\frac{\mathrm{d}F_{ij}}{\mathrm{d}t}e_k - \varepsilon_{ikl}A_{jk}\frac{\partial E_{h_l}}{\partial y_j} = 0, \tag{B.12}$$

$$\frac{\mathrm{d}we_i}{\mathrm{d}t} - we_k A_{jk}\frac{\mathrm{d}F_{ij}}{\mathrm{d}t} - w\varepsilon_{ikl}A_{jk}\frac{\partial \mathcal{E}_{h_l}}{\partial y_j} = 0. \tag{B.13}$$

Now, we add $0 \equiv we_k\dfrac{\mathrm{d}\delta_{ik}}{\mathrm{d}t}$ to the left hand side and then using that $\delta_{ik} = F_{ij}A_{jk}$ one can obtain that

$$\frac{\mathrm{d}we_i}{\mathrm{d}t} + we_k\frac{\mathrm{d}\delta_{ik}}{\mathrm{d}t} - we_k A_{jk}\frac{\mathrm{d}F_{ij}}{\mathrm{d}t} - w\varepsilon_{ikl}A_{jk}\frac{\partial \mathcal{E}_{h_l}}{\partial y_j} = 0, \tag{B.14}$$

$$\frac{\mathrm{d}we_i}{\mathrm{d}t} + we_k\frac{\mathrm{d}F_{ij}A_{jk}}{\mathrm{d}t} - we_k A_{jk}\frac{\mathrm{d}F_{ij}}{\mathrm{d}t} - w\varepsilon_{ikl}A_{jk}\frac{\partial \mathcal{E}_{h_l}}{\partial y_j} = 0, \tag{B.15}$$

$$\frac{\mathrm{d}we_i}{\mathrm{d}t} + we_k F_{ij}\frac{\mathrm{d}A_{jk}}{\mathrm{d}t} + we_k\frac{\mathrm{d}F_{ij}}{\mathrm{d}t}A_{jk} - we_k A_{jk}\frac{\mathrm{d}F_{ij}}{\mathrm{d}t} - w\varepsilon_{ikl}A_{jk}\frac{\partial \mathcal{E}_{h_l}}{\partial y_j} = 0. \tag{B.16}$$

After multiplying the last equation by A_{mi}

$$A_{mi}\left(\frac{\mathrm{d}we_i}{\mathrm{d}t} + we_k F_{ij}\frac{\mathrm{d}A_{jk}}{\mathrm{d}t} - w\varepsilon_{ikl}A_{jk}\frac{\partial \mathcal{E}_{h_l}}{\partial y_j}\right) = 0, \tag{B.17}$$

$$A_{mi}\frac{\mathrm{d}we_i}{\mathrm{d}t} + we_k\frac{\mathrm{d}A_{mk}}{\mathrm{d}t} - w\varepsilon_{ikl}A_{mi}A_{jk}\frac{\partial \mathcal{E}_{h_l}}{\partial y_j} = 0, \tag{B.18}$$

we have an intermediate result:

$$\frac{\mathrm{d}wA_{mk}e_k}{\mathrm{d}t} - w\varepsilon_{ikl}A_{mi}A_{jk}\frac{\partial \mathcal{E}_{h_l}}{\partial y_j} = 0. \tag{B.19}$$

Now, we introduce the change of unknowns (40): $wA_{mk}e_k = e'_m$, $wA_{mk}h_k = h'_m$, and we also change the energy potential $\mathcal{E}(e_i, h_i) = \mathcal{E}(w^{-1}F_{ij}e'_j, w^{-1}F_{ij}h'_j) = w^{-1}U(e'_j, h'_j)$. Hence, $\mathcal{E}_{h_i} = A_{ji}U_{h'_j}$. After this, the intermediate result (B.19) reads as

$$\frac{\mathrm{d}e'_m}{\mathrm{d}t} - w\varepsilon_{ikl}A_{mi}A_{jk}\frac{\partial A_{al}U_{h'_a}}{\partial y_j} = 0, \tag{B.20}$$

$$\frac{\mathrm{d}e'_m}{\mathrm{d}t} - w\varepsilon_{ikl}A_{mi}A_{jk}A_{al}\frac{\partial U_{h'_a}}{\partial y_j} - w\varepsilon_{ikl}A_{mi}A_{jk}\frac{\partial A_{al}}{\partial y_j}U_{h'_a} = 0. \tag{B.21}$$

Applying (B.6) and $(B.3)_3$ to the second term, we get

$$\frac{\mathrm{d}e'_m}{\mathrm{d}t} - \varepsilon_{mja}\frac{\partial U_{h'_a}}{\partial y_j} - w\varepsilon_{ikl}A_{mi}A_{jk}\frac{\partial A_{al}}{\partial y_j}U_{h'_a} = 0. \tag{B.22}$$

Now using the cofactor definition (B.3) and then applying (B.7) to the third term, we have

$$\frac{\mathrm{d}e'_m}{\mathrm{d}t} - \varepsilon_{mja}\frac{\partial U_{h'_a}}{\partial y_j} - \varepsilon_{ikl}A_{mi}C_{kj}\frac{\partial A_{al}}{\partial y_j}U_{h'_a} = 0, \tag{B.23}$$

$$\frac{\mathrm{d}e'_m}{\mathrm{d}t} - \varepsilon_{mja}\frac{\partial U_{h'_a}}{\partial y_j} - \frac{1}{2}\varepsilon_{ikl}\varepsilon_{lnk}\varepsilon_{pqj}F_{lp}F_{nq}A_{mi}\frac{\partial A_{al}}{\partial y_j}U_{h'_a} = 0. \tag{B.24}$$

Using (B.8) in the third term gives us

$$\frac{\mathrm{d}e'_m}{\mathrm{d}t} - \varepsilon_{mja}\frac{\partial U_{h'_a}}{\partial y_j} - \delta_{in}\varepsilon_{pqj}F_{lp}F_{nq}A_{mi}\frac{\partial A_{al}}{\partial y_j}U_{h'_a} = 0, \tag{B.25}$$

and subsequently,

$$\frac{\mathrm{d}e'_m}{\mathrm{d}t} - \varepsilon_{mja}\frac{\partial U_{h'_a}}{\partial y_j} - \varepsilon_{pqj}F_{lp}F_{iq}A_{mi}\frac{\partial A_{al}}{\partial y_j}U_{h'_a} = 0, \tag{B.26}$$

$$\frac{\mathrm{d}e'_m}{\mathrm{d}t} - \varepsilon_{mja}\frac{\partial U_{h'_a}}{\partial y_j} - \varepsilon_{mjp}F_{lp}\frac{\partial A_{al}}{\partial y_j}U_{h'_a} = 0. \tag{B.27}$$

Now, adding $0 \equiv \varepsilon_{mjp}\frac{\partial F_{lp}}{\partial y_j}A_{al}U_{h'_a}$ (see $(B.4)_2$), we get

$$\frac{\mathrm{d}e'_m}{\mathrm{d}t} - \varepsilon_{mja}\frac{\partial U_{h'_a}}{\partial y_j} - \varepsilon_{mjp}F_{lp}\frac{\partial A_{al}}{\partial y_j}U_{h'_a} - \varepsilon_{mjp}\frac{\partial F_{lp}}{\partial y_j}A_{al}U_{h'_a} = 0, \tag{B.28}$$

$$\frac{\mathrm{d}e'_m}{\mathrm{d}t} - \varepsilon_{mja}\frac{\partial U_{h'_a}}{\partial y_j} - U_{h'_a}\left(\varepsilon_{mjp}\frac{\partial A_{al}F_{lp}}{\partial y_j}\right) = 0, \tag{B.29}$$

$$\frac{\mathrm{d}e'_m}{\mathrm{d}t} - \varepsilon_{mja}\frac{\partial U_{h'_a}}{\partial y_j} - U_{h'_a}\left(\varepsilon_{mjp}\frac{\partial \delta_{ap}}{\partial y_j}\right) = 0. \tag{B.30}$$

Eventually, we have

$$\frac{\mathrm{d}e'_m}{\mathrm{d}t} - \varepsilon_{mja}\frac{\partial U_{h'_a}}{\partial y_j} = 0, \tag{B.31}$$

which is identical to (18c).

Appendix C. Euler-to-Lagrange momentum transformation

In this section, we shall use m'_i to denote the Lagrangian momentum and e'_i and h'_i to denote Lagrangian electro-magnetic fields, i.e. exactly those vector fields appearing in (18a), (18c) and (18d). Now, (18a) reads as

$$\frac{\mathrm{d}m'_i}{\mathrm{d}t} - \frac{\partial U_{F_{ij}}}{\partial y_j} = 0. \tag{C.1}$$

Using that $\mathrm{d}/\mathrm{d}t = \partial/\partial t + v_k\partial/\partial x_k$ and $F_{ij} = \partial x_i/\partial y_j$, equation (C.1) can be rewritten as

$$\frac{\partial m'_i}{\partial t} + v_k\frac{\partial m'_i}{\partial x_k} - F_{kj}\frac{\partial U_{F_{ij}}}{\partial x_k} = 0. \tag{C.2}$$

Subsequently, using the Eulerian stationary constraint for F_{ij} and time evolution of $w = \det(\boldsymbol{F})$ (e.g. see [72])

$$\frac{\partial w^{-1}F_{kj}}{\partial x_k} = 0, \quad \frac{\partial}{\partial t}\left(\frac{1}{w}\right) + \frac{\partial}{\partial x_k}\left(\frac{v_k}{w}\right) = 0, \tag{C.3}$$

(C.2) can be rewritten as

$$\frac{\partial}{\partial t}\left(\frac{m'_i}{w}\right) + \frac{\partial}{\partial x_k}\left(\frac{v_k m'_i - F_{kj}U_{F_{ij}}}{w}\right) = 0. \tag{C.4}$$

Finally, introducing the change of the variables $m_i = w^{-1}m'_i$, $wA_{mk}e_k = e'_m$ and $wA_{mk}h_k = h'_m$ and the change of the potential $\mathcal{E}(\rho, m_i, e_i, h_i, F_{ij}) = w^{-1}U(m'_i, e'_i, h'_i, F_{ij})$, equation (C.4) transforms into equation (37b).

References

[1] F. Abalos, F. Carrasco, E. Goulart, O. Reula, Nonlinear electrodynamics as a symmetric hyperbolic system, Phys. Rev. D 92 (2015) 084024.
[2] M. Abraham, Zur Elektrodynamik bewegter Körper, Rend. Circ. Mat. Palermo 28 (1) (1909) 1–28.
[3] D. Balsara, Second-order accurate schemes for magnetohydrodynamics with divergence-free reconstruction, Astrophys. J. Suppl. Ser. 151 (2004) 149–184.
[4] D. Balsara, D. Spicer, A staggered mesh algorithm using high order Godunov fluxes to ensure solenoidal magnetic fields in magnetohydrodynamic simulations, J. Comput. Phys. 149 (1999) 270–292.
[5] D.S. Balsara, A two-dimensional HLLC Riemann solver for conservation laws: application to Euler and magnetohydrodynamic flows, J. Comput. Phys. 231 (2012) 7476–7503.

[6] D.S. Balsara, Multidimensional Riemann problem with self-similar internal structure. Part I – application to hyperbolic conservation laws on structured meshes, J. Comput. Phys. 277 (2014) 163–200.
[7] D.S. Balsara, M. Dumbser, Divergence-free MHD on unstructured meshes using high order finite volume schemes based on multidimensional Riemann solvers, J. Comput. Phys. 299 (2015) 687–715.
[8] D.S. Balsara, C. Meyer, M. Dumbser, H. Du, Z. Xu, Efficient implementation of ADER schemes for Euler and magnetohydrodynamical flows on structured meshes – speed comparisons with Runge–Kutta methods, J. Comput. Phys. 235 (2013) 934–969.
[9] P.T. Barton, R. Deiterding, D. Meiron, D. Pullin, Eulerian adaptive finite-difference method for high-velocity impact and penetration problems, J. Comput. Phys. 240 (2013) 76–99.
[10] P.T. Barton, D. Drikakis, E.I. Romenski, An Eulerian finite-volume scheme for large elastoplastic deformations in solids, Int. J. Numer. Methods Eng. 81 (4) (2010) 453–484.
[11] H. Baty, H. Nishikawa, Hyperbolic method for magnetic reconnection process in steady state magnetohydrodynamics, Mon. Not. R. Astron. Soc. 459 (2016) 624–637.
[12] S. Benzoni-Gavage, D. Serre, Multidimensional Hyperbolic Partial Differential Equations, Oxford University Press, Oxford, 2007.
[13] D. Biskamp, Magnetic reconnection via current sheets, Phys. Fluids 29 (1986) 1520–1531.
[14] A.V. Bobylev, The Chapman–Enskog and Grad methods for solving the Boltzmann equation, Dokl. Akad. Nauk SSSR 262 (1982) 71–75.
[15] G. Boillat, Sur l'existence et la recherche d'équations de conservation supplément aires pour les systémes hyperboliques, C. R. Acad. Sci. Paris, Sér. A 278 (1974).
[16] D. Bolmatov, V.V. Brazhkin, K. Trachenko, Thermodynamic behaviour of supercritical matter, Nat. Commun. 4 (2013).
[17] D. Bolmatov, M. Zhernenkov, D. Zav'yalov, S. Stoupin, Y.Q. Cai, A. Cunsolo, Revealing the mechanism of the viscous-to-elastic crossover in liquids, J. Phys. Chem. Lett. 6 (15) (2015) 3048–3053.
[18] V.V. Brazhkin, Yu D. Fomin, A.G. Lyapin, V.N. Ryzhov, K. Trachenko, Two liquid states of matter: a dynamic line on a phase diagram, Phys. Rev. E 85 (3) (2012) 031203.
[19] S. Brown, P. Roe, C. Groth, Numerical Solution of a 10-Moment Model for Nonequilibrium Gasdynamics, in: 12th Computational Fluid Dynamics Conference San Diego, CA, USA, AIAA paper no. AIAA-95-1677-CP, 1995.
[20] C. Buet, B. Després, Asymptotic preserving and positive schemes for radiation hydrodynamics, J. Comput. Phys. 215 (2) (2006) 717–740.
[21] E. Burman, L. Sainsaulieu, Numerical analysis of two operator splitting methods for an hyperbolic system of conservation laws with stiff relaxation, Comput. Methods Appl. Mech. Eng. 128 (1995) 291–314.
[22] R.E. Caflish, S. Jin, G. Russo, Uniformly accurate schemes for hyperbolic systems with relaxation, SIAM J. Numer. Anal. 34 (1997) 246–281.
[23] M.J. Castro, J.M. Gallardo, A. Marquina, Approximate Osher–Solomon schemes for hyperbolic systems, Appl. Math. Comput. 272 (2016) 347–368.
[24] M.J. Castro, J.M. Gallardo, C. Parés, High-order finite volume schemes based on reconstruction of states for solving hyperbolic systems with nonconservative products. applications to shallow-water systems, Math. Comput. 75 (2006) 1103–1134.
[25] C. Cattaneo, Sulla conduzione del calore, Atti Semin. Mat. Fis. Univ. Modena 3 (1948).
[26] G.Q. Chen, C.D. Levermore, T.P. Liu, Hyperbolic conservation laws with relaxation terms and entropy, Commun. Pure Appl. Math. 47 (6) (1994) 787–830.
[27] S. Clain, S. Diot, R. Loubère, A high-order finite volume method for systems of conservation laws—multi-dimensional optimal order detection (MOOD), J. Comput. Phys. 230 (10) (2011) 4028–4050.
[28] B.D. Coleman, E.H. Dill, Thermodynamic restrictions on the constitutive equations of electromagnetic theory, Z. Angew. Math. Phys. 22 (4) (July 1971) 691–702.
[29] C.M. Dafermos, Hyperbolic Conservation Laws in Continuum Physics, Springer-Verlag, Berlin, 2005.
[30] R.B. Dahlburg, J.M. Picone, Evolution of the Orszag–Tang vortex system in a compressible medium. I. Initial average subsonic flow, Phys. Fluids B 1 (1989) 2153–2171.
[31] A. Dedner, F. Kemm, D. Kröner, C.-D. Munz, T. Schnitzer, M. Wesenberg, Hyperbolic divergence cleaning for the MHD equations, J. Comput. Phys. 175 (2002) 645–673.
[32] S. Diot, S. Clain, R. Loubère, Improved detection criteria for the multi-dimensional optimal order detection (MOOD) on unstructured meshes with very high-order polynomials, Comput. Fluids 64 (2012) 43–63.
[33] S. Diot, R. Loubère, S. Clain, The MOOD method in the three-dimensional case: very-high-order finite volume method for hyperbolic systems, Int. J. Numer. Methods Fluids 73 (2013) 362–392.
[34] V.N. Dorovsky, Kh.Kh. Imomnazarov, A mathematical model for the movement of a conducting liquid through a conducting porous medium, Math. Comput. Model. 20 (7) (1994) 91–97.
[35] M. Dumbser, Arbitrary high order PNPM schemes on unstructured meshes for the compressible Navier–Stokes equations, Comput. Fluids 39 (2010) 60–76.
[36] M. Dumbser, D. Balsara, E.F. Toro, C.D. Munz, A unified framework for the construction of one-step finite-volume and discontinuous Galerkin schemes, J. Comput. Phys. 227 (2008) 8209–8253.
[37] M. Dumbser, D.S. Balsara, High-order unstructured one-step PNPM schemes for the viscous and resistive MHD equations, Comput. Model. Eng. Sci. 54 (2009) 301–333.
[38] M. Dumbser, D.S. Balsara, A new, efficient formulation of the HLLEM Riemann solver for general conservative and non-conservative hyperbolic systems, J. Comput. Phys. 304 (2016) 275–319.
[39] M. Dumbser, M. Castro, C. Parés, E.F. Toro, ADER schemes on unstructured meshes for non-conservative hyperbolic systems: applications to geophysical flows, Comput. Fluids 38 (2009) 1731–1748.
[40] M. Dumbser, C. Enaux, E.F. Toro, Finite volume schemes of very high order of accuracy for stiff hyperbolic balance laws, J. Comput. Phys. 227 (2008) 3971–4001.
[41] M. Dumbser, A. Hidalgo, M. Castro, C. Parés, E.F. Toro, FORCE schemes on unstructured meshes II: non–conservative hyperbolic systems, Comput. Methods Appl. Mech. Eng. 199 (2010) 625–647.
[42] M. Dumbser, I. Peshkov, E. Romenski, O. Zanotti, High order ADER schemes for a unified first order hyperbolic formulation of continuum mechanics: viscous heat-conducting fluids and elastic solids, J. Comput. Phys. 314 (2016) 824–862.
[43] M. Dumbser, E.F. Toro, On universal Osher-type schemes for general nonlinear hyperbolic conservation laws, Commun. Comput. Phys. 10 (2011) 635–671.
[44] M. Dumbser, E.F. Toro, A simple extension of the Osher Riemann solver to non-conservative hyperbolic systems, J. Sci. Comput. 48 (2011) 70–88.
[45] M. Dumbser, A. Uuriintsetseg, O. Zanotti, On arbitrary-Lagrangian–Eulerian one-step WENO schemes for stiff hyperbolic balance laws, Commun. Comput. Phys. 14 (2013) 301–327.
[46] M. Dumbser, O. Zanotti, Very high order PNPM schemes on unstructured meshes for the resistive relativistic MHD equations, J. Comput. Phys. 228 (2009) 6991–7006.
[47] M. Dumbser, O. Zanotti, A. Hidalgo, D.S. Balsara, ADER-WENO finite volume schemes with space–time adaptive mesh refinement, J. Comput. Phys. 248 (2013) 257–286.

[48] M. Dumbser, O. Zanotti, R. Loubère, S. Diot, A posteriori subcell limiting of the discontinuous Galerkin finite element method for hyperbolic conservation laws, J. Comput. Phys. 278 (December 2014) 47–75.
[49] F. Dupret, J.M. Marchal, Loss of evolution in the flow of viscoelastic fluids, J. Non-Newton. Fluid Mech. 20 (1986) 143–171.
[50] B. Einfeldt, C.D. Munz, P.L. Roe, B. Sjögreen, On Godunov-type methods near low densities, J. Comput. Phys. 92 (1991) 273–295.
[51] A.C. Eringen, G.A. Maugin, Electrodynamics of Continua I: Foundations and Solid Media, Springer Science & Business Media, 2012.
[52] F. Fambri, O. Zanotti, M. Dumbser, Space–time adaptive ADER-DG schemes for dissipative flows: compressible Navier–Stokes and resistive MHD equations, Comput. Phys. Commun. (2017), submitted for publication, arXiv:1612.01410.
[53] N. Favrie, S.L. Gavrilyuk, R. Saurel, Solid–fluid diffuse interface model in cases of extreme deformations, J. Comput. Phys. 228 (16) (2009) 6037–6077.
[54] J. Frenkel, Kinetic Theory of Liquids, Dover, 1955.
[55] K.O. Friedrichs, Symmetric positive linear differential equations, Commun. Pure Appl. Math. 11 (3) (1958) 333–418.
[56] K.O. Friedrichs, P.D. Lax, Systems of conservation equations with a convex extension, Proc. Natl. Acad. Sci. 68 (8) (1971) 1686–1688.
[57] S.L. Gavrilyuk, N. Favrie, R. Saurel, Modelling wave dynamics of compressible elastic materials, J. Comput. Phys. 227 (2008) 2941–2969.
[58] I.M. Gelfand, S.V. Fomin, Calculus of Variations, Prentice–Hall Inc., Englewood Cliffs, NJ, 1963.
[59] I.M. Gelfand, R.A. Minlos, Z.Ya. Shapiro, Representations of the Rotation and Lorentz Groups and Their Applications, Pergamon Press, Oxford, London, 1963.
[60] V.L. Ginzburg, V.A. Ugarov, Remarks on forces and the energy-momentum tensor in macroscopic electrodynamics, Sov. Phys. Usp. 19 (1) (1976) 94.
[61] S.K. Godunov, An interesting class of quasilinear systems, Dokl. Akad. Nauk SSSR 139 (3) (1961) 521–523.
[62] S.K. Godunov, The problem of a generalized solution in the theory of quasilinear equations and in gas dynamics, Russ. Math. Surv. 17 (3) (1962) 145–156.
[63] S.K. Godunov, Symmetric form of the magnetohydrodynamic equation, Numer. Methods Mech. Continuum Medium 3 (1) (1972) 26–34.
[64] S.K. Godunov, Elements of Mechanics of Continuous Media, Nauka, 1978 (in Russian).
[65] S.K. Godunov, T.Yu. Mikhailova, E.I. Romenski, Systems of thermodynamically coordinated laws of conservation invariant under rotations, Sib. Math. J. 37 (4) (1996) 690–705.
[66] S.K. Godunov, I.M. Peshkov, Thermodynamically consistent nonlinear model of elastoplastic Maxwell medium, Comput. Math. Math. Phys. 50 (8) (2010) 1409–1426.
[67] S.K. Godunov, E.I. Romenski, Nonstationary equations of nonlinear elasticity theory in Eulerian coordinates, J. Appl. Mech. Tech. Phys. 13 (6) (1972) 868–884.
[68] S.K. Godunov, E.I. Romenski, Nonstationary equations of the nonlinear theory of elasticity in Euler coordinates, J. Appl. Mech. Tech. Phys. 13 (1972) 868–885.
[69] S.K. Godunov, E.I. Romenski, Thermodynamics, conservation laws and symmetric forms of differential equations in mechanics of continuous media, Comput. Fluid Dyn. Rev. 95 (1995) 19–31.
[70] S.K. Godunov, E.I. Romenski, Symmetric forms of thermodynamically compatible systems of conservation laws in continuum mechanics, in: ECCOMAS Conference on Numerical Methods in Engineering, 1996, pp. 54–57.
[71] S.K. Godunov, E.I. Romenski, Elements of Mechanics of Continuous Media, Nauchnaya Kniga, 1998 (in Russian).
[72] S.K. Godunov, E.I. Romenski, Elements of Continuum Mechanics and Conservation Laws, Kluwer Academic/Plenum Publishers, 2003.
[73] H. Goldstein, J.L. Safko, C.P. Poole, Classical Mechanics, 3rd edition, Addison–Wesley, 2001.
[74] A. Harten, B. Engquist, S. Osher, S. Chakravarthy, Uniformly high order essentially non-oscillatory schemes, III, J. Comput. Phys. 71 (1987) 231–303.
[75] A. Hidalgo, M. Dumbser, ADER schemes for nonlinear systems of stiff advection–diffusion–reaction equations, J. Sci. Comput. 48 (2011) 173–189.
[76] H. Jeong, D. Ryu, T.W. Jones, A. Frank, The magnetohydrodynamic Kelvin–Helmholtz instability. III. The role of sheared magnetic field in planar flows, Astrophys. J. 529 (2000) 536–547.
[77] G.S. Jiang, C.C. Wu, A high-order WENO finite difference scheme for the equations of ideal magnetohydrodynamics, J. Comput. Phys. 150 (1999) 561–594.
[78] S. Jin, C.D. Levermore, Numerical schemes for hyperbolic conservation laws with stiff relaxation terms, J. Comput. Phys. 126 (2) (1996) 449–467.
[79] D. Jou, J. Casas-Vazquez, G. Lebon, Extended Irreversible Thermodynamics, Springer, Berlin, Heidelberg, 1996.
[80] T. Kato, The Cauchy problem for quasi-linear symmetric hyperbolic systems, Arch. Ration. Mech. Anal. 58 (3) (1975) 181–205.
[81] R. Keppens, G. Tóth, R.H.J. Westermann, J.P. Geodbloed, Growth and saturation of the Kelvin–Helmholtz instability with parallel and antiparallel magnetic fields, J. Plasma Phys. 61 (1999) 1–19.
[82] S.S. Komissarov, Multidimensional numerical scheme for resistive relativistic magnetohydrodynamics, Mon. Not. R. Astron. Soc. 382 (December 2007) 995–1004.
[83] E.M. Landau, L.D. Lifshitz, Electrodynamics of Continuous Media, vol. 8, 2nd edition, Elsevier, 1984.
[84] S. Landi, L. Del Zanna, E. Papini, F. Pucci, M. Velli, Resistive magnetohydrodynamics simulations of the ideal tearing mode, Astrophys. J. 806 (2015) 131.
[85] R.J. LeVeque, H.C. Yee, A study of numerical methods for hyperbolic conservation laws with stiff source terms, J. Comput. Phys. 86 (1) (1990) 187–210.
[86] N.F. Loureiro, A.A. Schekochihin, S.C. Cowley, Instability of current sheets and formation of plasmoid chains, Phys. Plasmas 14 (10) (2007) 100703.
[87] R.B. Lowrie, J.E. Morel, Methods for hyperbolic systems with stiff relaxation, Int. J. Numer. Methods Fluids 40 (2002) 413–423.
[88] V.P. Makarov, A.A. Rukhadze, Force on matter in an electromagnetic field, Phys. Usp. 52 (9) (2009) 937.
[89] A. Mazaheri, H. Nishikawa, First-Order Hyperbolic System Method for Time-Dependent Advection–Diffusion Problems, Technical report March, NASA, 2013.
[90] A. Mazaheri, H. Nishikawa, Very efficient high-order hyperbolic schemes for time-dependent advection–diffusion problems: third-, fourth-, and sixth-order, Comput. Fluids 102 (2014) 131–147.
[91] L.A. Merzhievsky, A.D. Resnyansky, The role of numerical simulation in the study of high-velocity impact, Int. J. Impact Eng. 17 (4) (1995) 559–570.
[92] F. Miniati, P. Colella, A modified higher order Godunov's scheme for stiff source conservative hydrodynamics, J. Comput. Phys. 224 (2) (2007) 519–538.
[93] H. Minkowski, Die Grundgleichungen für die elektromagnetischen Vorgänge in bewegten Körpern, Nachr. Kgl. Ges. Wiss. (1908) 53–111.
[94] G.I. Montecinos, L.O. Müller, E.F. Toro, Hyperbolic reformulation of a 1D viscoelastic blood flow model and ADER finite volume schemes, J. Comput. Phys. 266 (2014) 101–123.
[95] G.I. Montecinos, E.F. Toro, Reformulations for general advection–diffusion–reaction equations and locally implicit ADER schemes, J. Comput. Phys. 275 (2014) 415–442.
[96] I. Müller, T. Ruggeri, Rational Extended Thermodynamics, vol. 16, Springer, 1998.
[97] A. Muracchini, T. Ruggeri, L. Seccia, Dispersion relation in the high frequency limit and non linear wave stability for hyperbolic dissipative systems, Wave Motion 15 (2) (1992) 143–158.
[98] G. Naldi, L. Pareschi, Numerical schemes for hyperbolic systems of conservation laws with stiff diffusive relaxation, SIAM J. Numer. Anal. 37 (4) (2000) 1246–1270.
[99] S. Ndanou, N. Favrie, S. Gavrilyuk, Criterion of hyperbolicity in hyperelasticity in the case of the stored energy in separable form, J. Elast. 115 (1) (2014) 1–25.

[100] H. Nishikawa, A first-order system approach for diffusion equation. I: Second-order residual-distribution schemes, J. Comput. Phys. 227 (1) (2007) 315–352.
[101] H. Nishikawa, A first-order system approach for diffusion equation. II: Unification of advection and diffusion, J. Comput. Phys. 229 (11) (2010) 3989–4016.
[102] G.S. Ohm, Bestimmung des Gesetzes, nach welchem Metalle die Contactelektricität leiten, nebst einem Entwurfe zur Theorie des Voltaischen Apparates und des Schweiggerschen Multiplikators, Z. Phys. Chem. 46 (1826) 137–166.
[103] S.A. Orszag, C.M. Tang, Small-scale structure of two-dimensional magnetohydrodynamic turbulence, J. Fluid Mech. 90 (1979) 129.
[104] C. Parés, Numerical methods for nonconservative hyperbolic systems: a theoretical framework, SIAM J. Numer. Anal. 44 (2006) 300–321.
[105] L. Pareschi, G. Russo, Implicit-explicit Runge–Kutta schemes for stiff systems of differential equations, Adv. Theory Comput. Math. 3 (2000) 269–288.
[106] Michal Pavelka, Václav Klika, Miroslav Grmela, Time reversal in nonequilibrium thermodynamics, Phys. Rev. E 90 (6) (2014) 062131.
[107] R.B. Pember, Numerical methods for hyperbolic conservation laws with stiff relaxation, I. Spurious solutions, SIAM J. Appl. Math. 53 (5) (1993) 1293–1330.
[108] R.B. Pember, Numerical methods for hyperbolic conservation laws with stiff relaxation. II. Higher order Godunov methods, SIAM J. Sci. Comput. 14 (4) (1993) 824–859.
[109] I. Peshkov, M. Grmela, E. Romenski, Irreversible mechanics and thermodynamics of two-phase continua experiencing stress-induced solid–fluid transitions, Contin. Mech. Thermodyn. 27 (6) (November 2015) 905–940.
[110] I. Peshkov, E. Romenski, A hyperbolic model for viscous Newtonian flows, Contin. Mech. Thermodyn. 28 (2016) 85–104.
[111] J.M. Picone, R.B. Dahlburg, Evolution of the Orszag–Tang vortex system in a compressible medium. II. Supersonic flow, Phys. Fluids B 3 (1991) 29–44.
[112] Kenneth G. Powell, Philip L. Roe, Timur J. Linde, Tamas I. Gombosi, Darren L. De Zeeuw, W.M. Keck, A solution-adaptive upwind scheme for ideal magnetohydrodynamics, J. Comput. Phys. 154 (1999) 284–309.
[113] J. Qiu, M. Dumbser, C.W. Shu, The discontinuous Galerkin method with Lax–Wendroff type time discretizations, Comput. Methods Appl. Mech. Eng. 194 (2005) 4528–4543.
[114] A.D. Resnyansky, DYNA-modelling of the high-velocity impact problems with a split-element algorithm, Int. J. Impact Eng. 27 (7) (2002) 709–727.
[115] A.D. Resnyansky, N.K. Bourne, J.C.F. Millett, E.N. Brown, Constitutive modeling of shock response of polytetrafluoroethylene, J. Appl. Phys. 110 (3) (2011) 033530.
[116] S. Rhebergen, O. Bokhove, J.J.W. van der Vegt, Discontinuous Galerkin finite element methods for hyperbolic nonconservative partial differential equations, J. Comput. Phys. 227 (2008) 1887–1922.
[117] P.L. Roe, D.S. Balsara, Notes on the eigensystem of magnetohydrodynamics, SIAM J. Appl. Math. 56 (1996) 57–67.
[118] E.I. Romenski, Hyperbolic equations of Maxwell's nonlinear model of elastoplastic heat-conducting media, Sib. Math. J. 30 (4) (1989) 606–625.
[119] E.I. Romenski, Hyperbolic systems of thermodynamically compatible conservation laws in continuum mechanics, Math. Comput. Model. 28 (10) (1998) 115–130.
[120] E.I. Romenski, Thermodynamics and hyperbolic systems of balance laws in continuum mechanics, in: E.F. Toro (Ed.), Godunov Methods, Springer, 2001, pp. 745–761.
[121] T. Ruggeri, Global existence of smooth solutions and stability of the constant state for dissipative hyperbolic systems with applications to extended thermodynamics, in: S. Rionero, G. Romano (Eds.), Trends and Applications of Mathematics to Mechanics, Springer, Milano, 2005, pp. 215–224.
[122] T. Ruggeri, A. Strumia, Convex covariant entropy density, symmetric conservative form, and shock waves in relativistic magnetohydrodynamics, J. Math. Phys. 22 (8) (August 1981) 1824–1827.
[123] V.V. Rusanov, Calculation of interaction of non-steady shock waves with obstacles, J. Comput. Math. Phys. USSR 1 (1961) 267–279.
[124] Z. Xin, S. Jin, The relaxation schemes for systems of conservation laws in arbitrary space dimensions, Commun. Pure Appl. Math. 48 (1995) 235–277.
[125] R. Samtaney, N.F. Loureiro, D.A. Uzdensky, A.A. Schekochihin, S.C. Cowley, Formation of plasmoid chains in magnetic reconnection, Phys. Rev. Lett. 103 (10) (2009) 105004.
[126] D. Serre, Hyperbolicity of the nonlinear models of Maxwell's equations, Arch. Ration. Mech. Anal. 172 (3) (May 2004) 309–331.
[127] A.H. Stroud, Approximate Calculation of Multiple Integrals, Prentice–Hall Inc., Englewood Cliffs, New Jersey, 1971.
[128] Struchtrup Henning, Manuel Torrilhon, Regularization of grad's 13 moment equations: derivation and linear analysis, Phys. Fluids 15 (9) (2003) 2668–2680.
[129] A. Taube, M. Dumbser, C.D. Munz, R. Schneider, A high order discontinuous Galerkin method with local time stepping for the Maxwell equations, Int. J. Numer. Model. 22 (2009) 77–103.
[130] V.A. Titarev, E.F. Toro ADER, Arbitrary high order Godunov approach, J. Sci. Comput. 17 (1–4) (December 2002) 609–618.
[131] V.A. Titarev, E.F. Toro, ADER schemes for three-dimensional nonlinear hyperbolic systems, J. Comput. Phys. 204 (2005) 715–736.
[132] E.F. Toro, V.A. Titarev, Derivative Riemann solvers for systems of conservation laws and ADER methods, J. Comput. Phys. 212 (1) (2006) 150–165.
[133] E.F. Toro, S.J. Billet, Centered TVD schemes for hyperbolic conservation laws, IMA J. Numer. Anal. 20 (2000) 44–79.
[134] E.F. Toro, A. Hidalgo, M. Dumbser, FORCE schemes on unstructured meshes I: conservative hyperbolic systems, J. Comput. Phys. 228 (2009) 3368–3389.
[135] E.F. Toro, G.I. Montecinos, Advection–diffusion–reaction equations: hyperbolization and high-order ADER discretizations, SIAM J. Sci. Comput. 36 (5) (2014) A2423–A2457.
[136] E.F. Toro, G.I. Montecinos, Implicit, semi-analytical solution of the generalized Riemann problem for stiff hyperbolic balance laws, J. Comput. Phys. 303 (2015) 146–172.
[137] E.F. Toro, V.A. Titarev, Solution of the generalized Riemann problem for advection–reaction equations, Proc. R. Soc. Lond. (2002) 271–281.
[138] Manuel Torrilhon, Modeling nonequilibrium gas flow based on moment equations, Annu. Rev. Fluid Mech. 48 (1) (2016) 429–458.
[139] M. Dumbser, W. Boscheri, R. Loubere, Cell centered direct arbitrary-Lagrangian–Eulerian ADER-WENO finite volume schemes for nonlinear hyperelasticity, Comput. Fluids 134–135 (2016) 111–129.
[140] T. Warburton, G. Karniadakis, A discontinuous Galerkin method for the viscous MHD equations, J. Comput. Phys. 152 (1999) 608–641.
[141] K.S. Yee, Numerical solution of initial boundary value problems involving Maxwell equation in an isotropic media, IEEE Trans. Antennas Propag. 14 (1966) 302–307.
[142] J.Y. Yoo, Daniel D. Joseph, Hyperbolicity and change of type in the flow of viscoelastic fluids through channels, J. Non-Newton. Fluid Mech. 19 (1985) 15–41.
[143] O. Zanotti, M. Dumbser, Numerical simulations of high Lundquist number relativistic magnetic reconnection, Mon. Not. R. Astron. Soc. 418 (2011) 1004–1011.
[144] O. Zanotti, F. Fambri, M. Dumbser, Solving the relativistic magnetohydrodynamics equations with ADER discontinuous Galerkin methods, a posteriori subcell limiting and adaptive mesh refinement, Mon. Not. R. Astron. Soc. 452 (2015) 3010–3029.
[145] O. Zanotti, F. Fambri, M. Dumbser, A. Hidalgo, Space–time adaptive ADER discontinuous Galerkin finite element schemes with a posteriori subcell finite volume limiting, Comput. Fluids 118 (2015) 204–224.